A 'NEW' MICROSPORIDIAN IN THE UK:
INVESTIGATIONS INTO THE UNKNOWN MICROSPORIDIAN
INFECTING JUVENILE SMELT (*OSMERUS EPERLANUS*) FROM
THE RIVER THAMES

A thesis submitted for the degree of Doctor of Philosophy

by

Georgina Fauconier (née Collins)

College of Health, Medicine and Life Sciences
Brunel University London

December 2021

Declaration

I, Georgina Beth Fauconier (née Collins) confirm that the work presented in this thesis is my own. Where information has been derived from other sources, I confirm that this has been indicated in the thesis.

Signature:

Georgina Fauconier

Date: 13/12/2021

Abstract

The European smelt *Osmerus eperlanus* is a small anadromous species, which resides in coastal waters with a broad distribution around Europe and the Baltic regions. UK populations were once abundant, inhabiting most rivers around the UK. However, pollution and overexploitation of this once commercial species led to its disappearance from most UK rivers during the 1800s. With the improved water quality and legal protection, the species returned to many rivers, including a breeding population in the River Thames since the 1980s. This species is severely understudied with knowledge gaps on life-history traits, dynamics between different populations in the UK and native parasitic fauna. In the summer of 2018, Environment Agency (EA) surveys in the Thames revealed that many juvenile smelt were infected with a microsporidian parasite, previously unreported in the UK smelt. This doctoral thesis aimed to identify and describe this newly reported microsporidian and assess the possible impacts of infection. Using traditional histological analysis and micro-computer tomography (micro-CT), I characterised the parasite as a species of the *Glugea* genus. The micro-CT imagery provided a novel approach for assessing a full 360° view of parasitic infections, allowing for visualisation of the distribution of disease and providing quantitative measures for the volume of cysts within the body cavity. Additional phylogenetic analysis confirmed the *Glugea* genus classification and revealed close sequence identity to several other *Glugea* species. Based on the morphological presentation, phylogenetic placement, and historical findings of a morphologically similar microsporidian infecting smelt from the Baltic regions and Rainbow smelt *Osmerus mordax* in the US and Canada; I suggest that the microsporidian infecting Thames smelt is likely *G. hertwigi*. This study was the first to provide a ribosomal DNA sequence for a microsporidian of the *Glugea* genus in European smelt and the first to report its presence in UK smelt. Furthermore, I assessed the surface pressure changes and drag forces associated with the disease due to the gross distortions caused to the fish's body by bulging cysts. To the best of my knowledge, this study is the first to attempt to apply computational fluid dynamics to calculate costs associated with parasitic infection in fish. The data presented in this thesis adds to the limited body of knowledge on smelt populations in the UK and provides novel complementary methods for assessing parasitic infections in fish.

Acknowledgments

TABLE OF CONTENTS

List of Figures

List of Tables

Chapter 1. General introduction

1.1 Introduction

The United Kingdom, like many other countries, is facing significant threats to terrestrial and aquatic biodiversity (Hulme, 2017). Global declines in species are leading to less resilient ecosystems, which are put under further pressure by increasing anthropogenic pressures and changing climatic regimes (Butchart et al., 2010). Many aquatic ecosystems across Europe are recovering from a history of mass industrial and urban development and the subsequent degradation of urban rivers (Grizzetti et al., 2017). Wetlands, peatlands, tidal wetlands and saltmarshes have been degraded and reduced in size across Europe and are recognised as critical habitats for biodiversity conservation (Verhoeven, 2014). Freshwater habitats are some of the most threatened, with freshwater fish facing the highest extinction rate worldwide among vertebrates in the 20th century (WWF, 2018). The World Health Organisation (WHO) categorised four main anthropogenic drivers of biodiversity and ecosystem change in riverine systems; habitat alteration, habitat fragmentation, introduced non-native species and water pollution (Corvalan et al., 2005). Legal frameworks such as the European Union Birds and Habitats Directives, Natura 2000 network and EU Water Framework Directive (WFD) have been established to protect, conserve, and restore threatened ecosystems. The WFD was one of the most ambitious EU frameworks to improve water quality and achieve "good water status" by 2015 (Boeuf & Fritsch, 2016).

The UK is no different, with a long history of polluted water bodies becoming anoxic and devoid of aquatic life during the 19th and 20th centuries (Miller & Hutchins, 2017). Many legal frameworks have been adopted to manage and conserve critical ecosystems, such as the UK's 25-year Environment Plan, Species of Conservation Importance and the UK Biodiversity Action Plan (BAP) priority species and habitats (Department for Environment Food & Rural Affairs, 2018; JNCC, 2010; H.M.Government, 1994). Under these frameworks, certain species are identified for focused conservation efforts. Indicator species for the WFD are selected based on their sensitivity to water quality and changes to their spawning habitat, i.e., their presence in an ecosystem may indicate good ecological status (Directive, 2000).

Legislation and conservation efforts have dramatically improved water quality in urban rivers steadily over the last 60 years. Recently, however, the status of rivers in the UK, especially England, has been receiving a lot of media and public attention due to their degraded state, primarily due to unregulated sewage and grey water releases and the perceived lack of government intervention. The River's Trust has recently published the "State of Our Rivers" report, which highlighted several major environmental concerns, including the fact that all English rivers are failing chemical standards and only 14% pass with "good ecological health" (The Rivers Trust, 2021). The Zoological Society of London (ZSL) have also recently released their 'State of The Thames' report, where they used seventeen indicators to assess the health of the Tidal Thames and estimate short and long term trends of the state of the environment, state of nature and state of play (Zoological Society of London, 2021). The state of the Thames environment highlighted improvements in the system, such as increasing concentrations of dissolved oxygen and reduction in phosphorus concentrations; however, nitrate concentrations have been increasing, along with increased average water temperatures and sea level rise (Zoological Society of London, 2021).

While improved water quality and legal protection has boosted the populations of a number of migratory species migrating into UK waters, such as European eel *Anguilla anguilla*, allis shad *Alosa alosa*, twaite shad *Alosa fallax*, sea lamprey *Petromyzon marinus* and river lamprey *Lampetra fluviatilis*, many of these species remain highly threatened with very low population numbers (Jolly et al., 2012; Davies et al., 2020; Masters et al., 2006). Another of these rare migratory species is the European smelt *Osmerus eperlanus* (Linnaeus 1758) (hereinafter referred to as smelt), an anadromous fish species now protected under EU and UK law. This thesis explores a newly reported microsporidian parasite infecting large numbers of juvenile smelt in the River Thames.

1.2 Study species – European smelt (*Osmerus eperlanus*)

The smelt family *Osmeridae* have a broad distribution throughout the northern hemisphere and contain six genera with thirteen species (Gorodilov & Melnikova, 2006). The species is tolerant to varying saline conditions and consists of migratory lacustrine and non-migratory freshwater populations (Maitland, 2003). European smelt is the only species of the genus which occurs in the British Isles (Maitland & Campbell,

1992). Most literature on smelt has originated in continental Europe, with few studies on the populations in the UK. The majority of studies from the British Isles have been conducted in the Cree in Scotland (where smelt are commonly referred to as Sparling) (Hutchinson, 1983; Hutchinson & Mills, 1987; Maitland & Lyle, 1996; Lyle & Maitland, 1997).

Ecological importance

Migratory smelt show large flexibility in their life-history traits and predator behaviour and, as a result, "can eat all, and be eaten by all" (Sandlund et al., 2005). Their ability to adapt to changing salinity and varied diet contributes to the biodiversity of pelagic food webs. As such, they are listed as a Species Feature of Conservation Importance under the ecological network guidance and a UK BAP Priority Species of principal importance to conserve biodiversity under the Natural Environment and Rural Communities Act S. 41 (2006) (JNCC, 2010, 2012). While flexible in some traits, smelt are very sensitive to poor water quality and environmental disturbances, and as a result, populations are particularly prone to crashes (Hutchinson & Mills, 1987). Due to their sensitivity, they have been listed as an ecological indicator species of Good Ecological Status under the Water Framework Directive (WFD) (Colclough, 2013). Furthermore, smelt were named a Focus for Conservation Importance (FOCI) species in 2010 (Colclough, 2013).

Smelt are an important food source for many recreational and economically important fish species in the northern hemisphere, including cod, *Gadus morhua;* pike, *Esos lucuis;* perch, *Perca flavenscens;* and Atlantic salmon, *Salmo salar*, to name a few (Hutchinson, 1983; Hammar et al., 2018). The ecological value of smelt as a prey item has not been specifically investigated in the UK, although some authors suggested they may be an essential food source for sea trout, *Salmo trutta* (Hutchinson, 1983). The species are also noted as an important trophic component in the Baltic Sea ecosystem, with their stock and condition being an essential determinant for the status of larger commercial species (Taal et al., 2014).

Commercial value

Smelt were a favoured food item until the mid-1800s, with a number of commercial fisheries on the Tyne, Humber, Thames, Medway and Conway (Colclough, 2013).

Fisheries in the 1700/1800s landed tons of smelt annually. At its peak, the Thames fishery supported 30 boats; however, by the 1850s, the fishery collapsed due to overexploitation and water pollution (Hutchinson, 1983). By 1858, smelt had disappeared from the River Thames, and other populations across Great Britain had significantly declined and remained absent for most of the late 1800s/early 1900s (Colclough, 2013). Stocks began to recover from the 1960s, and have now been described in the Wash, Norfolk Broads, Thames, Medway and Dee with some smaller populations in the Humber, Alde and Ribble, however their demand as a food fish remains almost non-existent (Colclough, 2013). Demand for smelt in the UK is now as dead bait for pike fishing. Currently, two authorised fisheries operate using fyke nets and pots. The rivers fished between 2013-2019 included the Aire, Wharf, Nene, Waveney, Bure, Trent, Yare and Great Ouse (Ian Dolbey, Environment Agency, pers. comm).

Pollution, overfishing, and habitat degradation have also resulted in declining migratory smelt populations across northern Europe. In the Dutch Wadden Sea, marked declines in smelt numbers have been observed due to extensive coastal defence structures that prevented migration and increased river-borne siltation in estuary mouths (Groot, 2002). In Germany, rivers such as the Elbe have noted historical declines of the species due to water pollution. However, recent improved water quality in the Elbe has led to the increased presence of migratory smelt. This increase has led to renewed interest in the fish as a modern commercial species in Germany (Svanberg, Bonow & Cios, 2016). The commercial demand for smelt as a food fish has declined in many northern European countries; however, they are still consumed in Germany, Russia and Estonia (Sendek & Bogdanov, 2019). Smelt are still a favourite food fish in Saint Petersburg, and the populations are exploited both commercially and recreationally. Commercial catches in the River Neva, Russia, averaged 292 tonnes between 2002-2017, while catches in the eastern Gulf of Finland reached a high of 595 tonnes in 2017, the highest catch in the previous 16 years (Sendek & Bogdanov, 2019). Smelt are also valued traditionally and towns, including St. Petersburg, Russia and Palanga, Lithuania, celebrate their migration by holding annual festivals (Svanberg, Bonow & Cios, 2016). Svanberg *et al.* (2016) have suggested that smelt may have the potential to be revived as a regional speciality in Sweden and adjacent countries as a more sustainable alternative to other declining

fish species. However, Švagždys (2009) suggested that long-term data on yearly catches of smelt from the Nemunas river and Curonian Lagoon, in the south-east Baltic, had a marked decline and fluctuated significantly in the second half of the twentieth century. Declining catches were likely a result of climatic changes, coupled with intensified fishing effort. Švagždys (2009) also suggested that a high abundance of cods in the Baltic Sea had a depressive effect on smelt stocks.

1.3 Biology and ecology of European smelt

Smelt have slender, elongated bodies with large scales and eyes and a fleshy adipose fin, and the lower jaw is projected and shows prominent teeth (Maitland & Campbell, 1992) (Fig. 1.1). Live fish appear translucent with a silvery green stripe and silvery-white body (Fig.1.2). Juveniles have very subtle colouration, appearing almost translucent. Adults have a characteristic cucumber scent which is localised in the skin and is referenced by their genus name of *Osmerus,* which was derived from the Greek 'osme' meaning smell or scent (Hutchinson, 1983).
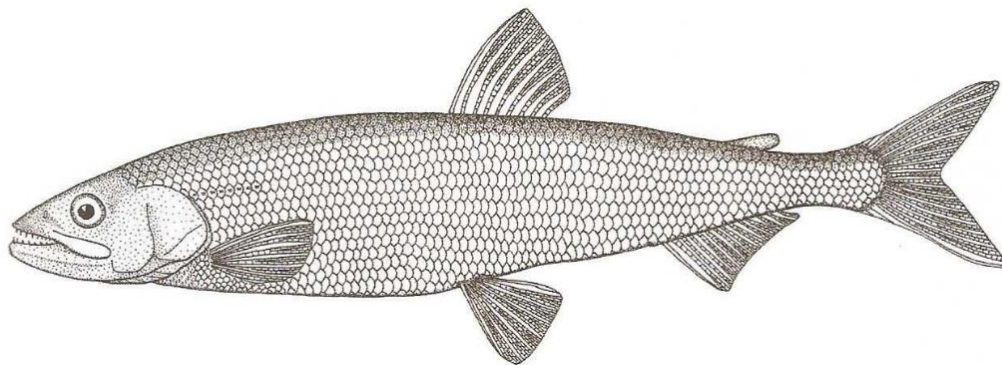
Figure 1. 1 A graphic representation of European smelt *Osmerus eperlanus* (taken from Maitland, 2007)

Figure 1. 2 A photograph of freshly caught adult smelt off Canvey Island, River Thames in November 2019.

Distribution

The European smelt is an anadromous, euryhaline species that migrate upstream from coastal marine waters into estuaries to breed (Colclough, 2013). The species have a broad distribution from southern Norway, around western Europe to northwest Spain, including the Baltic Sea, Southern North Sea and the British Isles, with several non-migratory populations in freshwater lakes in Finland, Sweden and Norway (Maitland & Lyle, 1996). Populations in the west of its distribution are primarily anadromous, while lacustrine in the east (Colclough, 2013).

UK distribution

The species used to occur in most estuaries around Great Britain prior to the 1850s but declined significantly due to overfishing, poor water quality from pollution, barriers to migration and urban development (Colclough, 2013). Smelt was classified as rare in the UK and vulnerable in Europe in the 1990s (Winfield, Fletcher & Cragg-Hine, 1994). The only UK freshwater population, which occurred in Rostherne Mere in Cheshire, became extinct in the 1920s (Maitland & Lyle, 1996).

More recently, smelt have been identified in 36 waterways in England and Wales, with large populations present in the Thames, Humber, Wash, Great Ouse, Norfolk Broads and the Dee (Colclough, 2013). Figure 1.3 shows the current distribution of smelt around the UK. In the Tidal Thames, the population has increased since the early 1980s due to improved water quality (Colclough et al., 2002).
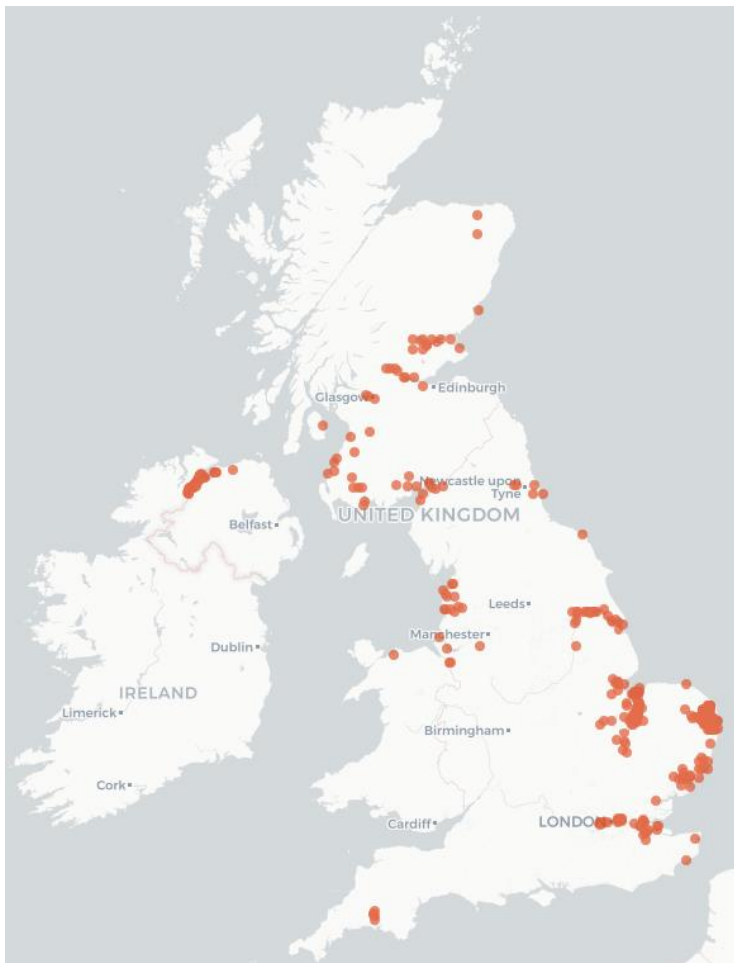
Figure 1. 3 Distribution of European Smelt around the UK based on data records from the Database for the Atlas of Freshwater Fishes, Environment Agency Rare and Protected Species records and Department of Agriculture, Environment and Rural Affairs (DAERA) Marine and Fisheries Division Marine Survey Data (NBN Atlas, 2021). The orange points represent locations where smelt have been identified and recorded in the aforementioned datasets. (NBN smelt distribution map - Link to an interactive map where the record for each point can be explored)

Diet

Smelt are known to be "gregarious and voracious" (Day, 1884). Their diet shifts as they mature, from feeding on small zooplankton to larger planktonic invertebrates, crustaceans and young fish (Maitland & Campbell, 1992; Taal et al., 2014). Their diet is reflected in their morphology, with their mouths featuring both dense gill rakers and prominent teeth (Sandlund et al., 2005). Diet composition differs amongst smelt populations and is influenced by local environmental conditions and prey availability, which in turn affects fish growth. A study of the diet of a smelt population from the Gulf of Finland revealed that crustaceans were the most common prey and that piscivorous feeding was particularly evident in larger fish during the summer and early autumn (Taal et al., 2014). This study also found that prey composition was significantly affected by the total length of individuals and during different seasons. Furthermore, seasonal diet shifted between smelt found in the near-shore and offshore regions. Personal investigations revealed whole amphipods (*Gammarus*) inside the stomachs of some dissected smelt from the Thames.

Age and growth

Smelt populations reside in a range of habitats across Europe and throughout their life; morphological characteristics, growth rates, maturation time and life span are all dependent on these conditions and habitats (Shpilev, Ojaveer & Lankov, 2005).

Populations of smelt in the UK have been reported as short-lived, living three years on average, with less than 2% surviving into their fourth year (Hutchinson, 1983). Whereas, in some Baltic populations, smelt reach maturity at 2-3 years old, with spawning shoals containing individuals of up to 10 years old, although most individuals are 2-6 years old (Shpilev, Ojaveer & Lankov, 2005).

The length of smelt varies with age and location but usually ranges from 10-29 cm in mainland Europe (Maitland & Campbell, 1992), whereas in the UK smelt have been reported as smaller with a length range of 10-20 cm (Maitland & Lyle, 1996). Males tend to be smaller than females with average weights of 28 g and 36 g, respectively (Maitland & Campbell, 1992), length differences between the sexes may become more apparent with increasing age (Hutchinson, 1983).

UK smelt tend to reach sexual maturity by two years old; however, some young-of-the-year from the Thames population have been recorded with developed gonads (Hutchinson, 1983; Hutchinson & Mills, 1987). Sexually mature smelt have been reported at age 1+ from the river Cree (Wootton, 2018; Hutchinson & Mills, 1987). The age of sexual maturity has been linked to the speed of growth of individuals, with rapidly growing individuals reaching sexual maturity earlier than slow-growing individuals (Hutchinson, 1983). When smelt reach sexual maturity, they aggregate and overwinter in shoals in the lower estuary (Doherty & McCarthy, 2004).

Variation in the age of sexual maturity of European smelt is also common in the Baltic Sea populations. Marine smelt from the Curonian Lagoon reach sexual maturity at 2-3 years, while lagoon smelt mature after their first year (Shpilev, Ojaveer & Lankov, 2005). Furthermore, smelt from the Gulf of Finland and Gulf of Riga mature between 2-6 years (Shpilev, Ojaveer & Lankov, 2005). Arula *et al.* (2017) reported that smelt from the Gulf of Riga reached maturity earlier and at a lower weight following periods of high exploitation compared to those sampled before 1980.

Reproduction

In UK waters, the spawning run occurs at night between late February to early April when water temperatures in the estuary are between 5-10°C (Colclough, 2013). The temperature threshold varies from estuary to estuary (Colclough, 2013). Spawning usually occurs in quite fast-flowing water, and young larvae and mature eggs likely drift downstream with the tide (Colclough, 2013). Tidal cycles, moon phase and river flows may also impact the timing of spawning (Lyle & Maitland, 1997). Eggs are very adhesive and adhere to gravel, stone, and soft vegetation. The eggs consist of a double envelope *zona radiate* around the oocytes; following spawning, the outer envelope bursts, becomes sticky and attaches to substrates. The outer envelope remains connected to the inner envelope, which results in the embryo being slightly suspended in the water (Gorodilov & Melnikova, 2006). From the limited studies in the UK, females are reported to lay between 10 000 to 106 000 eggs, and these eggs hatch after 20-35 days (Hutchinson & Mills, 1987; Maitland & Campbell, 1992).

A breeding population of national importance inhabits the Thames, and historic spawning has been recorded in the Wandsworth area of the estuary (Pilcher, 1989).

However, present-day spawning and juvenile rearing sites are not well defined (McCard, 2015). Recent smelt spawning surveys by the Zoological Society of London (ZSL) have suggested a stretch near Wandsworth Bridge is a likely spawning ground in the Thames (Anna Cucknell, ZSL, pers. comm), as eggs were collected at the site in 2015-2016. However, no eggs were collected between 2017-2019, and Cucknell suggested that percussive piling along the river may have affected spawning in those years (Anna Cucknell, ZSL, pers. comm). A spawning modelling report for smelt in the Thames suggested that fry do not hatch simultaneously but rather continuously over approximately two weeks (Barker, 2016). This report also suggested the fry hatch in an area close to the spawning grounds.

1.4 Threats to European smelt in the UK

<u>Habitat loss and degradation</u>
Rivers, particularly those close to or running through cities, have faced anthropogenic pressures and modifications for centuries. Channelization, water abstraction and damming have changed natural watercourses and the available foreshore habitat for local biodiversity. These modifications threaten breeding grounds due to the disruption of gravel substrates for egg laying and development and juveniles when flows reach critical velocities (Colclough et al., 2002). Juvenile smelt rely on tidal stream transport and the tidal foreshore (Colclough et al., 2002). The tidal foreshore also provides a low-velocity refuge against strong currents, which is critical habitat for juvenile fish which cannot swim against strong currents and need refuge from predators. It is important to conserve what is left of the remaining foreshore habitats, which are surrounded by heavily urbanised areas. Conservation advice, specifically for the tidal Thames, has suggested that no development affecting the subtidal habitat should occur when smelt are likely to spawn between late February to early April (Zoological Society of London, 2016).

Smelt are known to be particularly sensitive to changes in water quality. Alabaster (1982) suggested that for smelt to be present in an estuary, the air saturation value (ASV) needs to be at least 30-50%. Eutrophic waters with associated siltation can decrease fish recruitment to spawning grounds (Kangur et al., 2007). An example of this was given in a report by the Environment Agency (EA), which stated that a water

quality incident in May 2007 on the Thames decimated an entire 0+ year class and left a footprint in the length-frequency records of the species for two years (Colclough, 2013).

Habitat fragmentation is a significant driver of biodiversity loss and leads to a loss of connectivity for migratory fish species (Barry et al., 2018). These barriers to migration include weirs, dams and flood defences, which block access to historical breeding and feeding grounds (Colclough, 2013). Impacts from barriers can lead to short delays or complete obstruction, depending on the species swimming ability, barrier type, hydraulic conditions and timing of migration (Barry et al., 2018). A recent study by van Puijenbroek et al. (2019), who assessed species and river specific effects of river fragmentation on 16 anadromous fish species, suggested that a loss of connectivity is one of the most important reasons for Atlantic salmon *Salmo salar* decline across Europe.

While EU regulations have urged member states to restore connectivity in rivers, identifying and prioritising barriers for removal and budgetary constraints restrict restorations (King & O'Hanley, 2016). Furthermore, fish passages are not always effective for every species (van Puijenbroek et al., 2019). Belletti et al. (2020) highlighted that small and low-head barriers, such as bed sills, that are poorly mapped and difficult to detect, are causing major constraints to the free flow of rivers.

Climate change

Smelt are an Artic-Boreal species needing cool waters to spawn. The threat of warming waters as a result of global climate change may see populations shifting northward in the UK, with fewer numbers seen in southern estuaries such as the Thames (Colclough, 2013). Changing climates also directly or indirectly influence biological invasions and the prevalence of disease (Hulme, 2017). Changes in UK climate have been reported with mean annual temperatures rising since 1980 by 1 °C in the terrestrial environment, 0.7 °C in sea-surface temperatures around the UK coast, with changing rainfall patterns, with precipitation declining in summer and increasing in winter (Jenkins, Perry & Prior, 2008). A study on a population of non-migratory smelt in Lake Peipsi, Estonia suggested that smelt react quickly to weather-induced

changes, with populations declining when water remains above 20 °C for prolonged periods when they are unable to migrate to cooler waters (Kangur et al., 2007).

The ZSL State of the Thames report reported a long-term increase in both summer and winter water temperatures in the Tidal Thames (Zoological Society of London, 2021). Furthermore, the short-term predictions of summer temperatures showed a significant increase. The summer temperatures have increased on average by 0.19 °C each year in the upper Tidal Thames. Changes in water temperature significantly impact fish populations, especially migrating species like smelt, which rely on temperature cues to begin their spawning migration.

Commercial fishing

As previously mentioned, smelt are no longer consumed by the general UK population, but rather small-scale commercial fisheries exist to provide baitfish for recreational fishers. There are currently two licensed fisheries in England for smelt (Ian Dolbey, Environment Agency, pers. comm). As smelt are a protected species, it is important that we understand current population dynamics, to ensure that any exploitation is sustainable.

Parasites

Smelt are particularly vulnerable to parasites due to their migratory life cycle, range of salinity tolerances and opportunistic feeding (Dziekonska-Rynko et al., 2018; Pilecka-Rapacz et al., 2017). Smelt are open-bladder or physoclisti; which make them more sensitive to parasite invasion (Dziekonska-Rynko et al., 2018). A recent parasitological survey of smelt from the Baltic Sea aimed to provide an overview of the parasites commonly found in European smelt, as well as review historical literature on the subject (Pilecka-Rapacz et al., 2017). Baltic sea smelt parasitic fauna were represented by a range of taxa including Digenea, Cestoda, Nematoda, Acanthocephala, Crustacea, Hirudinea, Mollusca and Fungi. Three parasite species were very common and included parasitic worms, *Hysterothylacium aduncum* and *Cystidicola farionis*, which infect the viscera/intestines and swim bladder, respectively, and a bivalve mussel, Unionidae gen sp., which attaches to the gills of the fish (Pilecka-Rapacz et al., 2017). Furthermore, two parasite species were present in three of five survey sites and included a trematode species, *Diplostomum* sp., found in the

eye lenses of smelt and another tapeworm, *Proteocephalus longicollis*, which resides in the intestines.

Detailed studies of the parasitic fauna of smelt in the UK has not been attempted. Juvenile smelt surveyed from the Thames in 2018, presented with a high frequency of white cysts along their gut. These cysts were identified as microsporidians by Dr Amy Reading and team at the Environment Agency (pers. comms). Microsporidians or icthyosporidians have been previously reported in European smelt from the Baltic Sea, Lake Ladoga in Russia and the River Elbe in Germany (Costa, Melo-Moreira & De Carvalho, 2016; Pekcan-Hekim, Rahkonen & Horppila, 2005). These reported microsporidians were identified as *Glugea hertwigi* and *Pleistophora ladogensis*. A large body of literature is available on *G. hertwigi* outbreaks in American Rainbow smelt *Osmerus mordax,* where they were associated with the loss of whole year classes in lake smelt populations (Haley, 1954; Haley, Voge & Read, 1954; Nepszy, Budd & Dechtiar, 1978; Henderson & Nepszy, 1989; Lovy et al., 2009; Nepszy & Dechtiar, 1972).

1.5 Knowledge gaps on European smelt in the UK

A large proportion of English literature available on smelt comes from government agencies, such as Natural England and the Environment Agency. These agencies have produced reports on the status of smelt in England and Wales (Maitland, 2003; Colclough, 2013). The latest "status of smelt" report by the Environment Agency in 2013, built onto the previous review using data from extensive monitoring campaigns across estuaries in England and Wales. While this provided a good overview of the smelt populations, there are still significant knowledge gaps in the life history traits of current smelt populations. The Zoological Society of London conducted a study in 2015/2016 to determine where smelt spawned in the Thames (Barker, 2016). In order to conserve and protect the species, we first need to fully understand their population dynamics within UK waters.

Furthermore, little information is available on the parasitic fauna of smelt or risks from disease. As mentioned above, in 2018, Amy Reading and Chris Williams from the Environment Agency's National Fisheries Laboratory (NFL) were made aware of large numbers of juvenile smelt from the Thames with white cysts present along their gut.

This parasite was tentatively identified as the microsporidian *Glugea hertwigi* by the NFL. The identification was based on previous associations between *G. hertwigi* and European smelt from German rivers (Costa, Melo-Moreira & De Carvalho, 2016), and in *O. mordax* in Canada and the USA (Haley, 1954, 1952; Nepszy, Budd & Dechtiar, 1978; Lovy et al., 2009). Over 80% of sampled juveniles seemed to be infected in the 2018 sample (EA, pers. comm). The NFL wanted to identify if these parasites are just unsightly or if there is cause for concern, and therefore the topic warranted further investigation.

1.6 Thesis overview

This doctoral thesis aims to identify and describe a newly reported microsporidian parasite infecting large numbers of juvenile smelt *O. eperlanus* in the River Thames.

In **Chapter 2**, I explore current smelt population structures in England and Wales, using preliminary data provided by the Environment Agency National Fisheries Laboratory. Using established fisheries science metrics, I assess biological data on smelt collected from six English and one Welsh River between 2011 and 2018. I hope that analysis and assessment of these data on smelt can provide a starting point for future population studies and conservation efforts (outside of the scope of my thesis).

In **Chapter 3**, I provide a pathological description of the newly reported microsporidian parasite infecting juvenile Thames smelt. The microsporidian had been tentatively identified by EA fish pathologists at the National Fisheries Laboratory as *Glugea hertwigi* based on historical findings of this microsporidian in smelt from other European rivers. I briefly describe the basic characteristics of microsporidians and review their history of infection in European smelt. I aim to positively identify the microsporidian species based on morphological characteristics and to present a more in-depth study of the effects of the infection on the internal organs. Whole fish histological sections and 3D micro-computer tomography (micro-CT) imagery are used to provide this detail.

In **Chapter 4**, I aim to build onto the work of Chapter 3, by providing a molecular identification of the microsporidian using polymerase chain reaction (PCR) and DNA sequencing to target and amplify rDNA genes specific to microsporidia. I aim to

provide the first sequence from a *Glugea* microsporidian infecting European smelt (*O. eperlanus*), as only one current sequence of *G. hertwigi* is available on GenBank, which was extracted and sequenced from infected *O. mordax* in Canada. Furthermore, my research will be the first study (as far as I know) to sequence the ssrDNA of a microsporidian infecting European smelt across Europe.

In **Chapter 5**, I was interested in assessing the impact of the *Glugea* cysts on the swimming ability of infected smelt, as my findings in Chapters 3 and 4, revealed that the large cysts cause deformations in the infected fish's body shape. I investigate the drag coefficient and surface pressure changes produced by deformities in body shape caused by microsporidian cysts to assess potential negative impacts associated with increasing disease burden. This work was produced in collaboration with Dr Humberto G. Ferron and Dr Oscar Sanisidro.

In **Chapter 6**, I provide a final summary of the studies undertaken in this thesis and discuss how this work has contributed to the field. I describe some of the limitations of the work and outline another study I had planned to do but was unable to conduct due to the COVID 19 pandemic restrictions. I discuss how future studies could be improved and what the next steps should be regarding the presence of this microsporidian in the River Thames.

Chapter 2. Preliminary investigations into the biology and ecology of European smelt (*Osmerus eperlanus)* in several UK rivers

Abstract

The European smelt (*Osmerus eperlanus*) is a small anadromous migratory fish species that once flourished in the United Kingdom and supported a profitable fishery into the 1800s. However, rapid urbanisation and pollution caused populations to crash during the 20th century. Increasing concern and legislation to improve urban waterways have seen a resurgence in European smelt migrating into estuaries across the United Kingdom since the mid-1900s. Their ecological importance and sensitivity to pollution have noted them as a priority species for conservation. Smelt in the UK are an understudied species, with many knowledge gaps on biology, population dynamics and life-history traits. Using preliminary unpublished data (provided by the National Fisheries Laboratory), I assess several basic biology and life-history traits from 720 European smelt sampled across six English and one Welsh river between 2011 and 2018. The metrics included weight-length relationships, age and growth analyses and reproduction indices. The maximum age of any smelt captured was five, with approximately 80% of specimens aged two to three years old. Length and weights varied across rivers but were comparable with previous literature. All smelt captured ranged from <100 - <300 mm in total length. Smelt from the Great Ouse, Dee, Yare and Waveney presented a similar length-at-age trend, while smelt from the Thames and Tamar were smaller in comparison. Back-calculated length at age was applied to Von Bertalanffy growth functions to compare the growth trajectories of each population. These findings are reported as a starting point for future studies, however I acknowledge the limitations in the dataset. Differences in life-history traits between river locations may suggest that smelt populations could be separate. Further sampling is needed to validate this hypothesis and account for variations in population biology between seasons and during and after spawning.

2.1 Introduction

The European smelt, *O. eperlanus*, (hereon referred to as smelt) is a small-bodied, anadromous fish species, part of the Osmeridae family, native from the Northeastern Atlantic White Sea to the western coasts of France, including the Baltic Sea, Southern North Sea and British Isles (McAllister, 1984). Once an abundant fish in most rivers and estuaries throughout the UK (Maitland & Lyle, 1996), it was a favoured food item, with commercial fisheries in the 1700/1800s landing tons of smelt annually, especially in the River Thames (Colclough, 2013). However, by the mid-1800s, the fishery and population collapsed due to overexploitation and water pollution (Hutchinson, 1983).

Populations of migratory smelt have severely deteriorated across the UK, with an estimated decline of 33% in England and Wales and 80% in Scotland (JNCC, 2010) over the last 200 years (Moore et al., 2016). A Natural England report on the status of smelt published in 2003 suggested that there are approximately twenty-one populations around the coasts of England (19) and Wales (2) (Maitland, 2003), while the Environment Agency reported that smelt was found at thirty sites between 2000-2012 (Colclough, 2013) (Appendix 2. Table 1). Population declines and local extinctions have occurred due to various pressures, including water pollution, overfishing, habitat loss and reduced access to spawning grounds by weirs and other artificial barriers (Lyle & Maitland, 1997). Furthermore, dredging and development work on large estuaries, such as the Thames, have been suggested to cause decreased spawning and disruption to juveniles (pers. coms. Anna Cucknell ZSL). Smelt populations historically decimated in larger estuaries in England, such as the Thames and Humber, have been slowly recovering due to improved water quality and conservation efforts. While, smaller, more geographically isolated estuaries such as the Tyne are thought to be unlikely to recover through immigration alone (Maitland, 2003). Smelt are ecologically important in the food web, as essential prey items for larger piscivorous fish of commercial or recreational importance, such as the Atlantic salmon *Salmo salar* and European pike *Esox lucius*. In England, smelt are only commercially exploited in small quantities to provide bait for recreational fishermen (Colclough, 2013).

In the UK, the species has been reported as short-lived, living three years on average, with less than 2% surviving into their fourth year (Hutchinson, 1983). Whereas, in

some Baltic populations, smelt only reach maturity at 2-3 years old, with spawning shoals containing individuals of up to 10 years old, although most are aged between 2-6 years old (Shpilev et al. 2015). The smelt population dynamics have been reported to vary considerably, depending on environmental and anthropogenic pressures. Arula *et al.* (2017) investigated the impacts of overexploitation and climate on growth and reproductive development of smelt in the Gulf of Riga in the Baltic Sea. They found that after a population crash in the early 1990s, smelt were reaching maturity significantly younger than before (Arula et al., 2017). Understanding life-history traits at a regional and local population level are essential to guide conservation management with such a plastic species. Current published data on smelt biology and ecology in the UK are incredibly sparse. A Web of Science search (conducted December 2021) revealed only three peer-reviewed publications on smelt from UK waters in the last decade; these included a proposal for optimum larval culture for conservation aquaculture with broodstock acquired from the River Cree (McCarthy et al., 2020), microplastic ingestion by fish in the Thames (McGoran et al. 2017), and telemetry in two East Anglian rivers (Moore et al. 2016). In addition to these peer-reviewed publications, three recent reports on local smelt projects are available online (Wootton, 2018; Barker, 2016; Cotterell & Hillman, 2016).

Smelt are a listed species of conservation importance in the UK and an ecological indicator species of Good Ecological Status under the Water Framework Directive (WFD) (Colclough, 2013). Smelt were also highlighted in the recently published "State of the Thames" report, as the Thames provides a nationally significant spawning ground for this species (Zoological Society of London, 2021). There is a resurgent interest in investigating this poorly studied species in the UK. Several new monitoring programs have been set up by rivers trusts, the Environment Agency (EA) and projects run by the Zoological Society of London to collect information on the reproduction, occurrence, abundance, and growth of smelt. The clear knowledge gap on the population dynamics of smelt in UK rivers means that the impacts of climate change or habitat modification could be underestimated, and local populations may once again decline.

The EA's National Fisheries Laboratory (NFL) started to monitor smelt populations with ad hoc surveys and catches from commercial fishers in 2011. This unpublished

dataset (provided by the NFL) on smelt collected from six English and one Welsh river between 2011-2018 provides valuable preliminary data on the biology and life-history traits of smelt. In this chapter, I aim to use the EA data to explore current smelt population structures in England and Wales and to begin to address the significant knowledge gaps in this species in the UK. I hoped that analysis and assessment of these data on smelt can provide a starting point for future population studies and conservation efforts (outside of the scope of my thesis).

2.2 Materials and methods

Study sites, sample collection and processing

Smelt samples were obtained from six English rivers and one Welsh river through samples submitted to the EA by commercial netsmen and bespoke investigatory surveys undertaken by the EA (Figure 2.1). All fish were collected between 2011-2018 in February, March or April, except for juvenile fish collected in August from the River Dee. Samples were collected using fyke nets and seine nets complying with specific permit conditions.
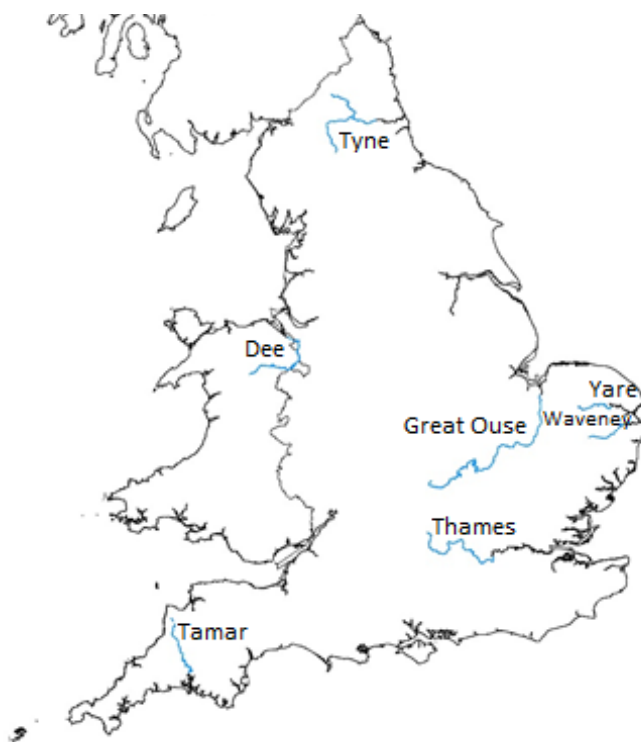
Figure 2. 1. Map of England and Wales showing the rivers where smelt were sampled between 2011-2018.

All samples were transported to the EA NFL and frozen upon arrival, except for fish obtained from the River Thames, which were either stored in 4% neutral buffered formalin (NBF) for histological analysis or frozen immediately after capture. Measurements and samples were collected from defrosted smelt; total length (mm) and weight (g) were recorded for each fish, and 5-10 scales were removed from the dorsal flank for age and growth assessment. Any abnormal pathology was noted during dissections.

Age and growth analyses

Scales were viewed under a projecting microscope (Projectina) at x 30 magnification to determine their age. Two experienced scale readers (from the EA NFL) read the scales for validation (Musk, Britton & Axford, 2006). For each scale, measurement of the annuli and scale radius along the anterio-lateral axis were recorded to enable me to back-calculate the length at age using the Fraser-Lee model (Fraser, 1916; Lee, 1920) (Equation 1); where L_i = back-calculated length at age, L_c = length at capture, S_i = scale radius to annulus i, S_c = total scale radius, and c = a correction factor. Linear regression of total fish length on scale radius was performed to determine constant c.

$$L_i = c + (L_c - c)(\frac{S_i}{S_c}) \tag{1}$$

Growth was described by von Bertalanffy (VB) (1938) and used in the form described by Beverton and Holt (1959) to describe fish growth (Equation 2). Where L_t is the length at age t, L_∞ is the maximum or asymptotic length, k is the growth coefficient, t is the age, and t_0 is a constant used to calculate the size when age is 0.

$$L_t = L_\infty\left[1 - e^{-k(t-t_0)}\right] \tag{2}$$

Growth curves were calculated by fitting the von Bertalanffy growth function (VBGF) using Fraser-Lee back-calculated length at age data for five rivers (Dee, Great Ouse, Thames, Waveney and Yare). The rivers Tamar and Tyne were excluded as the growth function requires at least three age groups to be included in the model (Ogle, Brenden & McCormick, 2017). The models were processed in RStudio (Version

1.2.1335) using code from Ogle et al. (2017). The "typical" parameterisation of the VBGF was used with the Fisheries Stock Analysis (FSA) package (Ogle, Wheeler & Dinno, 2021). Model fitting using the Francis parametrisation was also assessed. Male and female data were fitted together to provide a more robust dataset due to low sample numbers.

Weight-length relationship

Total length to mass relationships was examined using Equation 3, where a and b are the coefficients, L is the total length (cm), and W is the wet weight (g) (Froese, 2006). Coefficients a and b were calculated using linear regression models where $\ln(a)$ is the intercept, b is the slope or regression coefficient and R^2 is the coefficient of determination. Models were run using Graphpad Prism 8.0.2.

$$W = aL^b \tag{3}$$

Fulton's condition factor (K) was calculated using Equation 4 (Nash et al., 2006).

$$K = 100 * \frac{W}{L^3} \tag{4}$$

Fecundity

The ovaries and testis had been dissected from each fish and weighed (to the nearest 0.1g) by staff at the lab. Gonado-somatic index (GSI) was calculated (Equation 5) for both male and female fish for each population (Mcadam, Liley & Tan, 1999). Where W_G is the weight of the gonads and W_T is the total weight of the fish. Immature females and those with abnormal ovaries were omitted from these calculations.

$$\text{GSI} = (W_G/W_T) \times 100 \tag{5}$$

Ethical statement

Samples were collected as part of EA surveys or by permitted netsmen.

2.3 Results

<u>Age and growth analyses</u>

A total of 720 smelt individuals were collected between 2011 and 2018 from the Rivers Dee (n=187), Great Ouse (n=103), Tamar (n=62), Thames (n=154), Tyne (n=40), Waveney (n=74) and Yare (n=100). As smelt were collected opportunistically from commercial netsmen, in addition to EA surveys, sample numbers between rivers vary. The maximum age of any smelt caught was five years old (from the River Dee); however, more than 85% of the fish were between 2 and 3 years old (Table 2.1). Length frequencies showed that smelt from the Thames and Tamar had a higher percentage of smaller (total length) individuals sampled than the other rivers (Figure 2.2). While smelt from the Dee had a high frequency of individuals between 200-300 mm. The mean length at age showed a broadly similar size trend in smelt sampled from the Great Ouse, Yare and Waveney with age 1 individuals approximately 150 mm, age 2 between 150-200 mm, and age 3 individuals just over 200 mm (Figure 2.3.a,b,c). Smelt from the Thames had the smallest mean length at age, with all year classes under 200 mm (Figure 2.3.d). Samples from the River Dee had the greatest mean lengths at all ages compared to other rivers, with age 4 individuals reaching between 250-300 mm (Figure 2.3.e).

Using back-calculated length at age data, growth trajectories were fitted using VB growth for the River Dee, Great Ouse, Thames, Waveney and Yare (Figures 2.3, 2.4, 2.5, 2.6 and 2.7). The calculated parameters of asymptotic length (L_∞), the growth coefficient (K) and the theoretical length at age zero (t_0) (Table 2.2) varied between the populations. The river Dee smelt had the largest asymptotic length and lowest growth coefficient estimates, while Thames smelt had the lowest asymptotic length and highest growth coefficient.

Table 2. 1 Descriptive data for smelt by river, year sampled, sex, number of fish (n), age range, mean fish length (+ standard deviations and min/max) and weight (+ standard deviations and min/max).

River	Year	Sex	n	Age/age range	Mean length ± SD (mm)	Min - max	Mean weight ± SD (g)	Min - max
Dee	2011	Juvenile	15	0+	85 ± 11	63 - 99	4 ± 1	1 - 6
Dee	2011	Male	6	1	176 ± 16	154-200	33 ± 13	19 - 56
Dee	2011	Male	9	2	255 ± 20	224-281	104 ± 22	70 - 131
Dee	2012	Female	8	2	230 ± 9	220 - 246	96 ± 11	70 - 108
Dee	2012	Female	29	3	239 ± 24	200 - 300	110 ± 38	60 - 215
Dee	2012	Female	3	4-5	290 ± 9	280 -295	196 ± 29	178 -230
Dee	2012	Male	34	2	224 ± 15	189 - 268	81 ± 16	60 - 143
Dee	2012	Male	49	3	234 ± 20	209 - 311	93 ± 24	57 - 184
Dee	2014	Female	6	3-5	265 ± 21	254 - 296	148 ± 35	135 - 203
Dee	2014	Male	10	3	247 ± 23	205 - 272	118 ± 34	58 - 157
Dee	2014	Male	7	4	270 ± 12	245 - 280	151 ± 17	126 - 179
Gt. Ouse	2015	Female	6	2	196 ± 4	192 - 202	56 ± 5	48 - 62
Gt. Ouse	2015	Female	9	3	207 ± 20	190 - 256	68 ± 18	46 - 110
Gt. Ouse	2015	Male	2	1	/	152 - 160	/	23 - 25
Gt. Ouse	2015	Male	63	2	191 ± 11	174 - 222	51 ± 9	34 - 71
Gt. Ouse	2015	Male	22	3	204 ± 17	182 - 243	61 ± 14	45 - 92
Tamar	2015	Juvenile	30	0+	85 ± 9	67 - 103	3 ± 1	1 - 6
Tamar	2016	Not sexed	13	1	158 ± 9	145 - 173	28 ± 8	15 - 41
Tamar	2016	Not sexed	17	2	192 ± 24	135 - 218	46 ± 17	10 - 68
Thames	2014	Juvenile	100	0+	138 ± 8	115 - 157	16 ± 3	10 - 25
Thames	2018	Female	22	2-3	169 ± 12	146 - 193	29 ± 9	17 - 47
Thames	2018	Male	32	2-3	163 ± 10	137 - 181	23 ± 8	15 - 38
Tyne	2015	Female	5	2	198 ± 7	191 - 206	64 ± 10	51 - 80
Tyne	2015	Male	29	2	191 ± 17	118 - 215	50 ± 8	31 - 67
Tyne	2015	Male	5	3	247 ± 12	235 - 266	101 ± 14	85 - 123
Waveney	2014	Male	2	1	/	130 - 139	/	13 - 19
Waveney	2014	Male	12	2	172 ± 31	134 - 217	38 ± 22	16 - 73
Waveney	2014	Male	50	3	208 ± 11	186 - 234	61 ± 10	40 - 88
Waveney	2014	Male	10	4	217 ± 13	200 - 244	70 ± 10	54 - 88
Yare	2014	Juvenile	6	1	130 ± 7	120 - 138	11 ± 2	9 - 15
Yare	2014	Female	10	1	141 ± 12	119 - 156	16 ± 6	8 - 25
Yare	2014	Female	13	2	162 ± 9	144 - 177	26 ± 7	14 - 37
Yare	2014	Female	3	3	203 ± 10	197 - 215	49 ± 5	45 - 55
Yare	2014	Male	22	1	136 ± 12	114 - 161	14 ± 5	8 - 24
Yare	2014	Male	36	2	177 ± 25	135 - 215	35 ± 16	12 - 67
Yare	2014	Male	9	3	207 ± 7	194 - 221	55 ± 6	46 - 67
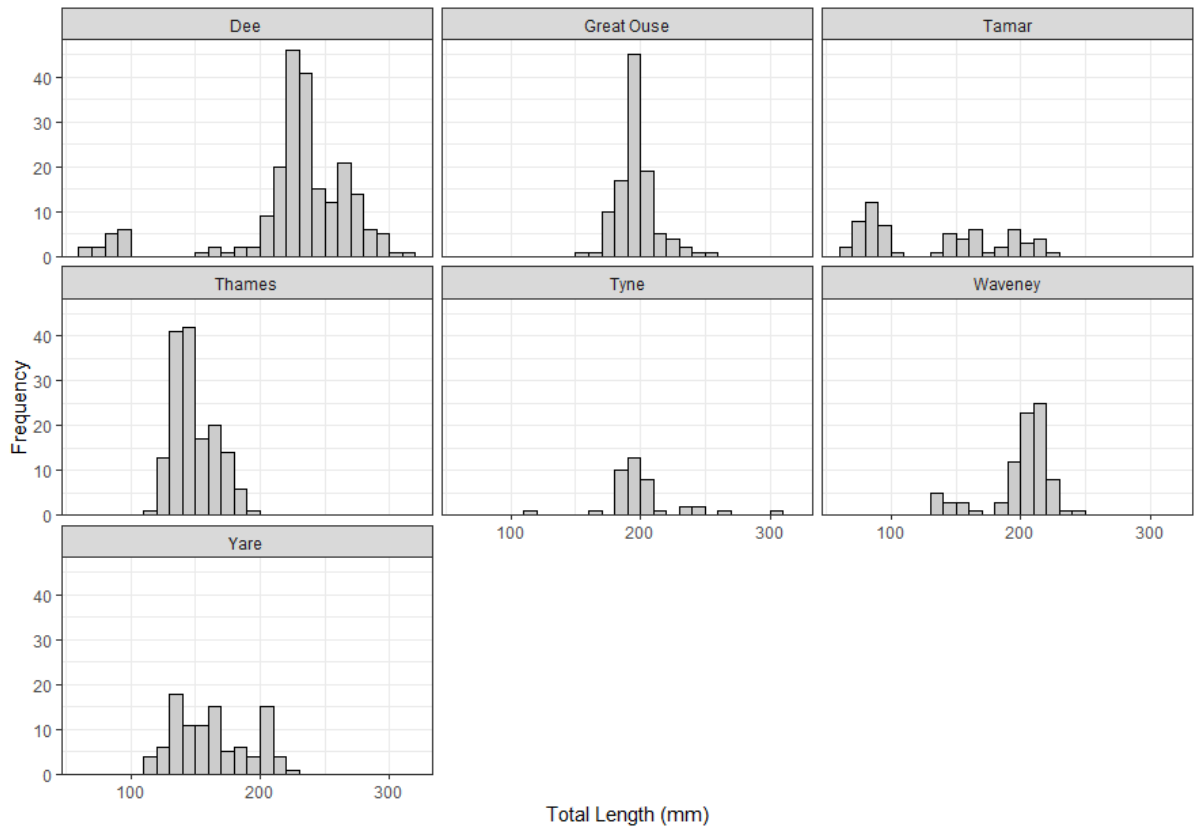
Figure 2. 1. Length frequency data of smelt from the Rivers Dee, Great Ouse, Thames, Waveney and Yare.
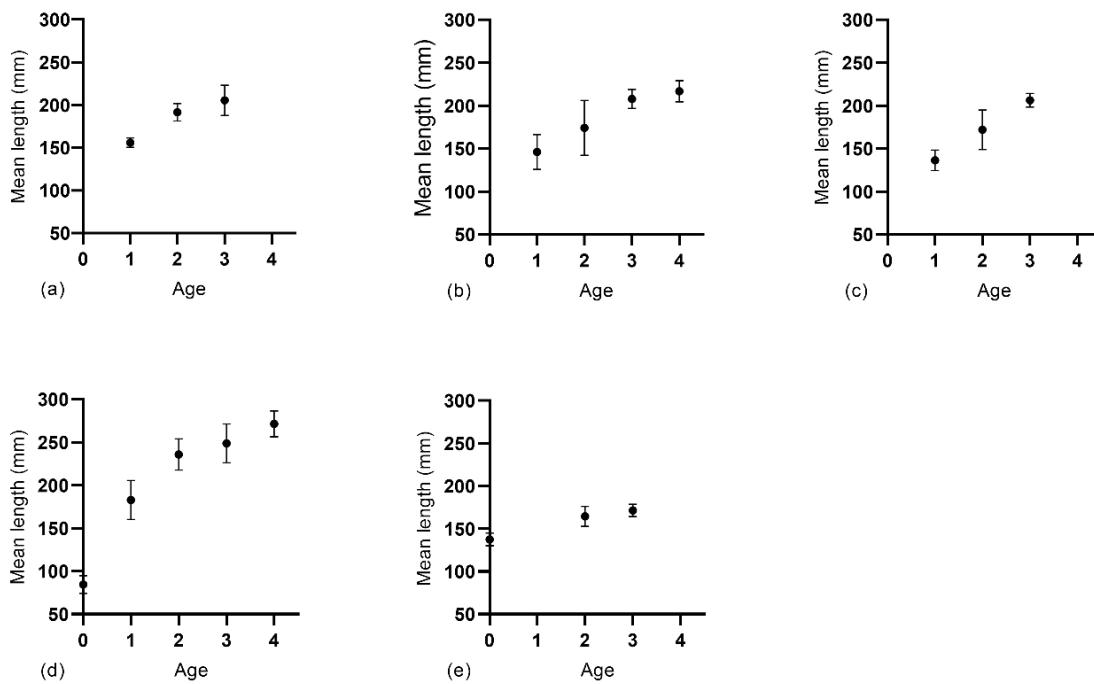
Figure 2. 2 Mean length at age (with standard error bars) of smelt from the rivers (a) Great Ouse (n=106), (b) Waveney (n=85), (c) Yare (n=90), (d) Dee (n=174) and (e) Thames (n=149).

Table 2. 2 Estimated von Bertalanffy growth parameters for smelt from five rivers in the UK. Estimates of asymptotic length (L_∞), growth coefficient (K), theoretical age at zero-length (t_0) and sample size are presented.

River	L_∞	K	t_0	Sample size
Dee	300.96	0.68	0.33	143
Great Ouse	211.23	1.35	0.48	106
Thames	172.68	2.06	0.66	49
Waveney	232.79	0.73	0.25	85
Yare	212.63	0.93	0.18	100
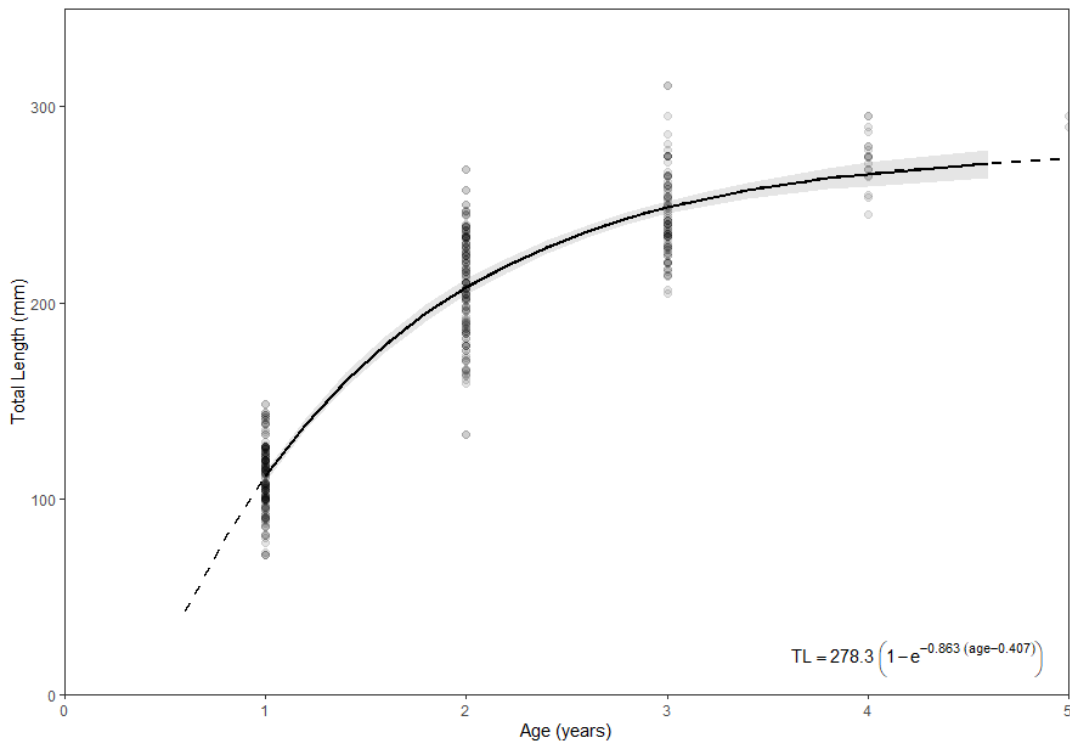
Figure 2. 3. Von Bertalanffy growth function fitted to back-calculated length at age data from the River Dee smelt. Both sexes fitted together.

$$TL = 278.3 \left(1 - e^{-0.863\,(age-0.407)}\right)$$
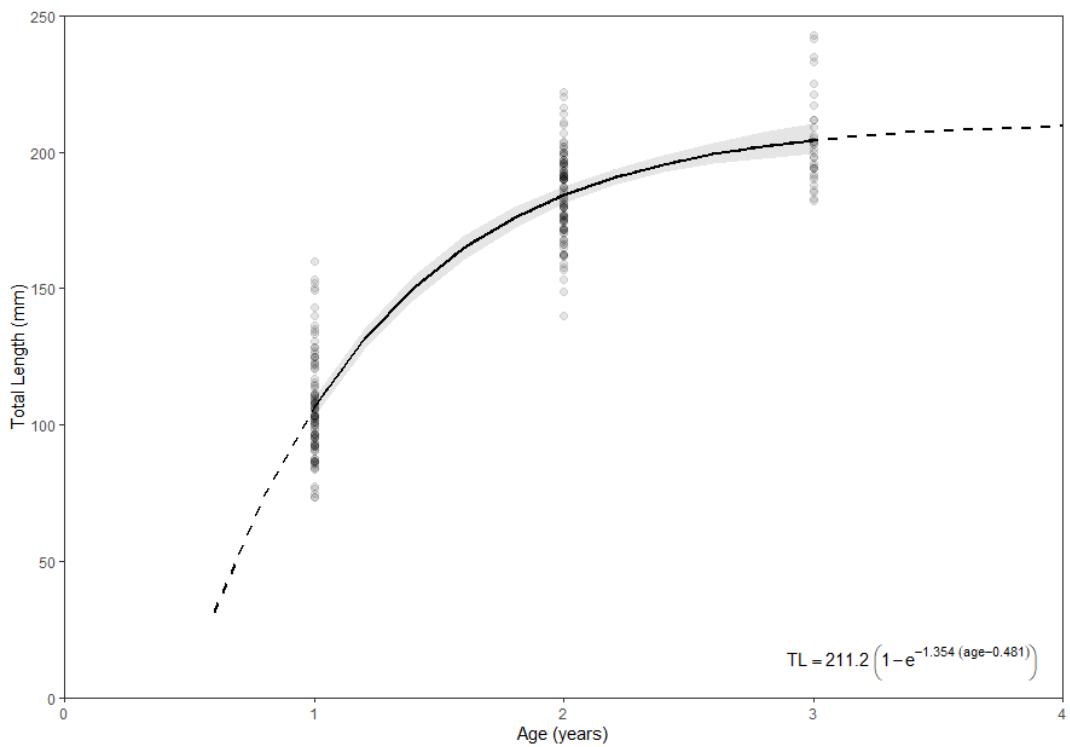
Figure 2. 4. Von Bertalanffy growth function fitted to back-calculated length at age data from the River Great Ouse smelt. Both sexes fitted together.

$$TL = 211.2 \left(1 - e^{-1.354\,(age-0.481)}\right)$$
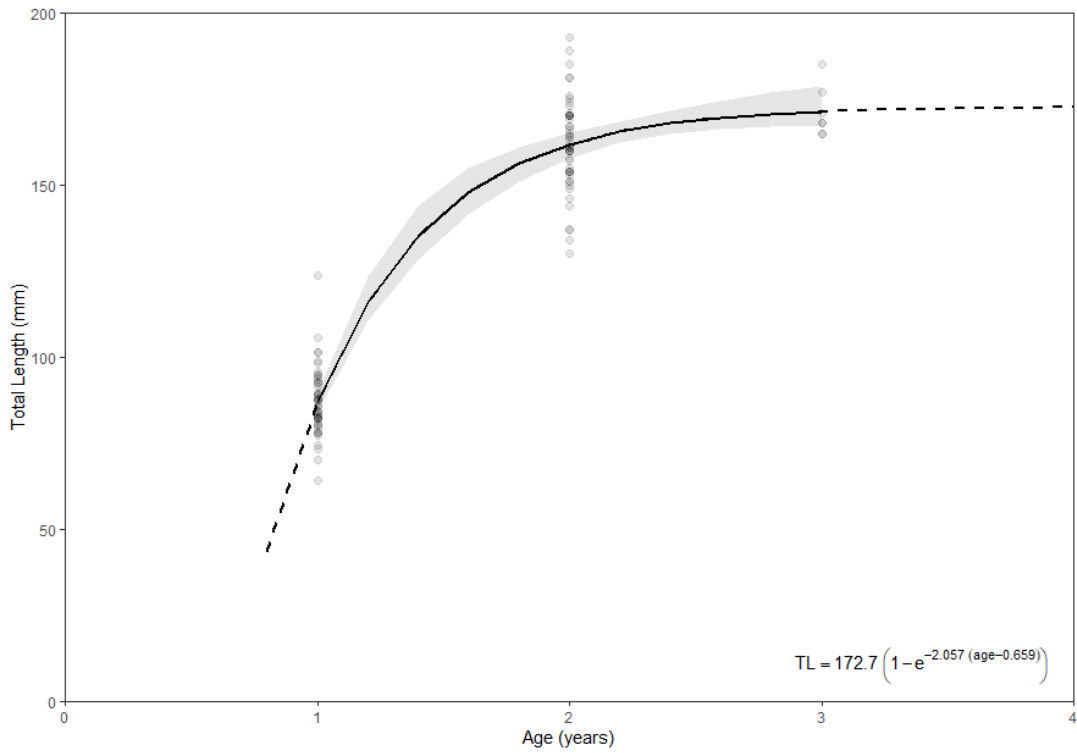
Figure 2. 5. Von Bertalanffy growth functions fitted to back-calculated length at age data from the River Thames smelt. Both sexes fitted together.
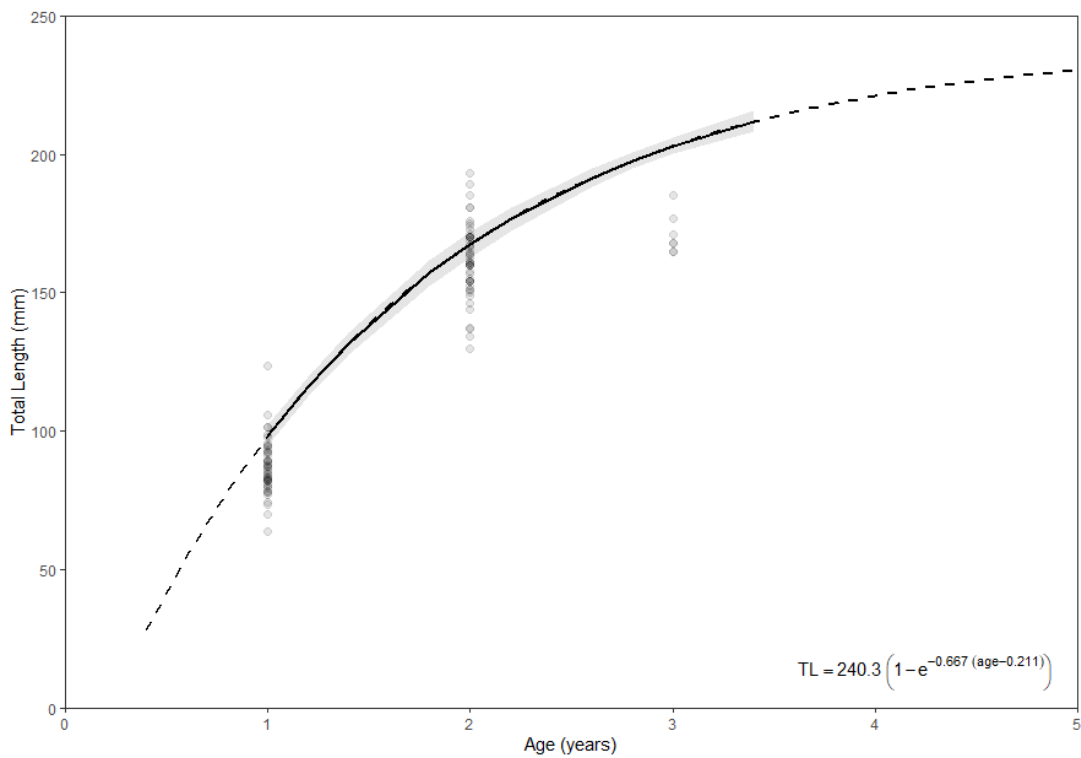
Figure 2. 6. Von Bertalanffy growth functions fitted to back-calculated length at age data from the River Waveney smelt. Both sexes fitted together.

41
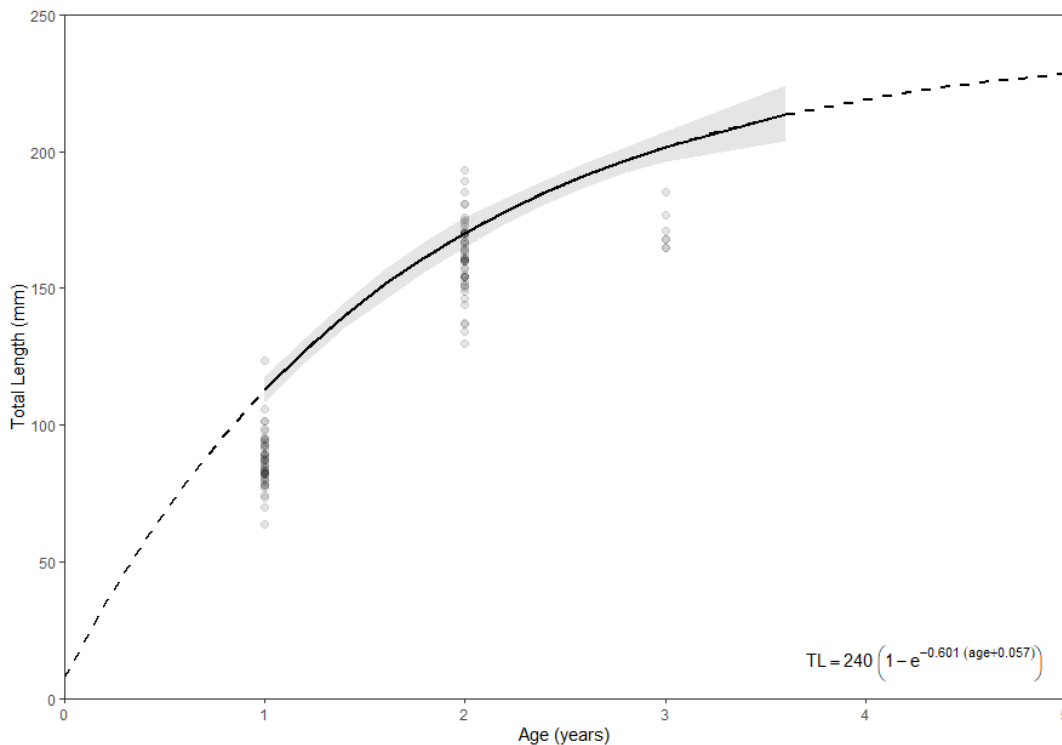
Figure 2. 7. Von Bertalanffy growth functions fitted to back-calculated length at age data from the River Yare smelt. Both sexes fitted together.

Weight-length parameters are used to estimate a weight corresponding to a given length (Froese, 2006). The *b* parameter represents the slope of the regression line in the logarithmic form and describes the form of growth, with the "ideal" of *b* = 3 representing isometric growth (Ricker, 1958). Carlander (1969) reported that *b* should typically fall between > 2.5 and < 3.5. Values outside these ranges suggest allometric growth (Carlander, 1969). Most smelt sampled had *b* values within this expected range (Table 2.3). However, females sampled from the Dee in 2014 and males sampled from the Tyne in 2015 had *b* values less than 2, suggesting that large fish were more elongated or smaller fish were in a better nutritional condition at the time of sampling. Furthermore, females obtained from the River Thames in 2018 had *b* values greater than 3.5, suggesting that fish had increased in height or width more than in length.

Table 2. 3 Weight-length relationship parameters and Fulton's condition factor (K_C + SD) for female, male, and juvenile smelt by year sampled and river.

River	Year	Month	Classification	n	a	b	R²	Mean K_C (±SD)
Dee	2012	March	Female	43	0.1472	2.864	0.83	0.79 (± 0.10)
Dee	2014	March	Female	6	0.8382	1.672	0.32	0.82 (± 0.12)
Dee	2011	March	Male	17	0.1005	3.050	0.93	0.60 (± 0.90)
Dee	2012	March	Male	89	0.2013	2.600	0.83	0.72 (± 0.07)
Dee	2014	March	Male	17	0.0904	3.203	0.95	0.76 (± 0.54)
Dee	2011	August	Juvenile	15	0.1913	2.369	0.5	0.62 (± 0.29)
Gt. Ouse	2015	April	Female	15	0.2178	2.539	0.82	0.75 (± 0.07)
Gt. Ouse	2015	April	Male	88	0.1372	2.878	0.82	0.72 (± 0.08)
Tamar	2016	March	Not sexed	32	0.1465	2.778	0.61	0.17 (± 0.17)
Thames	2014	March	Juvenile	100	0.1854	2.536	0.69	0.6 (± 0.07)
Thames	2018	Feb/March	Female	22	0.0498	3.644	0.72	0.5 (± 0.08)
Thames	2018	Feb/March	Male	32	0.1582	2.634	0.7	0.5 (± 0.08)
Tyne	2015	April	Female	6	0.1165	3.046	0.97	0.82 (± 0.07)
Tyne	2015	April	Male	34	0.6618	1.664	0.58	0.76 (± 0.40)
Waveney	2014	March	Male	74	0.1012	3.093	0.97	0.68 (± 0.05)
Yare	2014	April	Female	26	0.0600	3.476	0.94	0.58 (± 0.08)
Yare	2014	April	Male	68	0.0736	3.303	0.98	0.58 (± 0.07)
Yare	2014	April	Juvenile	6	0.1079	2.927	0.66	0.49 (± 0.06)

Condition factor represents a measure of fish health and will vary seasonally and during reproductive disturbances (Froese, 2006). Maitland (2003) reported that condition factor (K_C) values usually range between 0.7-1.3, with 0.7 representing a fish in poor condition and 1.3 representing a fish in good condition (Maitland, 2003). When calculating condition factor, Maitland (2003) used fork length, whereas this study used the total length of smelt to calculate K_C, which may account for the lower K values (Table 2.3). The condition factor (K_C) was generally higher in female smelt, with an overall mean K_C of 0.71 and a range between 0.5-0.82. Males had a mean K_C of 0.67 with a range of mean K_C values between 0.5-0.76. Female and male smelt from the Thames and Yare populations had low mean K values below 0.6.

Reproductive traits

GSI is used as an index for gonadal activity and to estimate readiness for spawning (Devlaming, Grossman & Chapman, 1982). Female smelt GSI values varied, with

Tyne females averaging >30 while the Yare females averaged <10 (Figure 2.8a). GSI values were similar between male smelt of all ages and across all rivers assessed (Figure 2.8b).

Table 2. 4 GSI for female smelt across rivers and years.

River	Year	n	Mean	Range
Dee	2012	36	22.26	2 - 48
Dee	2014	5	28.16	12 - 45
Gt. Ouse	2015	12	23.70	9 - 34
Tyne	2015	6	36.43	6 - 47
Thames	2018	17	21.78	8 - 37
Yare	2014	18	8.87	1 - 21
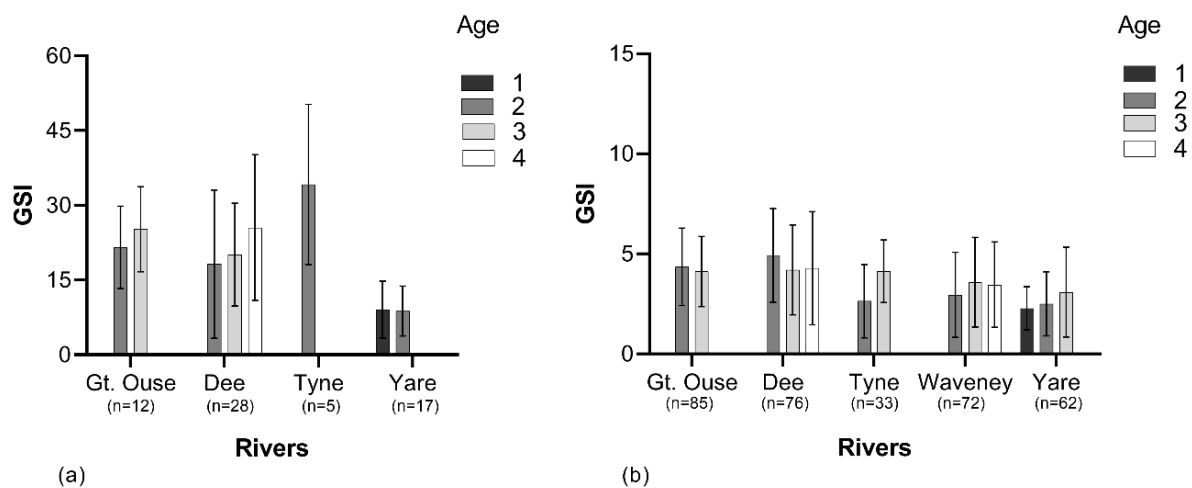
Figure 2. 8. Mean Gonado-somatic index (GSI) with standard deviation (error bars) of (a) female and (b) male *O. eperlanus* in each river sampled. Age of smelt represented by different colour bars (see legend). The number of fish sampled from each river (*n*) is included.

2.4 Discussion

The data presented in this chapter aimed to provide preliminary biological and ecological data on the understudied populations of smelt in several riverine systems across England and Wales. This study, to date, is the largest spatial survey of European smelt populations in the UK. Understanding the different population dynamics of this species is critical for its conservation and management.

Age and growth analyses

My preliminary findings suggest that the size of smelt varied considerably between different sampling locations. Variability in length and weight is a reported characteristic feature of smelt, with growth rates and dietary preference dependent on the season and environmental conditions (Doherty & McCarthy, 2004; Froese, 2006). For example, Repečka (2003) found lengths and weights fluctuated between regions and seasons in smelt from the coastal zone of the Baltic Sea and the Curonian Lagoon, and Pilecka-Rapacz *et al.*(2017) reported similar regional variations in five major estuaries in the Southern Baltic Sea. The results of this study agree with previous findings regarding the growth plasticity of populations, thus highlighting the need for seasonal monitoring of populations to detect abnormal fluctuations in population dynamics accurately. The size of smelt in most estuaries sampled in this study was comparable with those previously reported for smelt from English and Scottish estuaries (Colclough, 2010, 2013; Wootton, 2018; Cotterell & Hillman, 2016). Hutchinson (Hutchinson, 1983) reported comparable lengths at age for Thames smelt to my findings, with average lengths remaining below 200 mm. In my study, the Thames population had the smallest mean length at age, while smelt from the River Dee had the largest mean length at age. These differences may be due to local environmental drivers and may also result from regional segregation amongst populations with little mixing during the marine phase of their lives along the UK coastline. However, more regular fixed-seasonal sampling would need to be performed, to account for changes in weight during and after spawning, before statistically significant differences between populations could be assessed. Condition factor was used to assess and compare the condition of smelt populations in this study. As most samples were collected in March/April, females were likely to be gravid, which would increase their condition factor as the weight of the eggs was not excluded. Condition factor in our study was calculated using total length rather than fork length, which was used in comparative studies (Hutchinson, 1983), which limited direct comparisons with previously cited values. As many of the samples used in my study were collected during the known spawning period between March and April, some individuals may have already spawned, resulting in a lower weight recording, and equally, gravid females would have been heavier.

The average age of both males and females sampled in our study was 2+, with males reaching a maximum age of 4+ and only two females aged 5+. This age structure is comparable to previously reported age structures of smelt in UK waters, with mature smelt sampled in Ireland aged between 2+ and 5+ (Doherty & McCarthy, 2004) and three age classes recorded in smelt sampled in Scotland in 2018 (Wootton, 2018). *O. eperlanus* from other European populations have been shown to reach greater ages than those observed in this study, with smelt from the Eastern Gulf of Finland aged up to 7+ (Sendek & Bogdanov, 2019), smelt from Lake Syamozero, Russia, aged to 6+ and smelt from the Gulf of Riga up to 10+ (Shpilev, Ojaveer & Lankov, 2005). However, smelt in our study appear to attain greater lengths at a younger age than smelt from other European populations in the Baltic regions, where it was noted that individuals only exceeded 200 mm in length at ages greater than 4 (Shpilev, Ojaveer & Lankov, 2005; Sendek & Bogdanov, 2019; Švagždys, 2009). Comparison of age structures and length at age suggested that whilst the UK smelt populations mature earlier, they have shorter longevity when compared to other European populations. As previously mentioned, the collection time of some samples in this study during spawning may have resulted in the increased collection of running males and low numbers of females, which may have affected the age ranges described. Additionally, adult smelt are usually only present in estuaries during spawning, and therefore future studies should consider sampling at estuary mouths or the near shore outside of spawning times.

While the VB growth curves have provided valuable insight into somatic growth in fish (Chen, Jackson & Harvey, 1992), the data used to produce the curves in this study had some limitations. Some authors suggested that pre-and post- maturation growth cannot be accurately represented using the VB growth equation, due to the change in energy allocation during maturation (Day & Taylor, 1997). Lester, Shuter and Abrams (2004) suggested that the VB equation should only be applied to adult fish. Furthermore, as data were produced from the back-calculated length at age, the multiple observed lengths at age were not independent and, therefore, not considered accurate. However, this was the only option, as there were not enough independent samples in this study to produce realistic models. The Fraser-Lee equation for estimating back-calculated length at age is an accepted model for providing more data points (Klumb, Bozek & Frie, 1999). Therefore, finding ways to maximise the value of

limited data is especially needed when studying a species with legislated protection or conservation priority status. Issues producing VB growth models have also been reported when using data with only young or old individuals (Ogle, Brenden & McCormick, 2017). I tried to correct these limitations by applying different growth parametrisations. However, the best fit model utilised the "typical" parameterizations. The growth curves produced in this study need to be validated using independent sample points (i.e. the collection of more smelt at different ages).

GSI

The following GSI data were calculated to give an insight into the reproductive health of the smelt populations sampled. However, due to the limited and sporadic nature of the sampling, I do not wish to put forward the following metrics as fact, but rather as a starting point from which to guide future studies. Fecundity and GSI are important metrics used in fisheries science to estimate the reproductive potential of a fish population (FAO, 1974). These metrics are especially important for a short-lived species which only spawns once a year, as reproductive failure can lead to the loss of an entire year class. Regional historical data on smelt egg counts are limited. However, Maitland and Campbell (1992) reported a range of 10,000-40,000 eggs per female across the British Isles; similarly, an average of 33,818 eggs per female was reported in smelt from the Watford Estuary in Ireland (Doherty & McCarthy, 2004). In Scotland, Hutchinson and Mills (1987) reported greater values from River Cree smelt, 40,000-106,000 eggs per female. The mean female GSI was above 20 for all rivers except the Yare, which was very low at 8.87. Several female smelt obtained from the River Yare were already spent, and others may have already started to spawn, which may account for the lower GSI values in this river.

Monitoring and conservation of smelt

As a listed priority species under the UK Biodiversity Action Plan (BAP), experts identified the following actions in BAP Version 2, December 2010 to monitor smelt in UK rivers; 1. Review the case for the introduction or reintroduction of smelt to new or previously occupied sites, 2. Investigate the impact of climate change on smelt populations, and 3. Complete a sampling programme for genetic analysis to determine the origin of fish around the UK and report (Colclough, 2013). Furthermore, actions were suggested to ensure existing fisheries are monitored and sustainable. While

many institutions are undertaking research, including the EA, ZSL and CEFAS (Centre for Environment, Fisheries and Aquaculture Science), I believe many knowledge gaps still exist, and further studies need to be prioritised to ensure healthy populations remain stable.

Small, short-lived species have been assumed to be less vulnerable to threats, such as overfishing, due to their "fast" life-history strategies (Jennings, Reynolds & Mills, 1998). Pinsky *et al.* (2011) analysed two fisheries datasets to determine the life-history traits of species whose populations have collapsed due to human pressures. Their findings suggested that up to twice as many populations of small, low trophic level species have collapsed compared with fisheries for predator species. The authors propose several theories why this may occur. For instance, fisheries management often recommend higher exploitation levels for species with faster life-history strategies on the assumption that populations can recover quickly. This, however, may not be the case, with short-lived species either growing rapidly or declining rapidly in response to a stressor (Pinsky et al., 2011). Population collapses, even temporary, of low trophic level populations can impact the structure and function of the ecosystem, especially where a few species play a prominent role in transferring energy up the food web (Pinsky et al., 2011). Reynolds *et al.* (2005) suggested that simple life-history traits can be used directly to assess the threat status to fishes through quantitative assessment criteria or preliminary screening criteria. After population crashes, few have a rapid recovery and may take up to fifteen years to exhibit changes in their abundance and life history strategies (Hutchings & Reynolds, 2004). Thames smelt are still recovering from their decimation in the 1850s, with Colclough (2013) raising concern for a further decline in the fishery. As smelt are sensitive and prone to sudden population crashes due to environmental pressures (Hutchinson & Mills, 1987), seasonal monitoring is vital to indicate potential threats to other species residing in the Thames.

As there is an active commercial fishery for this species, even though it may be relatively small-scale, up-to-date data are critical for ensuring the proper regulation and management of this fishery. Furthermore, the current regulation of the smelt fisheries assumes that the UK riverine smelt populations are admixed. The findings from this study suggest that they could be distinct, isolated smelt populations with little

genetic admixture. Therefore, I agree with suggestions made in BAP version 2 that genetic studies (such as single nucleotide polymorphisms (SNPs) analysis) should be conducted to identify the origin/possible genetic isolation of local populations around the UK.

Chapter 3. Pathological description of a microsporidian infecting juvenile European smelt in the Thames

Abstract

In the summer of 2018, Environment Agency (EA) surveys revealed that a large number of juvenile European smelt (*Osmerus eperlanus*) were infected with a microsporidian parasite, presenting as large white cysts in the gut. Fish pathology experts at the EA tentatively identified this parasite as *Glugea hertwigi*, based on its morphological presentation and historical reporting in European smelt in the Baltic regions, and in Rainbow smelt (*O. mordax*) in the United States and Canada. This microsporidian had not been previously reported in smelt in the UK. This chapter aims to provide a pathological description of the microsporidian using traditional histology, and less widely used micro-computer tomography (micro-CT). Histopathological analysis revealed that most of the cysts occurred within the peritoneal cavity, alongside the digestive tract, and were occasionally seen within the stomach or pyloric caeca. Cysts also developed in the liver tissues. The morphological presentation of cysts showed typical characteristics to those of the *Glugea* genus. In heavy infections, internal organs were compressed, and the muscular wall of the peritoneal cavity was thinned and deformed by the bulging cysts. The micro-CT imagery allowed me to visualise the infection in three dimensions, further adding to knowledge on the distribution and placement of cysts throughout the body. The micro-CT images also provided quantitative data on the volume of cysts. There was a negative correlation found between the volume of cysts and length of smelt, suggesting that heavy infections adversely affect growth. Additional photographic data (provided from an external source) revealed the presence of the same microsporidian cysts in adult smelt from the River Thames; conflicting with previous historical reports which found only juveniles to become infected with *G. hertwigi*. This chapter provided valuable information on the pathological presentation of the microsporidian infecting Thames smelt and indicated that the microsporidian is from the *Glugea* genus. Furthermore, this study highlighted a novel use of micro-CT imagery to complement histological examination when exploring fish parasitology.

3.1 Introduction

As outlined in Chapters 1 and 2, one of the main study species of my thesis is the European smelt *Osmerus eperlanus*, hereon referred to as smelt. Smelt are a small migratory fish species which occur along the coasts of northern Europe (Maitland, 2003). Adults live in marine coastal waters and migrate up estuaries to spawn. Migratory fish species are known to host diverse groups of parasites which are representative of the multiple environments which they inhabit (Pilecka-Rapacz et al., 2017). The parasitic fauna of European smelt are understudied, with approximately only 100 original articles published since 1771 (Pilecka-Rapacz et al., 2017). When compared to the literature available on the parasitic fauna in other species, for example, Salmon *Salmo salar* or Common Carp *Cyprinus carpio* (Mennerat et al., 2010). Unsurprisingly, these studies often focus on diseases and parasites in fish species of high economic value and cultured fish (Chapman et al., 2021). This has led to huge knowledge gaps in fish species of perceived lower economic value. New approaches to fisheries management are developing onto the "ecosystem approach", with the UK's "One Health" approach for aquaculture and sustainable fisheries. The principles of the One Health approach are defined "as the collaborative, multisectoral and transdisciplinary approach to achieving beneficial health and well-being outcomes for people, non-human organisms and their shared environment" (Stentiford et al., 2020). In order for the UK to achieve this approach, a better basic understanding of relevant species in an ecosystem is needed. As previously highlighted, smelt are a species of conservation importance in the UK, and it is therefore vital that we monitor any potential new threats to populations inhabiting UK rivers.

An unknown microsporidian detected in juvenile smelt from the River Thames

A strange parasite had been noticed in a few juvenile smelt in 2010, however infection numbers were low and there were not enough samples for the Environment Agency (EA) to accurately assess the infection (Dr C. Williams, pers. comm). It wasn't until the summer months of 2018, where the EA routine survey noticed a large number of juvenile smelt collected (> 80%) were heavily infected with an unknown parasite presenting the same way as previously noted in 2010 (Dr C. Williams, pers. comm). The parasite presented as large masses of white cysts in the body cavity. The infections were easily noticed, as juvenile smelt are largely translucent in colour (Fig. 3.1). Fish pathology experts at the EA National Fisheries Laboratory (NFL) tentatively

identified the parasite as a microsporidian, likely to be *Glugea hertwigi,* based on historical findings of this microsporidian species in smelt from other European rivers. However, *G. hertwigi* had not been reported in UK smelt prior to this possible occurrence in the River Thames. This gap in our knowledge provided the perfect opportunity for my Doctoral research to conduct an in-depth study to positively identify the parasite and describe its infection in UK smelt.

Figure 3. 1. An infected juvenile smelt collected in 2018 from the River Thames (credit: EA National Fisheries laboratory). Note the body cavity filled with white cyst-like growths.

The following introduction provides background on microsporidia and reports of *G. hertwigi* in European and North American smelt species. The rest of the chapter focuses on describing the infection in smelt using histopathological and micro-computer tomography (micro-CT) imaging techniques.

Microsporidia

Microsporidians are unicellular organisms which live as obligate parasites in a range of animal hosts (Lom, 2002). The spores range in size from 1-20 μm (Cali, Becnel & Takvorian, 2017). There are approximately 16 genera and 120 species of microsporidia which infect fish, with some causing severe disease (Weiss & Becnel, 2014). Some examples include mortalities associated with microsporidian infections in rainbow trout *Salmo gairdneri* and young gizzard shad *Dorosoma cepedianum* infected with species of the *Pleistophora* genus (Putz, Hoffman & Dunbar, 1965). Furthermore, Cali *et al.* (1986) reported a 63% mortality following experimental infection of American winter flounder *Pseudopleuronectes americanus* with *Glugea stephani*. Most microsporidians infecting fish induce the formation of xenomas, or cyst like structures (Cali, Becnel & Takvorian, 2017). The term 'xenon' was first described by Weissenberg in 1922, then changed by Weissenberg in 1949 to 'xenom' to describe the xenoparasitic complex which developed in sticklebacks *Gasterosteus aculeatus* infected with *Glugea anomala* (Weiss & Becnel, 2014). Genera such as *Glugea*,

Spraguea and *Ichthyosporidium,* are known as xenoma-forming; whereby the microsporidia are embedded directly into the host cell cytoplasm and stimulate hypertrophic growth creating a xenoma (Lom & Dyková, 2005). Xenomas are defined by completely transformed host cells which have changed structure both morphologically and physiologically, to form a separate entity with its own development, at the expense of the host (Lom & Dyková, 2005; Weissenberg, 1968). The way in which microsporidia invade hosts cells is unique as they are able to penetrate the plasma membrane without destroying it or forming a phagosome (Cali, Becnel & Takvorian, 2017).
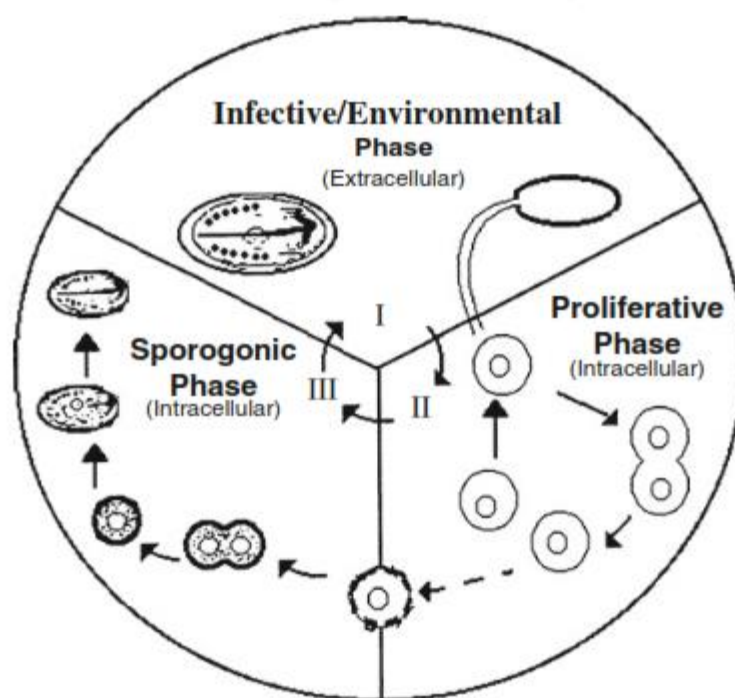
Figure 3. 2. A typical microsporidian lifecycle, showing the three phases of development (Taken from Cali & Takvorian, 1999).

These xenomas produce millions of spores in three stages (Dyková & Lom, 1980). The three stages are environmental, proliferative and sporogonic (Fig. 3.2). The spore is ingested indirectly via its presence in the water column or directly via the consumption of spore-carrying filter feeders on which the fish prey (Scarborough & Weidner, 1979). Following ingestion, the spore is activated (by the digestive environment) and results in the polar filament being expelled and piercing the host cell (Cali, Becnel & Takvorian, 2017). The spore contents and infectious sporoplasm is

injected into the host cell and the proliferative phase begins. For *Glugea*, early stage xenomas consist of the developmental stages of the parasite surrounded by the peripheral host cytoplasm. The maturing xenoma develops a multi-layered coat, incorporating fibroblast (the most common cells of connective tissue) and epithelial cells, while increasing the number of proliferative cells by binary or multiple fission (Cali, Becnel & Takvorian, 2017). The transition to the third phase (sporogonic) is represented by the cell's development of spores. During maturation, the xenoma is surrounded by a light refractile cell wall, with the centre filled with spores and the host cell cytoplasm pushed to the edges of the cell (Dyková & Lom, 1980). A mature xenoma becomes totally filled with spores and the host cell is reduced to only the cell wall (Dyková & Lom, 1980). The final stage occurs when the mass of spores is eliminated by phagocytosis and subsequent degradation of the xenoma wall (Dyková & Lom, 1980). Xenomas will be referred to as cysts throughout the chapter, in keeping with previous literature. Lom (2002) provides a detailed catalogue of microsporidian genera and species infecting fish.

Many microsporidia which infect fish are host specific, however there are a few which have been reported in multiple hosts; such as *Glugea stephani* found in winter flounder *P. americanus* (Cali et al., 1986), plaice *Pleuronectes platessa* (McVicar, 1975), and English sole *Parophrys vetulus* (Olson, 1981) *and Pleistophora hyphessobryconis* which infects fish from multiple families (Characidae, Cyprinidae, Cyprinodontidae, Poecilidae, Cichlidae), including *Danio rerio*, a common species used in clinical studies (Steffens, 1962; Sanders et al., 2010). Microsporidians of the genus *Glugea* are some of the most studied of those infecting fish, both wild and cultured. Microsporidians with characteristics of *G. anomala* have been associated with high mortalities in several species of ornamental killifishes (*Nothobranchius korthausae*, *N. eggersi*, *Fundulopanchax filamentosus* and Cynolebias nigripinnis) (Lom, Noga & Dykova, 1995). Numerous *Glugea* spp. show adaptations to prevent an immune response from host cells (Dyková & Lom, 1978). Laudan et al. (1986) found that *G. stephani* spores when phagocytized suppressed immunoglobulin levels in winter flounder, *P. americanus*. Weidner & Sibley (1985) reported that *G. hertwigi* spores were able to increase rigidity and prevent fusion with a lysosome when bonding with the phagosome membrane.

History of *Glugea hertwigi* in European smelt in Europe

Weissenberg (1913) first briefly described *G. hertwigi* in 1911, and in 1913 found the parasite infecting smelt in Lietzow, Germany while studying *G. anomala* in three-spined stickleback. Weissenberg described the infection as similar to *G. anomala,* however noted that the cysts were not limited to individual nodules (like that in Stickleback), but rather a large number of cysts in the body cavity that were clearly visible due to the transparent and delicate texture of smelt skin. A clear example of this observation can be seen in young-of-the-year smelt; Figure 3.3. Prevalence of *G. hertwigi* infections in smelt reported from the Baltic region vary greatly with low levels (1-2%) of infection in one-year-old smelt reported by Weissenberg (1913) in Lietzow, Germany. Higher prevalence (6-23%) were seen in smelt studied in the Enonselkä Basin in Southern Finland in 1990 (Horppila et al., 1996) and approximately 30% of smelt were infected in a 2000 study from Lake Tuusulanjärvi, also in Southern Finland (Pekcan-Hekim, Rahkonen & Horppila, 2005). While in the North Sea region, Costa, Melo-Moreira and De Carvalho (2016) reported a low prevalence (< 1%) of infection in smelt from the river Elbe, Germany, The literature suggests that infection level increases throughout the summer months and varies year to year (Costa, Melo-Moreira & De Carvalho, 2016; Pekcan-Hekim, Rahkonen & Horppila, 2005).
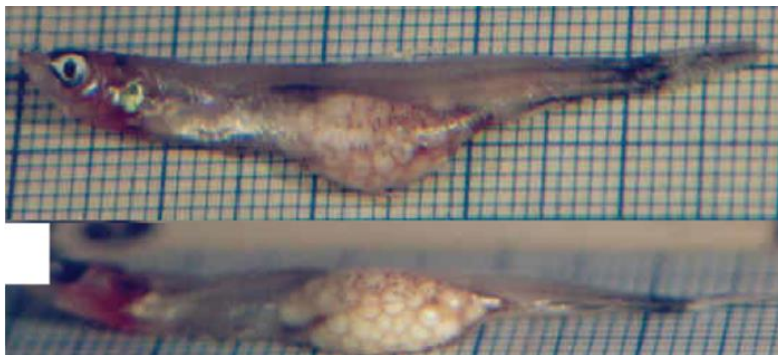
Figure 3. 3. Photo taken from Pekcan-Hekim, Rahkonen & Horppila (2005) showing a young-of-the-year smelt from Lake Tuusulanjärvi in September 2000 with a large infection of *G. hertwigi* cysts.

History of *Glugea hertwigi* in rainbow smelt (*Osmerus mordax*) in North America

Infections of *G. hertwigi* have been described in smelt occurring in North America, namely *Osmerus mordax* or Rainbow smelt (Fig.3.4). Infections were first described by Schrader in 1921 who studied samples from Lakes Massabesic and Sunapee in New Hampshire, and Dennysville and Casco Bay on the coast of Maine (Schrader,

1921). Schrader reported a much higher prevalence of infection in smelt from lake populations (53% in Lake Massabesic and 28% in Sunapee Lake) than in smelt populations migrating between fresh and salt water (1.5% in Dennysville and 16% in Casco Bay). Schrader (1921), like Weissenberg (1913), reported that adults were only rarely infected, with the majority of infection occurring in young smelt (< 1 year) under 10 cm long (Schrader, 1921). Monitoring of *G. hertwigi* infections began in Lake Eerie in 1960, when the parasite was first reported in the lake (Dechtiar, 1965). A mass die-off of young-of-the-year smelt in Lake Eerie in 1969, led to the collection of 1150 dead and dying smelt with a reported prevalence of *G. hertwigi* infection of 90% (Nepszy, Budd & Dechtiar, 1978). The intensity of *G. hertwigi* infections and associated histopathological changes observed within the body cavity were identified as the main cause of mortality, due to the mechanical damage caused to internal organs by the cysts (Nepszy, Budd & Dechtiar, 1978). Nepszy, Budd & Dechtiar (1978) and Haley (1954) suggested that death was likely due to multiple factors associated with a high intensity of disease, including impacts on swimming ability, malformation of organs and physiological stress. Haley (1954) and Sindermann (1966) also reported that reproduction can be impaired by mechanical obstruction of the vent by cysts. The above reports in Europe and North America suggested that high levels of *G. hertwigi* infections can lead to mass die offs of young smelt, which could negatively impact the breeding success of subsequent generations of smelt.
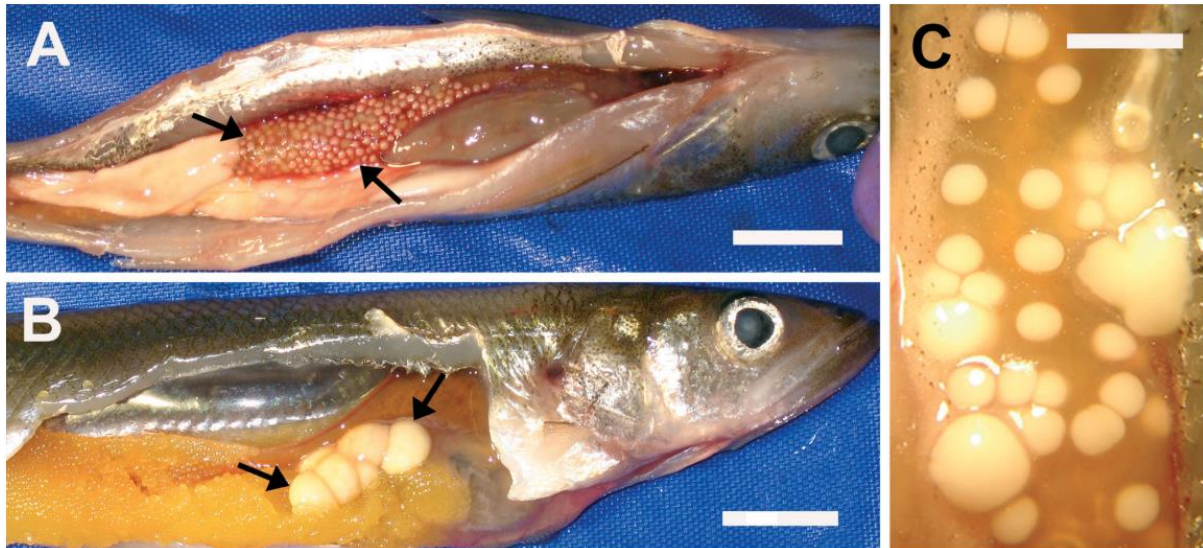
Figure 3. 4. Photo taken from Lovy *et al.* (2009) showing *Glugea hertwigi* infections in *Osmerus mordax*. A shows a heavy infection with small cysts (scale bar = 1 cm). B shows a moderate infection with uniformly larger cysts (scale bar = 1 cm). C shows a mixed infection of cyst sizes (scale bar = 4 mm).

Aims

This chapter examines the microsporidian infecting juvenile smelt collected from the River Thames in 2018 and 2020. The main aim of this chapter is to provide a pathological description of the microsporidian, based on histology and micro-computer tomography (micro-CT) imagery. Historically, *Glugea* infections have been described based on morphological presentation and histological analysis of the cysts. This chapter aims to identify the species based on morphological characteristics and to present a more in-depth study of the effects of the infection on internal organs. Whole fish histological sections as well as 3D micro-CT imagery are used to provide this detail. Micro-CT analysis allows for tissues to be visualised without physical tissue manipulation and disturbance.

3.2 Methodology

Study sites and smelt sample collection

Juvenile smelt (< 1 year) were collected by the Environment Agency (EA) from the River Thames at sampling points at Battersea and Chiswick (Fig. 3.5 shown by red dots) in March/April 2018. Forty juvenile smelt were collected at Chiswick and twenty juveniles at Battersea. Samples were collected using fyke nets and seine nets

complying with specific permit conditions. Fish were first euthanased by being placed in a bucket for 15 minutes with a lethal dose of benzocaine, and then preserved in 4% neutral buffered formalin (NBF) and transported to the EA, National Fisheries Laboratory for processing. The juveniles ranged from no visible infections to heavily infected, with ~ 80% visibly infected (see Appendix 3 Table A3.1 & A3.2). These samples were used for histological analysis, micro-CT and genetic analysis. Teddington lock represents the full tidal range of the Thames, with mostly low salinity conditions (Richardson & Soloviev, 2021). The Chiswick and Battersea sites are mostly freshwater, with more brackish conditions occurring between Hammersmith and Greenwich, and marine conditions from Greenwich to the coast (Zoological Society of London, 2021).

Figure 3. 5. Graphic representation of the tidal limit of the River Thames from the English Channel to Teddington lock. Red dots represent EA sampling locations at Battersea and Chiswick. The green dot represents the sampling at Erith.

Map adapted from map created at http://magic.defra.gov.uk/MagicMap.aspx.

A. McGoran[1] provided biological data for 207 smelt which were collected by commercial fishermen using a trawling vessel near Erith (Fig. 3.5 green dot) in the River Thames in March, June, October and December 2019, and March, July and September 2020 (See Appendix 3. Table A3.10). Smelt were collected during 15-minute midwater and benthic trawls (80mm cod end with 16 mm insert). Samples were

---

[1] A. McGoran is funded by the London NERC DTP and the Fishmonger's Company. She is based at the Natural History Museum London and a registered PhD student at Royal Holloway University of London. McGoran's PhD project investigated the movement of microplastic up the food web, using the Thames Estuary as a model system.

immediately frozen at -20°C. Samples were defrosted and dissected, as McGoran was collecting gut samples. Smelt samples infected with the microsporidian were used for genetic analysis to compare with infected samples collected in 2018 by the EA.

<u>Descriptive statistics for smelt sampled at Battersea and Chiswick in 2018</u>
The smelt were visually ranked at the EA based on the number and intensity of cysts present within the peritoneal cavity. Smelt were ranked as uninfected, low, moderate, heavy, and very heavy infections (Appendix 3. Table A3.1 and A3.2). Bar graphs were computed to depict severity of infection at each site.

<u>Preliminary findings of microsporidian infection in adult smelt (Erith samples)</u>
Following dissection of the smelt collected during the trawls at Erith in 2019 and 2020, McGoran noted 52 samples were potentially infected with a microsporidian, due to the presence of white cysts in the gut (pers.comm). McGoran provided length and weight data as well as noting the presence or absence of cysts in the gut. These data were of particular interest as many of the collected samples were considered as adults (body length >150 mm) presenting with microsporidian cysts (A.McGoran, pers.comm). McGoran also provided photographs of the infected individuals following dissection for me to assess. The smelt were visually ranked based on the number and intensity of cysts present within the peritoneal cavity. Smelt were ranked as low, moderate, heavy, and very heavy infections (Appendix 3. Table A3.10).

Using these data, I performed a two-way ANOVA in GraphPad Prism (Version 9.2) to compare the lengths and weights between uninfected and infected individuals at their classified levels of infection. Bar graphs were also computed to represent the data.

<u>Histopathology and light microscopy analysis</u>
Smelt collected in 2018 by the EA NFL and Thames area teams were used for the histopathological analysis of infected and uninfected smelt. Initial processing and blocking, and embedding were performed at the EA NFL. Smelt samples for light microscopy were fixed in 4% Neutral buffered formalin (NBF) and placed as either whole fish or staked sections in labelled cassettes. The whole fish were positioned to be sectioned longitudinally, while the staked samples provided transverse sections. The process of dehydration and clearing was performed using a Shandon Excelsior

ES (ThermoFischer Scientific) automated tissue processor, with an ascending series of IMS alcohol and xylene. Next, the tissues were embedded by surrounding the tissues in molten wax using the Shandon Histocentre 3 (ThermoFischer Scientific). Embedded tissues were sectioned using a rotary microtome (Leica RM2235), disposable microtome blades (Shannon MB35 premier) at a thickness of 3 µm. Sections were flattened by floating in a water bath at 42°C before being placed on glass slides. Slides were left to dry on warming racks (45°C) overnight (minimum 12 hours) prior to staining.

Tissue sections were stained with either haematoxylin and eosin (H&E) or Luna stain (Luna, 1968). H&E is a widely used stain in pathology and was also the stain of choice in the historical literature used to identify microsporidians in smelt (Lom & Dyková, 2005). The Luna stain was recommended by Peterson *et al.* (2011) as the selective stain of choice for the detection of microsporidian spores in histological sections. The Luna stain was prepared as per Luna (1968), with a premixed Weigert′s iron haematoxylin solution (Sigma-Aldrich HT1079-1SET) and Biebrich scarlet (Sigma-Aldrich B6008-25G). See Appendix 3 Table A3.5 for working solutions for the Luna stain. For the H&E stain protocol, slides were dehydrated in a descending alcohol series, cleared in Histoclear and mounted with Histomount (Appendix 3. Table A3.3). For the Luna stain protocol slides were dehydrated in a descending alcohol series, cleared in xylene, and mounted with Histomount (Appendix 3. Table 3.4).

Slides were examined under a light microscope using the 2X, 10X and 40X objectives (Olympus BX51) and images were captured using an attached camera (Teledyne Photometrics MicoPublisher 6). Images were captured and scale bars were added using Ocular Imaging 2.0.

<u>X-Ray micro-computer tomography</u>

Fourteen smelt samples were selected to represent different infection intensities. Selection was classified by number or clusters of visible cysts, and at least 3 samples were chosen to represent non-infected fish, mild, moderate, and heavy/very heavy infections (Table 3.3). These smelt came from the 2018 EA collection and were preserved in formalin. The smelt were soaked in a 5% iodine solution for 3 days prior to scanning. The iodine is used as a contrast agent to enhance the visibility of the

internal features. A contrast agent is needed to increase the contrast between the soft tissue structures due to the low density and chemical make-up of soft tissues (O'Sullivan et al., 2018). The samples were then washed in ethanol and mounted in plastic falcon tubes using sponge to keep the sample in place. A small amount of ethanol was also added into each tube to keep the samples preserved. Samples were taken to the Imaging and Analysis Centre at the Natural History Museum, London. The samples were then washed in ethanol and mounted in plastic falcon tubes with a small amount of ethanol added into each tube. Two fish were placed in each tube at a time to maximise available scanning time. Scans were taken using the Nikon Metrology HMX ST 225, with the support of Dr Vincent Fernandez (CT facility manager) and Brett Clark. One tube was placed in the instrument for each scan (Fig. 3.6). See Appendix 3. Table A3.6 for the instrument set up details for each tube scanned. Each tube is rotated 360° during the scan. Scan time was between 20 – 40 minutes for each tube and depended on the exposure time, frame average and number of projections (Scan time in minutes = [((exposure time / 1000) X frame avg.) X projections] / 60).

Post-scanning image analysis and volumetric measurements were completed by Brett Clarke (Natural History Museum) using Avizo (2019.1). Each scan was segmented to generate separate masks for visualising different organs and the cysts and were assigned different colours. This process assigns a label to all the voxels which correspond to specific structures and therefore allows for structures to be separated from the background voxels (Rovaris et al., 2018). The segmented features were then used to measure associated volumes of specific structures and to produce 3D images. The structures measured included the volume of total cysts, digestive tract, body cavity and full body volume. Individual cyst sizes were measured in two heavily infected smelt samples. Smelt samples were visually ranked based on the number and intensity of cysts present within the peritoneal cavity. Smelt were ranked as "healthy", "mild infection", "moderate infection", "heavy infection" and "very heavy".

A two-tailed Pearson correlation was performed between the body length of each smelt and their associated volume of cysts using GraphPad Prism 9.2.0 (n = 14). The null hypothesis stated that the volume of cysts was not correlated to the body length of the fish.

Table 3. 1 Levels of infection classification based on the number of individual cysts or clusters of cysts (with examples for reference). Deformity refers to any deformation caused to the natural body shape by the cysts.

Overall infection	Distribution of cysts	Deformity?	Xenoma size	Infection example
None	N/A	No	N/A	18.109.02
Very low	1 - 5 cysts	No	Medium - large	18.109.05
Moderate	1 lobe (cluster of cysts)	Yes	Small	18.109.08
Heavy	1 lobe (cluster of cysts)	Yes	Small - large	18.109.11
Very Heavy	2 lobes (clusters of cysts)	Yes	Small - large	18.109.13
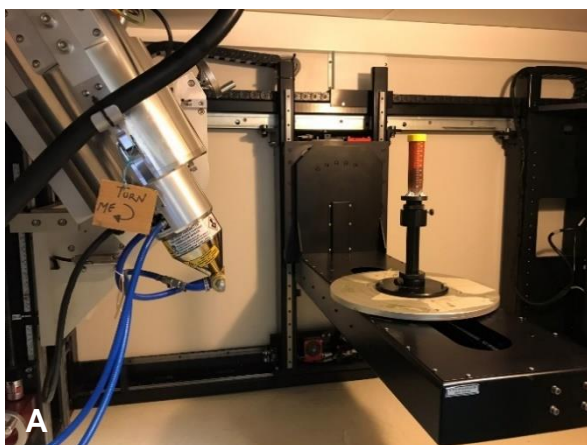
Figure 3. 6. (**A**) A sample tube placed in the instrument prior to scanning. (**B**) A representation of samples during x-ray scanning.

3.3 Results

Descriptive statistics for smelt sampled at Battersea and Chiswick in 2018

Of the twenty smelt sampled at Battersea, 85% were infected while 65% of the forty smelt sampled at Chiswick were infected. Severity of infection varied; however, a large majority were ranked with very heavy infections (Fig. 3.7).
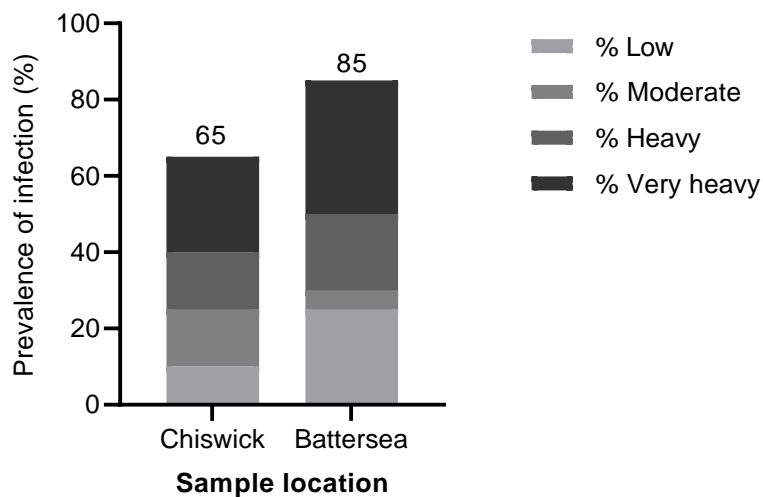
Figure 3. 7 Stacked bar graph of infection severity and prevalence of infection in smelt by sample location. Numbers on top of each bar represent the percentage of infected smelt from each site. The legend depicts the different severities of infection by colour.

Preliminary findings of microsporidian infection in adult smelt (Erith samples)

My analysis of the forty-four photographs provided, confirmed McGoran's correct identification of white microsporidian cysts in smelt (Fig.3.10, 3.11 & 3.12). The photographs revealed the same morphological presentation of cysts inside the peritoneal cavity and along the digestive tract, that was previously highlighted in this study. The infection levels were ranked as follows; 26 mild, 10 moderate, 8 heavy and 8 unknowns (no photograph provided) (see Appendix 3 Table A3.10). Cysts varied in number, size and site location as shown by the representative selection of photographs in Figure 3.12. As seen in Figure 3.11 **A**, cysts are not clearly visible beneath the skin, even when the infection is heavy. Cysts would not be visible in cases of mild infection, unless fish were dissected, as shown in the fish with only one or two small cysts along the gut (Fig. 3.12).

Prevalence of infection amongst smelt sampled at Erith differed between months, however these differences were not statistically significant, and the majority of those infected were considered to have low infection levels (Fig. 3.8). The lengths and weights of infected (n = 52) versus uninfected smelt (n = 153) were similar (Fig. 3.9). Two-way ANOVA showed no significant differences (p > 0.05) between the lengths and weights of uninfected, mild, moderate, and heavy infections. The large ranges in 95% confidents limits for heavy and very heavy infections was due to the limited number of samples with those infection severities.
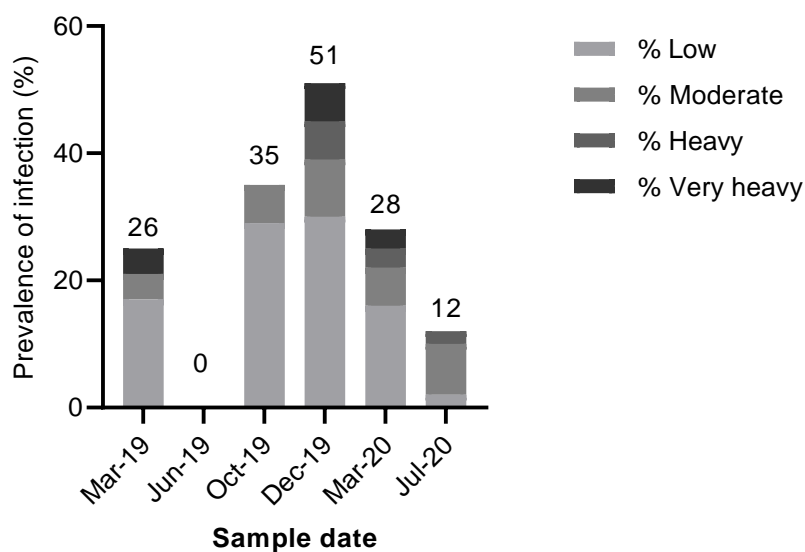
Figure 3. 8 Stacked bar graph of infection severity and prevalence of infection by month sampled. Numbers on top of bar represent the total percentage of smelt infected. The legend depicts the different severities of infection by colour.
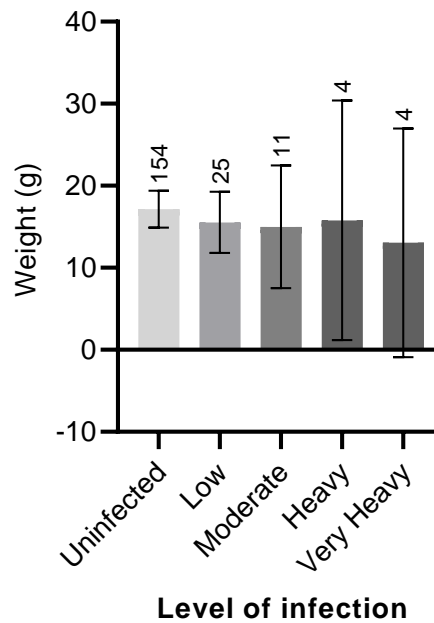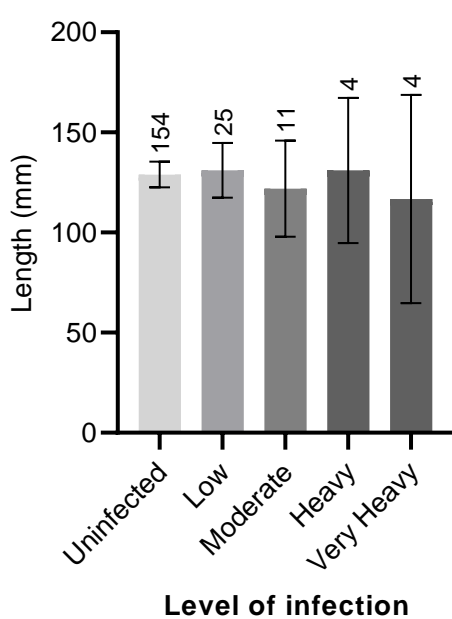
Figure 3. 9 Bar graphs comparing the length **(A)** and weights **(B)** of smelt based on level of infection (McGoran 2019 & 2020 trawl data). Error bars represent 95% confidence limits.

Figure 3. 10. A photograph of a dissected adult smelt (ID #191219OE20) with a heavy burden of white microsporidian cysts (shown with red arrow) clearly visible along the length of the digestive tract. Scale represented by black and white ruler with each square representing 1 cm. (Photograph provided by A. McGoran)

Figure 3. 11. Photograph of an adult smelt (ID #021019OE1), prior to dissection (**A**) and post dissection (**B**). The smelt has a distension along the dorsal line and obscured view of microsporidian cysts prior to dissection. Scale represented by black and white ruler with each square representing 1 cm. (Photographs provided by A. McGoran)
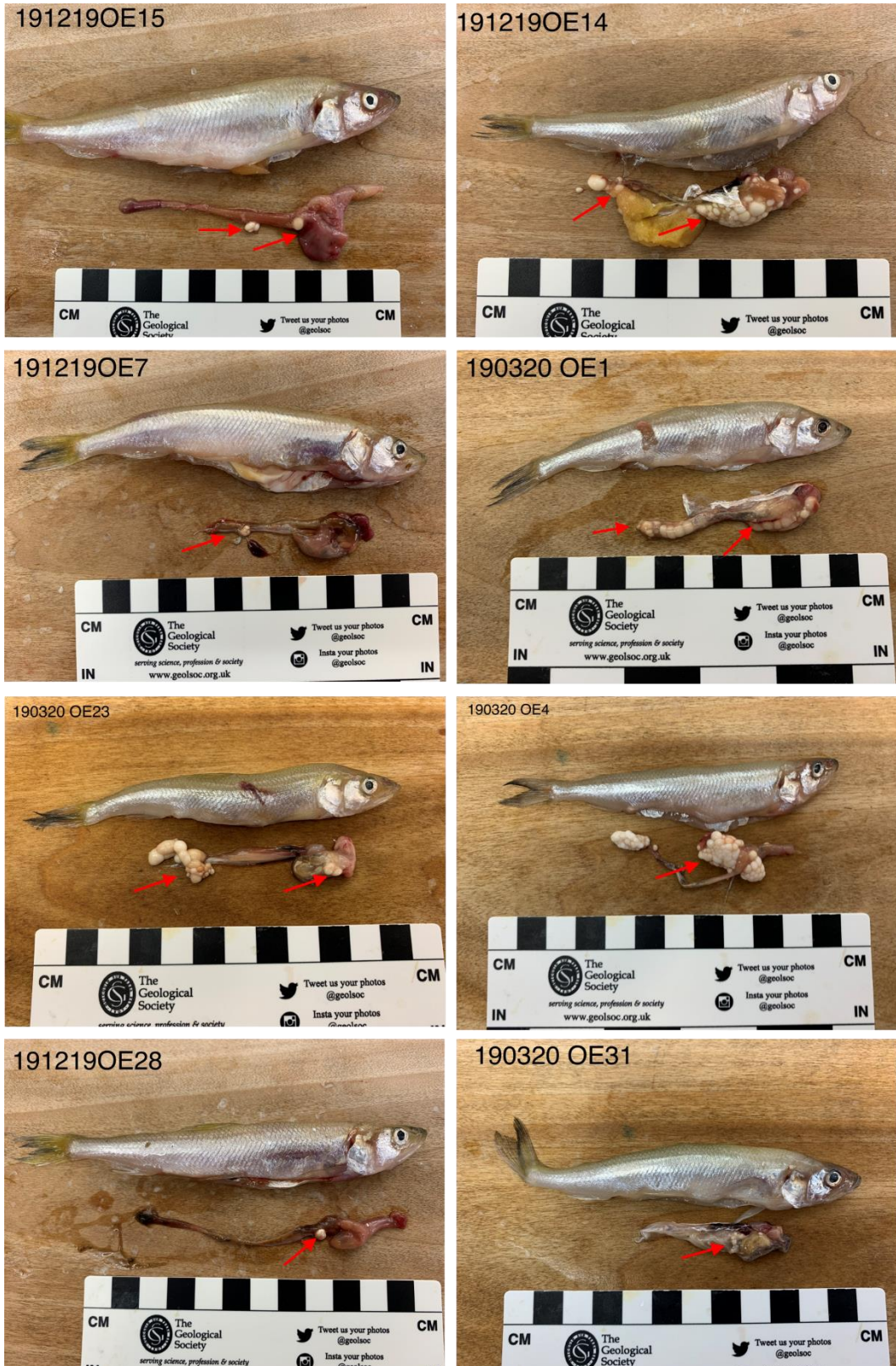
Figure 3. 12. A selection of photographs of dissected adult smelt with the digestive tract removed and placed below the fish. Fish ID written on top left of each photo and microsporidian cysts shown by red arrows. Scale represented by black and white ruler with each square representing 1 cm. (Photographs provided by A. McGoran)

Histopathology and light microscopy analysis

Histopathology of uninfected juvenile smelt

Due to the limited data on smelt, it was important to first understand the normal appearance and internal structures of uninfected juvenile smelt (Fig. 3.14 and 3.15). Healthy juveniles presented with a thick muscle layer surrounding the peritoneal cavity and a thick strong muscular wall surrounding the stomach. The livers in healthy smelt also appeared quite large. In healthy fish the majority of the peritoneal cavity is filled with liver and gut/digestive tissues. Smelt are known to be voracious eaters, as evidenced in Fig. 3.15, which showed the stomach enlarged and filled with food.

Histopathology of infected juvenile smelt

The spores of the microsporidian are ellipsoidal, measuring on average 4.14 x 1.6 µm (n=15), with posterior vacuoles filling approximately one third of the cell (Fig. 3.13). For H&E stained tissues, cysts were not always obvious, due to the similar staining colour of surrounding tissues. The Luna stain assisted in highlighting cysts in smelt with mild infections (Fig. 3.16). Using the Luna stain, microsporidian spores stained brick red, as well as erythrocytes, bones and any eosinophilic granular cells, with other background tissues staining blue (e.g. Fig. 3.16.B).

After close inspection of approximately 160 slides produced from 15 infected smelt samples, it was clear that the parasites did not follow a particular pattern of infection. Cysts of varying size and number presented in different positions along the digestive tract. Most of the cysts occurred within the peritoneal cavity, alongside the digestive tract, and were occasionally seen within the stomach or pyloric caeca (Fig. 3.19.A & 3.21.B). Different developmental stages of cysts were also observed. The early sporogenic stage is shown by a dense cytoplasm filled with a few spores and a less defined wall (Fig. 3.17.A). A maturing cyst with a defined cyst wall composed of collagen fibres and filled with spores is seen in Fig. 3.17.B.

In heavy infections, cysts filled the peritoneal cavity and were also associated with the connective tissue of the gut submucosa (Fig. 3.19 & 3.21) and liver (Fig. 3.18 & 3.21). Large cysts caused significant distention of the peritoneal cavity and displacement of internal organs (Fig. 3.18 & 3.20). In cases of severe infection, the digestive tract and

liver tissues became fragmented, and some internal organs were difficult to identify (Fig. 3.22.).

Increased magnification of cysts showed clear association with liver cells (Fig. 3.21.B & C, 3.22.B & C). Only one sample showed a cyst within the muscle tissue (Fig. 3.23.). Interestingly fish C.37 was first recorded as "uninfected", however early-stage cysts were seen in the histology (Fig. 3.24). On closer inspection, it seemed that these early-stage cysts were developing in the liver tissue, while the gut looked normal (Fig. 3.24B). No lymphocytes or granulomatous inflammation was seen surrounding the cysts or in organs, suggesting that the presence of the microsporidian does not cause a significant immune response.

Figure 3. 13. Wet mount of microsporidium spores sampled from an infected juvenile smelt (X1000). Arrows show posterior vacuoles. (Photomicrograph provided by the EA National Fisheries Laboratory)
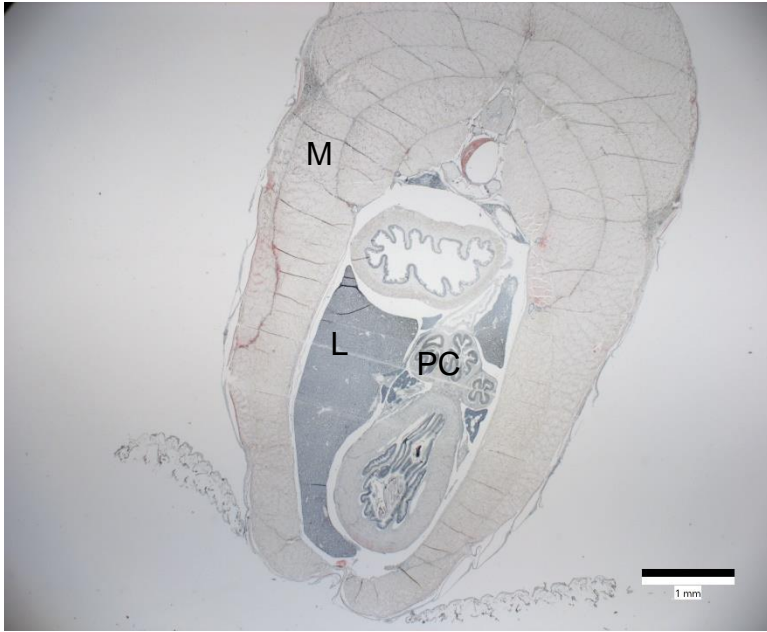
Figure 3. 14. A transverse section of a whole, healthy juvenile smelt stained with Luna stain (Fish C.18). PC = pyloric caeca, L = liver, M = muscle. (scale bar = 1 mm)

Figure 3. 15. A transverse section of a whole, healthy juvenile smelt stained with H&E (Fish C.31). S = stomach, PC = pyloric caeca (scale bar = 1 mm)
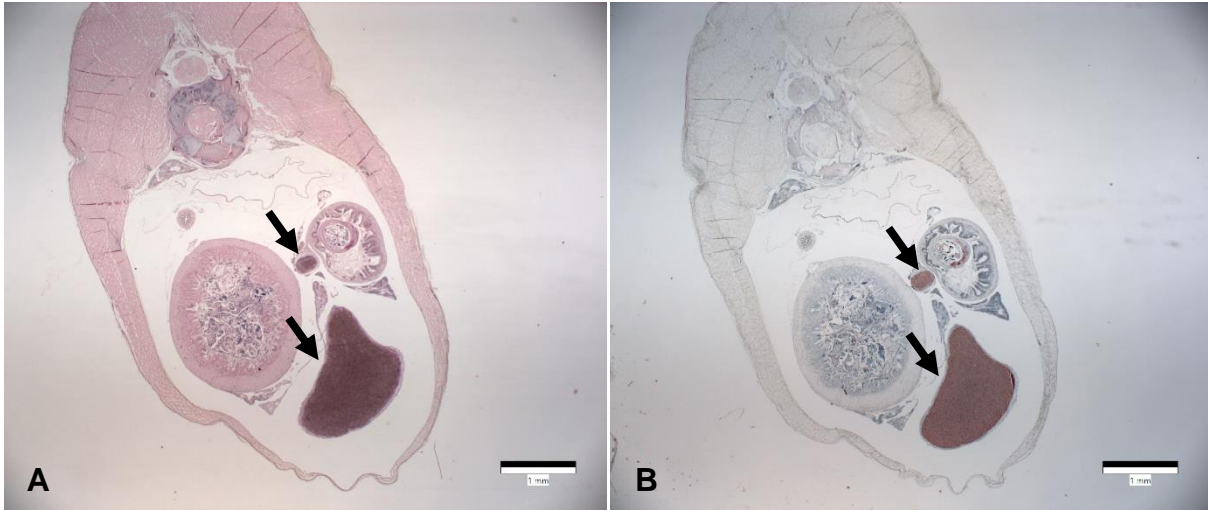
Figure 3. 16. Comparative staining of the same fish (Fish B.7). Photomicrograph **A** shows a whole, transverse section stained with H&E. Photomicrograph **B** shows a whole, transverse section stained with Luna stain. Arrows indicate xenomas. (scale bar = 1 mm)
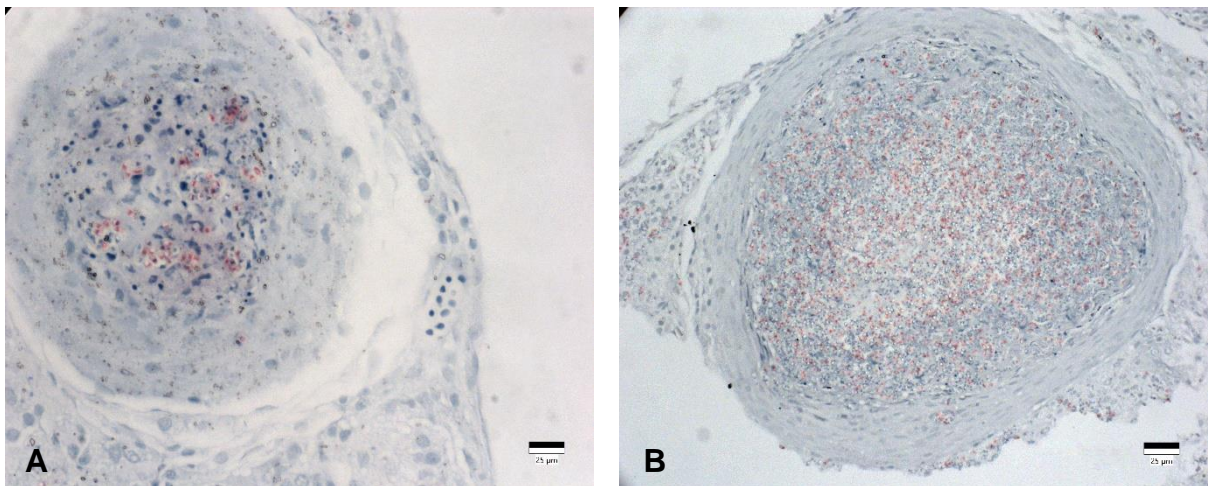
Figure 3. 17. Photomicrographs **A** and **B** show xenoma development with surrounding liver cells (Fish C.37). (**A)** Early stage xenoma formation with xenoma wall still developing and only a few spores present. (**B**) Secondary stage of xenoma growth, showing a defined wall of connective tissue and increasing number of spores within the xenoma. Spores visible in red. (scale bar = 25 μm).
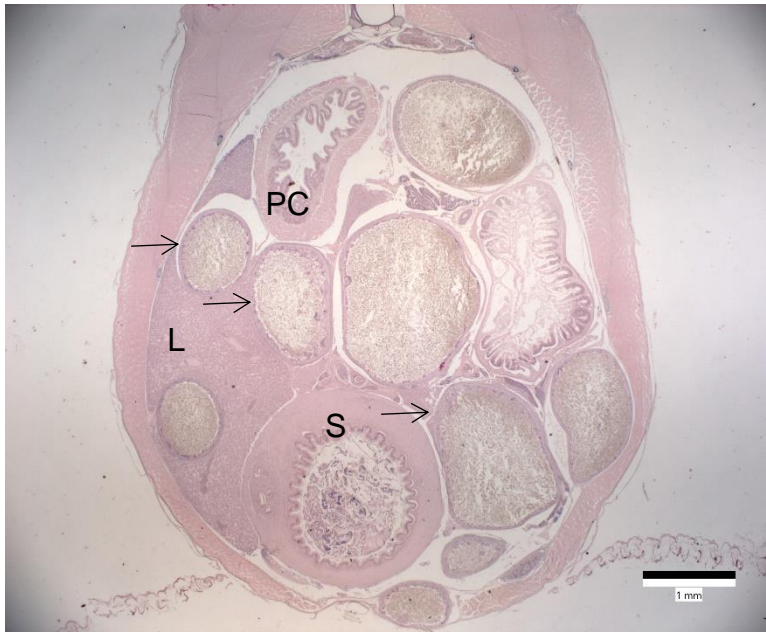
Figure 3. 18. H&E stained whole transverse section of a juvenile smelt (Fish B.17), showing multiple cysts (with highly eosinophilic walls (→)) within the body cavity and in the liver (L) (scale bar = 1 mm). The stomach of the digestive tract is identified by its thick muscular wall. PC = pyloric caeca, S = stomach. Early formation of a cyst can be seen in the liver (►).
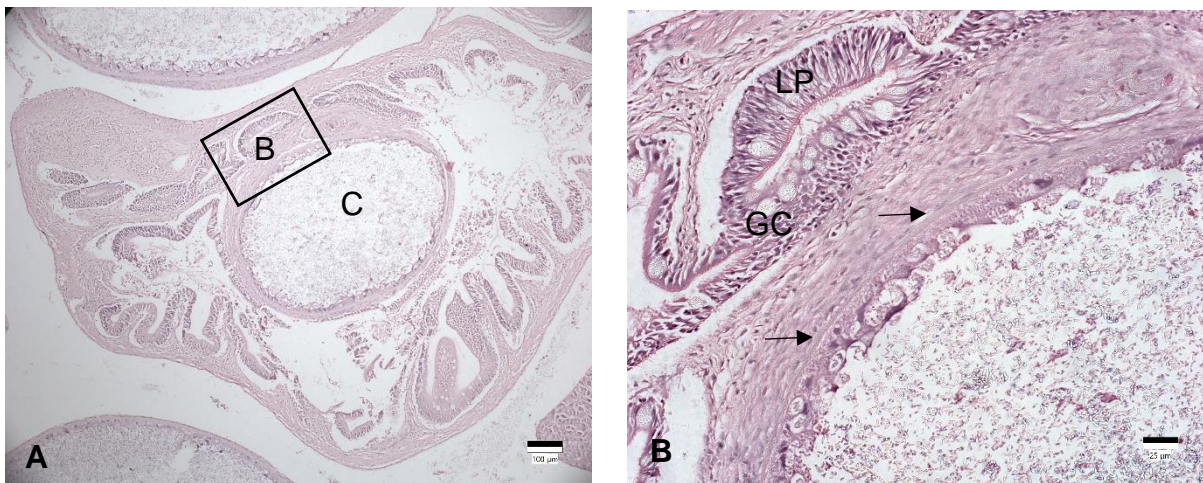
Figure 3. 19. (**A**) A *Glugea* xenoma formed inside the gut along the lamina propria (scale 100 μm) (Fish C.9). (**B**) The box outlined section of **A** at higher magnification (scale 25 μm), showing the cyst wall, which consists of a thin layer of collagen (→) and surrounding host cells (X 400). LP = lamina propia, GC = goblet cells, SM = submucosa, C = cyst.
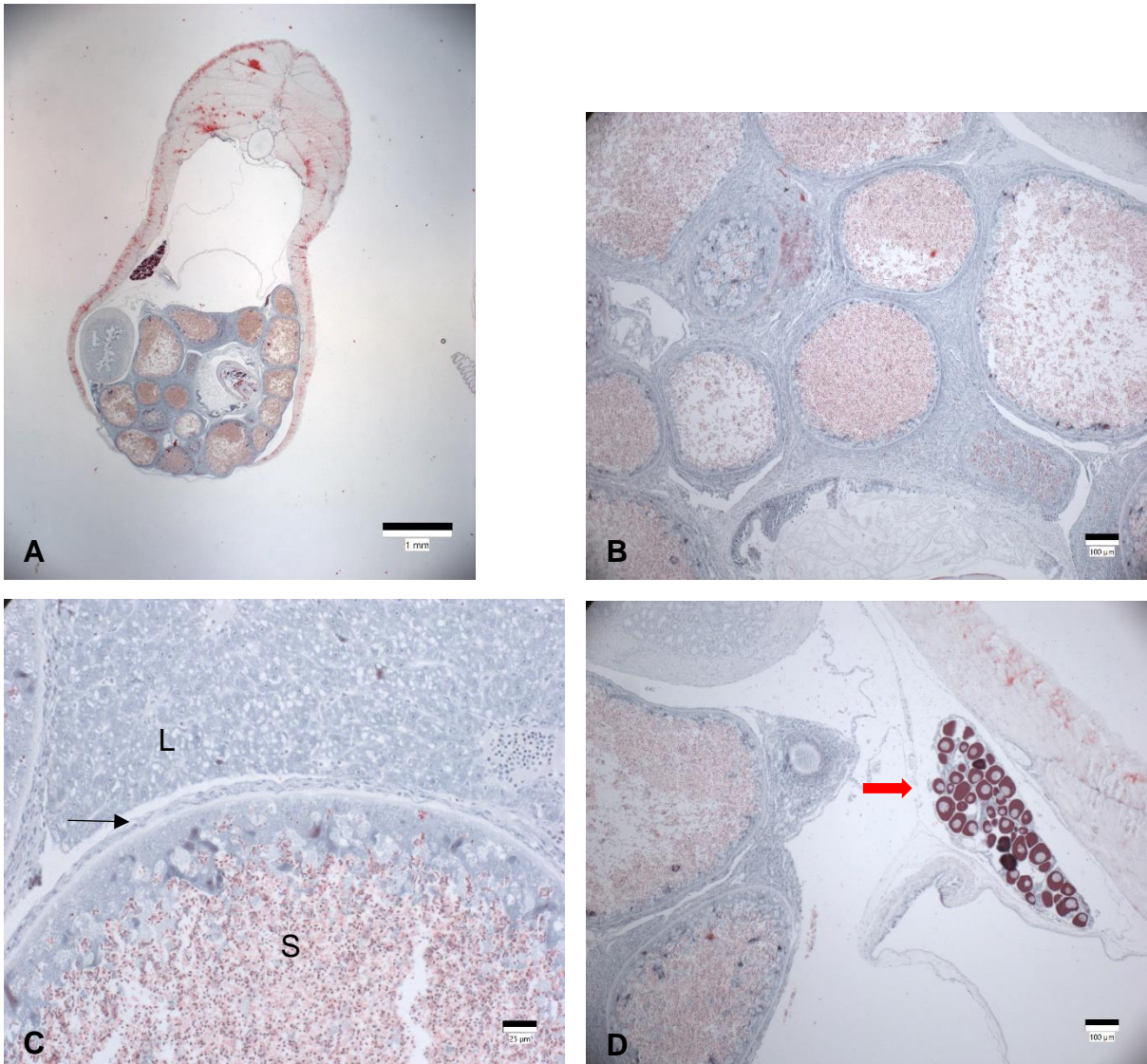
Figure 3. 20. (**A**) A whole transverse section of a juvenile smelt (Fish C.6) with a heavy infection of *Glugea* cysts (scale bar = 1 mm). (**B**) Magnified image of **A** showing different stages of xenoma growth, filled with spores (S); X 200 (scale bar = 100 um). (**C**) Magnified image of **B** showing cyst wall (arrow), surrounded by host liver cells (L); X 400. (**D**) Ovarian lamellae containing follicles in primary growth (shown by red arrow) (scale bar = 100 μm).
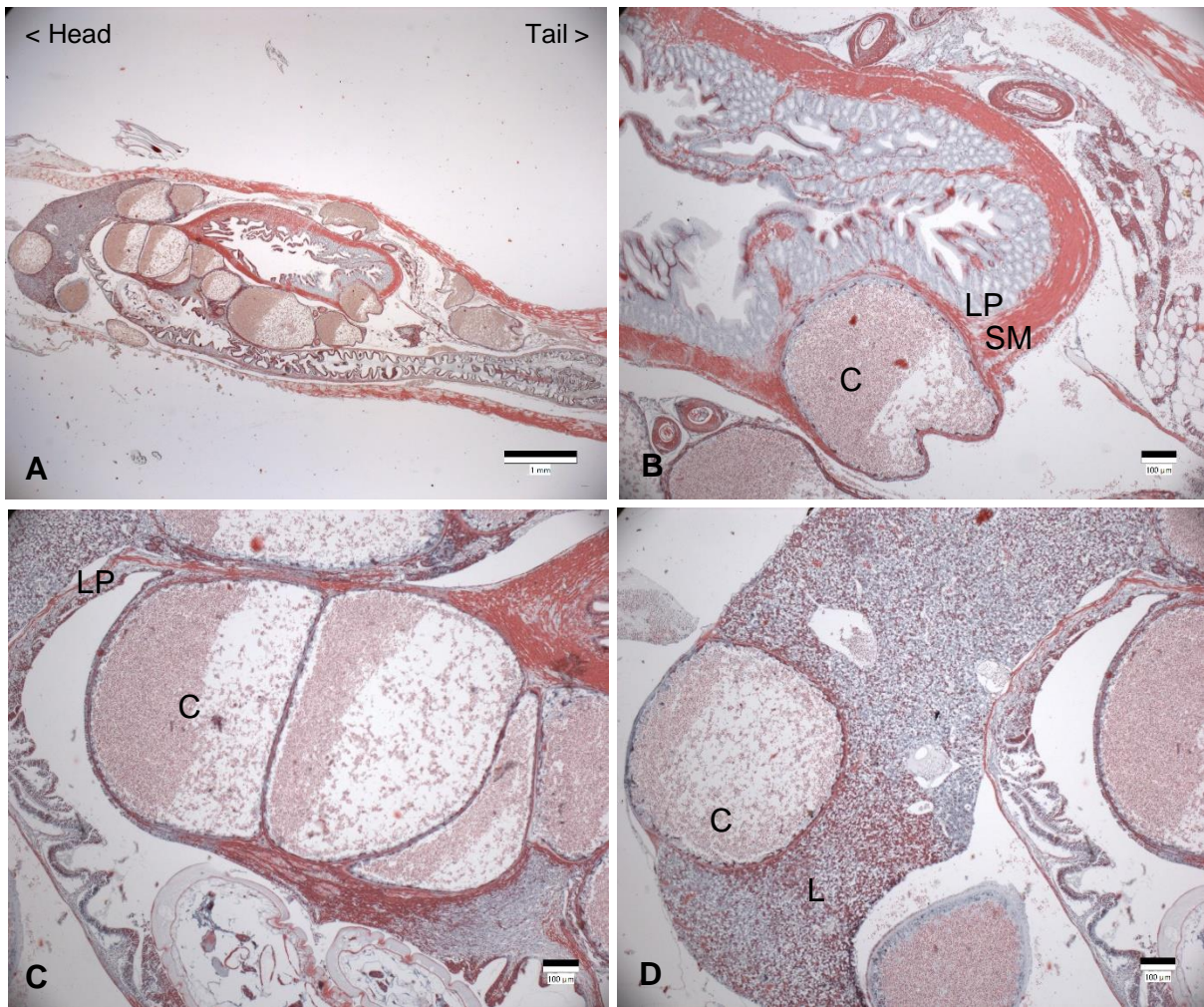
Figure 3. 21. (**A**) Whole, longitudinal section of a heavily infected juvenile smelt filled with xenomas, stained with Luna stain (scale bar = 1 mm). **B, C** and **D** show magnified sections of image **A** (scale bar = 100 μm). **B** and **C** show xenomas formed within the gut lining at 400 X. **D** shows a xenoma formed within the liver tissues. C = cyst, L = liver, LP = lamina propia, SM = submucosa.
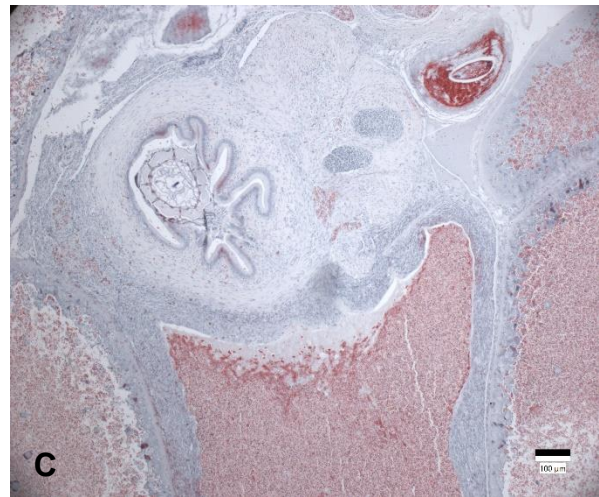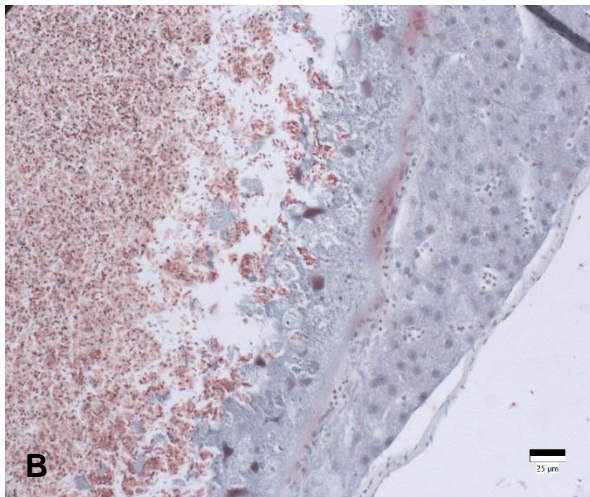
Figure 3. 22. (**A**) Longitudinal section of a whole juvenile smelt (Fish B.12), with a severe infection of *Glugea* xenomas displacing all internal organs (scale bar = 1 mm). (**B**) Magnified section of **A**, showing a xenoma connected to liver cells (scale bar = 25 µm). (**C**) Magnified section of **A**, showing xenomas closely associated with the submucosa of the gut (scale bar = 100 µm). SB = swim bladder, H = heart.
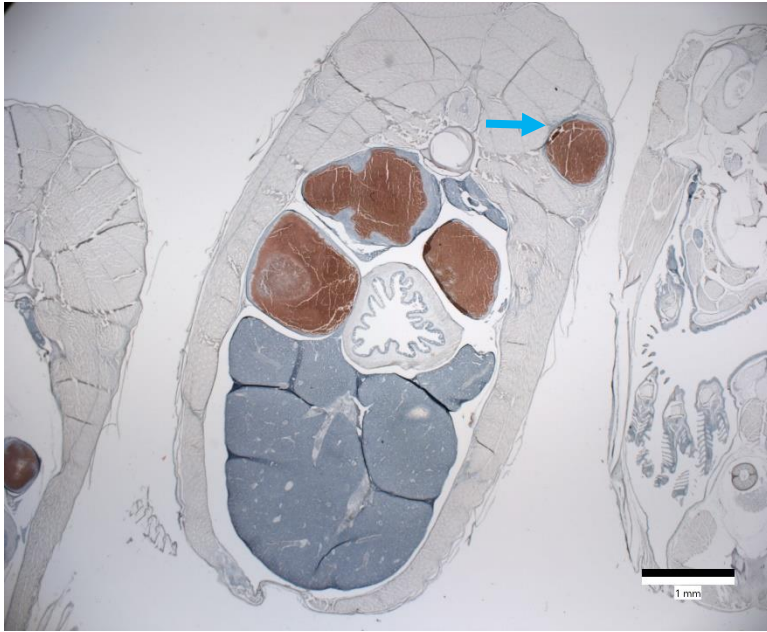
Figure 3. 23. Transverse section of a juvenile smelt (Fish B.18) with cysts in the peritoneal cavity and one cyst in the ventral muscle tissue (light blue arrow) (scale bar = 1 mm).
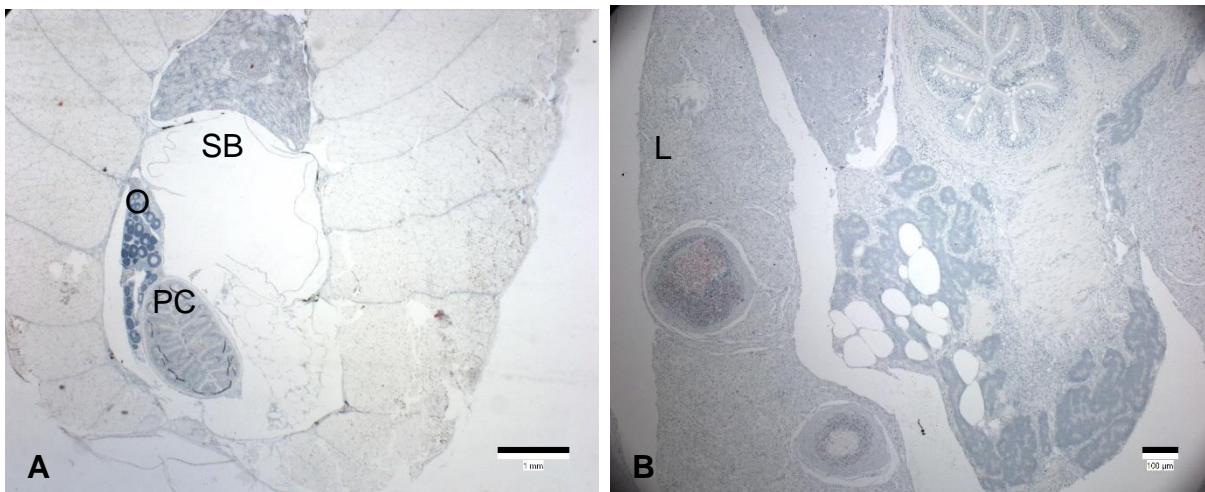
Figure 3. 24. Photomicrograph showing what first appeared to be a healthy juvenile smelt (Fish C.37) in **A** (scale bar = 1 mm), while in reality, photomicrograph **B** shows early-stage cysts developing in the liver. SB = swim bladder, PC = pyloric caeca, O = ovarian lamellae, L = liver (scale bar = 100 µm).

X-Ray micro-computer tomography

The micro-CT images allowed us to visualise the entire peritoneal cavity of each smelt scanned and to highlight structures of interest (See Appendix 3 Table A3.4). Healthy, uninfected, smelt were usually longer in length than infected samples and presented with normal organ placement (Fig. 3.26). Mild infections were characterised by the

presence of only a few cysts within the peritoneal cavity and did not appear to be causing displacement of internal organs (Fig. 3.24). In mild infections, cysts were present near the stomach in the upper digestive tract (Fig. 3.27.A) but also found near the lower intestines (Fig.3.27.B). This seemingly 'random' placement of cysts was also observed in moderately infected smelt, with some samples presenting with clusters of small cysts near the upper digestive tract (Fig.3.28.A), and others presenting with larger individual cysts spread along the length of the digestive tract (Fig.3.28.B). Minimal organ displacement was observed in moderately infected samples. Smelt with heavy infections presented with clusters of differently sized cysts throughout the peritoneal cavity, causing severe organ displacement, and compression of the digestive tract (Fig.3.29). The digestive tract was visibly intact in all smelt scanned with micro-CT, including those with very heavy cyst burdens. The 3D image rendering allowed us to "remove" the cysts and identify only the digestive tract (Fig. 3.30). In smelt with very heavy burdens, the digestive tract was often compressed but was not "burst" by the cysts. In heavily infected smelt, the cysts caused distention of the body cavity, causing large bulges, particularly along the ventral region below the operculum and between the pelvic and anal fins (Fig.3.29 & 3.30).

Smelt with moderate and very heavy infections became increasingly thin, with less muscle mass and shorter in total length. A significant negative correlation was found between body length and volume of cysts (%) (n = 14) (Fig. 3.25). The 'r' value was -0.6518, and 'P' value was 0.0115. The negative correlation suggested that as the volume of cysts increased, the body length of smelt decreased. The diameter of individual cysts (n=68) averaged 1.18 mm (std. deviation = 0.64), with a minimum diameter of 0.06 mm and maximum diameter of 3.86 mm (See Appendix 3 Table A3.8 & A3.9).
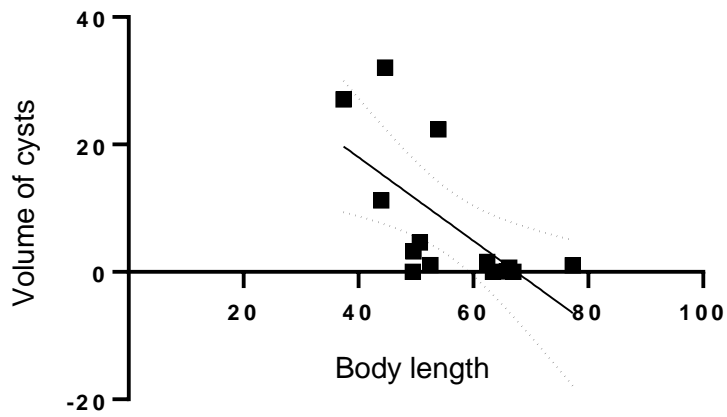
Figure 3. 25 Pearson correlation graph between the volume of cysts and body length of infected smelt. Dotted lines show

20 mm
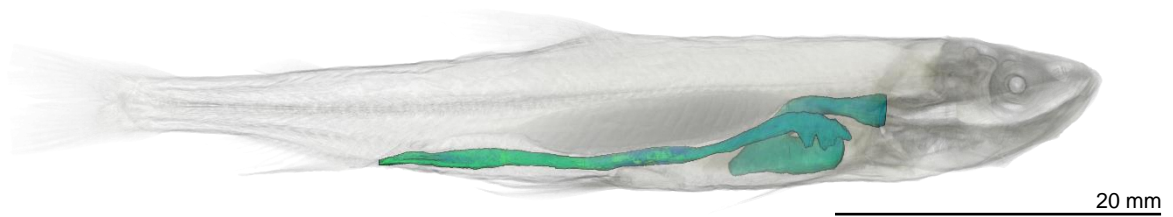
Figure 3. 26. False-coloured 3D volume rendering of a healthy smelt, with the digestive tract coloured in blue/green (ID #2).
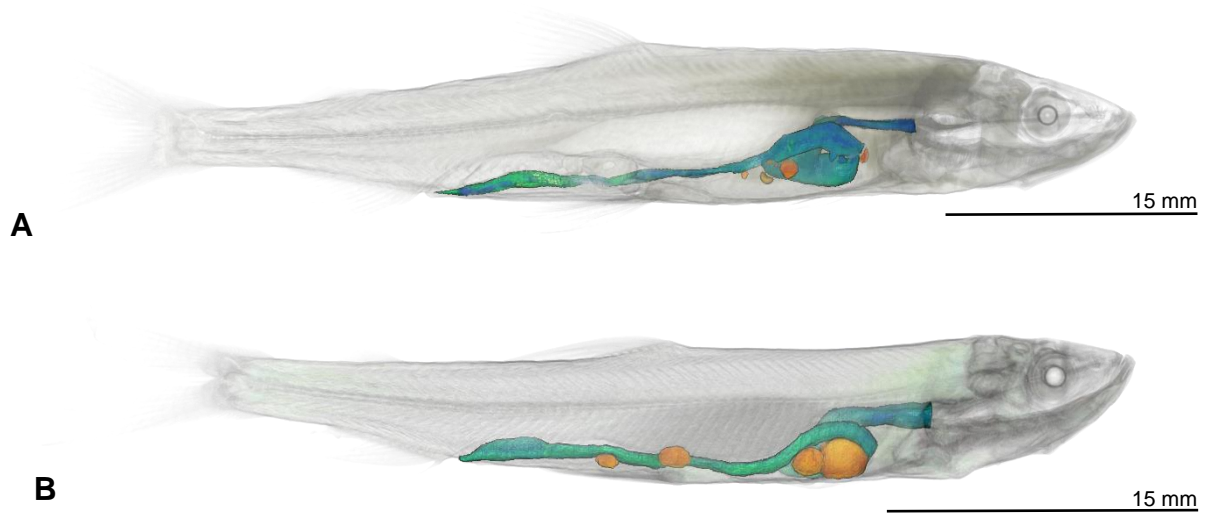
Figure 3. 27. (**A** & **B**) False-coloured 3D volume rendering of smelt with mild *Glugea* infections. The digestive tract is coloured in blue/green and the microsporidian cysts coloured in orange. (A = ID #10, B = ID #22)
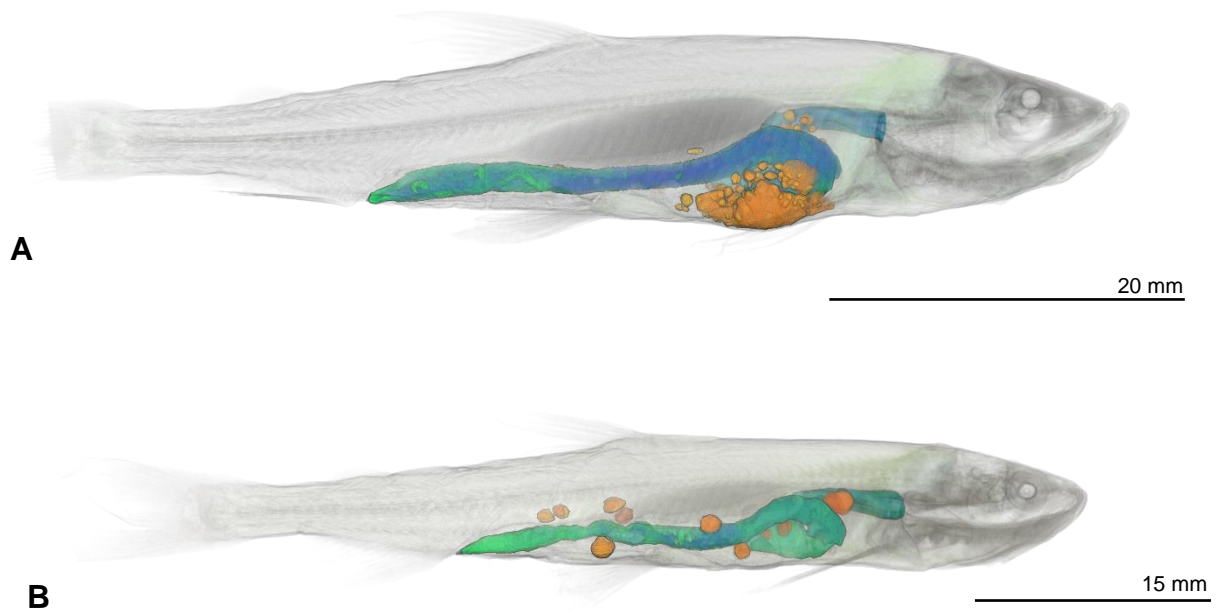
Figure 3. 28. (**A** & **B**) False-coloured 3D volume rendering of smelt with moderate *Glugea* infections. The digestive tract is coloured in blue/green and the microsporidian cysts coloured in orange. (A = ID #36, B = ID #3)
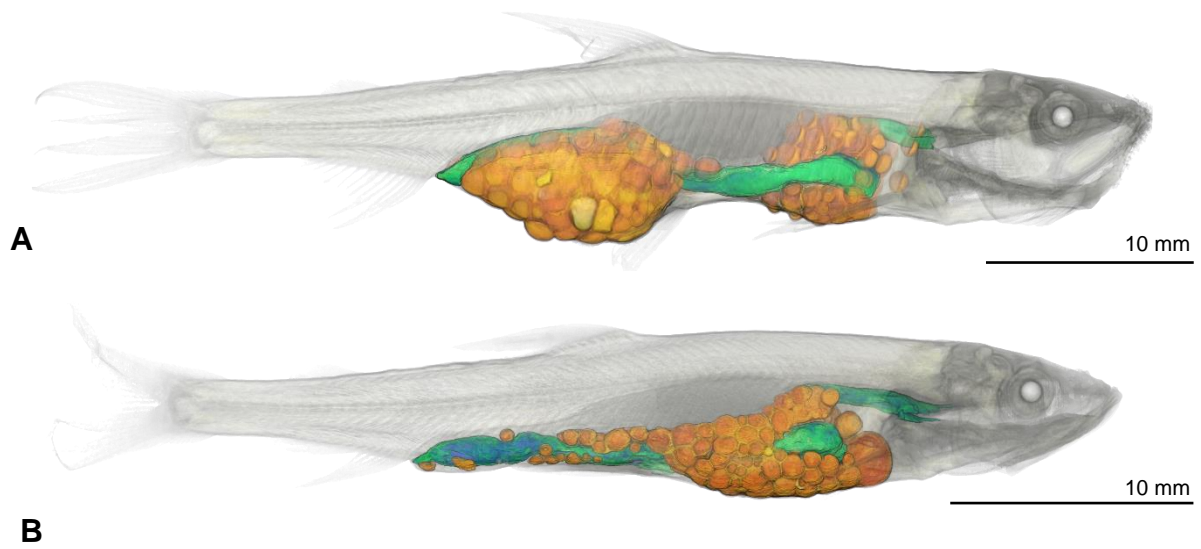
Figure 3. 29. (**A** & **B**) False-coloured 3D volume rendering of smelt with very heavy *Glugea* infections. The digestive tract is coloured in green and the microsporidian cysts coloured in orange. (A = ID #6, B = ID #5)
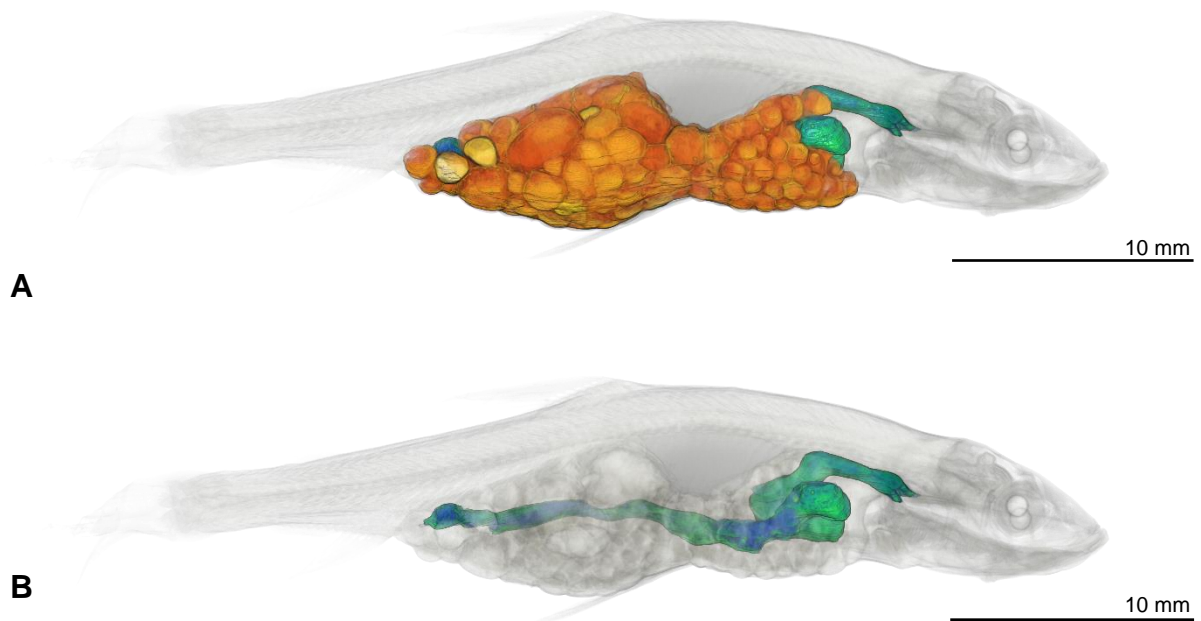
Figure 3. 30. False-coloured 3D volume rendering of a smelt with a very heavy *Glugea* infection (**A**). (**B**) shows the same image but with only the digestive tract highlighted in green. (ID #1)

3.4 Discussion

This chapter provides a histopathological overview of the microsporidian infecting juvenile smelt in the River Thames. The study also provided a unique view of the parasite in-situ using micro-CT 3D imagery to further understand the development and internal impact of this parasite.

Historically, identification of microsporidian parasites has been based on morphology, using light microscopy to identify specific ultrastructural features and cell structure characteristics of spores and developmental stages (Nilsen, Endresen & Hordvik, 1998; Weiss & Becnel, 2014). Fish microsporidia can be classified into two broad groups; the first being xenoma (cyst) forming and the second being non-xenoma forming (Dyková & Lom, 1980). The xenoma forming genera, which applies to this study, include *Glugea*, *Ichthyosporidium*, *Jirovecia*, *Loma*, *Microfilum, Microgemma, Nosemoides, Spraguea* and *Tetramicra* (Weiss & Becnel, 2014). Identification of different genera is primarily based on the host species, size of the spores, the primary site of infection and any inflammatory reaction to cysts (Rodriguez-Tovar, Speare & Markham, 2011). Inflammatory responses include the infiltration of cells such as macrophages and lymphocytes (Rodriguez-Tovar, Speare & Markham, 2011). Different genera also use different mechanisms to infect host cells; for example, *Ichthyosporidium* and *Tetramicra* form microvillus-like structures, while *Glugea* and *Loma* species use pinocytotic vesicles (Canning & Lom, 1986).

The morphological and histological presentation of the microsporidian infecting juvenile smelt in this study showed characteristics typical of the genus *Glugea,* specifically the development of cysts along the digestive tract. *Glugea* species typically infect the submucosal and intestinal cells (Weiss & Becnel, 2014). *G. anomala*, one of the most well studied *Glugea* species, usually infects sticklebacks (*G. aculeatus*). Dyková & Lom (1978) experimentally infected sticklebacks with *G. anomala* to study tissue reactions and reported cyst formation in the subepithelial connective tissue of the glandular part of the stomach. Their findings contrasted with the findings of Delisle (1972), who reported a closely related microradian species, *G. hertwigi,* which showed low organ specificity and a primary site of infection along the digestive tract (Dyková & Lom, 1978). *G. stephani* is another species which presents with opaque cysts developing primarily on the external wall of the digestive tract of pleuronectiform (flat)

fishes (Canning & Lom, 1986). McVicar (1975) reported that the primary site of infection of *G. stephani* was the intestine submucosa, specifically in the rectum, with a ring of cysts close to the anus. Interestingly, cysts were not found in the stomach wall, with a clear line of demarcation observed by McVicar (1975) between the intestine and stomach. Multifocal cysts of *G. stephani* have also been reported in the liver, kidney and ovaries of winter flounder (*P. americanus*) (Khan, 2004). The microsporidian *G. plecoglossi,* which infects ayu (*Plecoglossus altivelis*), has similar morphology to that of *G. hertwigi* (Takahashi & Egusa, 1977)*. G. plecoglossi* has also been reported in ayu in Mainland China (Zhou, Chai & Chen, 2018)*.*

Fish pathology experts at the EA had suggested that the microsporidian infecting juvenile Thames smelt in this study could be *G. hertwigi.* This work aimed to determine if this tentative species identification was correct. The primary site of infection by *G. hertwigi* in European (*O. eperlanus*) and Rainbow smelt (*O. mordax*) occurs in the digestive tract, more evidently in the anterior portion (Chen & Power, 1972); however, in heavy infections, it can infect the liver and gonads (Haley, 1954; Lovy et al., 2009; Costa, Melo-Moreira & De Carvalho, 2016). Bogdanova (1957) and Chen and Power, (1972) also reported that heavy infections caused degenerative changes in the gonads, that would negatively affect fecundity. My findings largely agree with the morphology described for *G. hertwigi* in *O. eperlanus* in the literature. However, some of my samples with mild/moderate infections had cysts sporadically located along the entire length of the digestive tract, which did not seem defined to a specific region. The liver, pyloric caeca, heart and gonads have been reported as secondary sites for infection (Haley, 1952). However, I found that some smelt with mild infections had more cysts associated with the liver than the anterior digestive tract, suggesting that the liver may also be a primary site for infection. Legault and Delisle (1967) also reported cysts infecting the liver while not observed in other organs. Legault and Delisle (1967) also reported that cysts of *G. hertwigi* may occlude the stomach and intestine, ultimately leading to death through starvation. This was not observed in the smelt assessed in my study. Indeed, the micro-CT imagery of infected smelt clearly showed the digestive tract intact, but with compression in heavy infections. Therefore, my findings suggest that mortality may also result from starvation, possibly via reduced swimming ability and feeding efficiency. As for the micro-CT scanned fish, heavily infected individuals were smaller and thinner than uninfected fish.

Previous literature has suggested that adult smelt are rarely infected with *G. hertwigi*, with authors suggesting that heavily infected juveniles die before maturity (Schrader, 1921; Haley, 1954; Nepszy, Budd & Dechtiar, 1978). However, Nepszy and Dechtiar (1972) reported unusually severe mortality in adult rainbow smelt *O. mordax*, in Lake Erie in May 1971. In November 2019, I joined an EA (Estuarine and Coastal Monitoring Assessment Service team) trawl survey of smelt in the mouth of the River Thames (near Canvey Island) (Unpublished data). We assessed 73 adult smelt by external visual inspection (not dissection), and only one individual appeared very thin and had visible white cysts (potentially *Glugea*). Based on this personal experience, it seemed that infection levels in adult smelt in the mouth of the Thames was indeed low, however in comparison to the juveniles, the adult smelt are no longer translucent, hindering internal observation. However, the preliminary data from trawl samples at Erith in the Thames (in 2019 & 2020) provided by McGoran refutes these earlier assessments, with around 25% of smelt infected with cysts. Unfortunately, the age of individuals could not be classified based on length alone as smelt are known to have considerable overlap in lengths between year classes, with Hutchinson reporting considerable overlap between Thames smelt in the 0+, 1+ and 2+ age groups (Hutchinson, 1983; Bailey, 1964). My findings in Chapter 2 on length at age for Thames smelt, also agreed with Hutchinson's findings. Future studies should include age in analyses of infection now that adults have been shown to carry infections. The McGoran-dissected Thames samples suggest that adult smelt either remain infected from juvenile infections or may become infected as adults. Some of the photographs I assessed showed only one or two cysts along the digestive tract, so either these are new infections, or the infection has not proliferated as the fish matured. Therefore, more adults could be carrying mild infections that would not be visible without dissection. Future work could look to survey adult smelt throughout the year, to see if juveniles with mild infections are maturing and carrying cysts into adulthood. Another interesting finding was the similarity between the lengths and weights of infected versus uninfected individuals. Half of the infections (~26) reported were ranked as mild, and therefore any negative impacts from low infection might be minimal.

Past studies on the microsporidian *G. hertwigi* in European smelt have presented histological microscopy and SEM (scanning electron microscopy) of the cysts and

spores (Bogdanova, 1957; Costa, Melo-Moreira & De Carvalho, 2016; Weissenberg, 1913). Comparatively, data are limited on the effects of the cysts on surrounding organs and the fish as a whole. My study, therefore, provides a novel way to explore microsporidian pathology using micro-CT imagery. To the best of my knowledge, this is the first study using micro-CT to explore a microsporidian infection in a fish host. The 3D volume renderings allowed us to view infections without destructive physical manipulation of the samples (as often found in histologically fixed and processed tissues) and provided a full 3D view of different infection levels. Grading levels of infection was easier when viewing the whole specimen when compared to histological sections. Furthermore, the positioning of the parasites within the host can be better viewed without the risk of potential sectioning-related displacement (O'Sullivan et al., 2018).

Based on the histological evidence in this study, it is impossible to suggest the initial site of infection due to the varied locations of cysts present in mildly infected fish. However, it seems most likely that spores are orally ingested through the water or infected food sources and then travel into the digestive tract cells, as that is where most of the cysts were found in mild infections. Future studies could look to experimentally infect smelt to analyse early stages of infection. Experimental infection of *O. mordax* with *G. hertwigi* was performed in the 1970s by Scarborough & Weidner (1979). Weissenberg (1968) also reported a successful infection of *G. hertwigi* in sticklebacks (*G. aculeatus*), although Lom (2002) suggested that it should be reconfirmed to ensure it was not *G. anomala*. To the best of my knowledge, experimental infection of European smelt (*O. eperlanus*) with *G. hertwigi* has not been attempted.

The use and applications of micro-CT in biological and ecological studies has grown in recent years and is highlighted by its ability to explore internal morphology in 3-dimensional space (Gutiérrez et al., 2018). The technique is becoming more widely applied in teleost studies, for example, morphometric analyses (Weinhardt et al., 2018; Ceballos-Francisco et al., 2020b, 2020a) and histological phenotyping in zebrafish (Ding et al., 2019). A few recent studies applied micro-CT imagery to study parasite/host interactions in aqua-cultured species, including a study on a myxosporean parasite infecting cultured red seabream (*Pagrus major*) (Katharios et

al., 2020) and the parasitic isopod *Ceratothoa oestroides* infecting farmed European sea bass (*Dicentrarchus labrax*) (Mladineo et al., 2020). The studies used a combination of histological and micro-CT techniques and suggested that using both methods provide a much more detailed pathological report of the interaction and effects of the parasitic infection. Histological sections are still needed to view the cellular level impact of cysts on surrounding tissues and identify any immune responses.

For this study, I was able to scan 14 fish samples using micro-CT, with at least three fish to represent healthy fish and three fish to represent each stage of infection (mild, moderate, and heavy). My sample size was comparable with the other mentioned studies on fish parasites using micro-CT, with Katharios *et al.* (2020) analysing 15 red seabream (*P. major*) infected with a myxosporean and Mladineo *et al.* (2020) analysing five infected European sea bass (*D. labrax*) infected with *C. oestroides*. The higher cost associated with using micro-CT and likely post-scan image analysis performed by an expert is an important factor to consider for future work, as the cost, while not huge, is much higher than producing histological slides. I strongly agree with other authors, such as O'Sullivan *et al.* (2018), who have suggested that using both histological and micro-CT imaging to study parasite pathology is better than each method on its own.

Based on the literature, *G. hertwigi* is the only *Glugea* species reported to infect smelt (*O. eperlanus* and *O. mordax*)*.* From my histopathological and micro-CT assessment, many of the pathologies are similar to those described in previous publications. However, without molecular confirmation, it is difficult to make a positive identification to the species level of this microsporidian. This leads to my next chapter (Chapter 4), which explores the molecular methods for species identification and the phylogenetic placement of this parasite.

Chapter 4. Molecular identification and phylogenetic placement of the microsporidian infecting juvenile European smelt from the River Thames

Abstract

Fish infecting microsporidia can have significant negative impacts on the health of a population. Identification of microsporidians was historically determined using light microscopy and morphology in host species. While scanning electron microscopy (SEM) allowed for further ultrastructure's to be identified, phylogenetic placement at species level was limited. More recently, molecular identification specifically looking at the small subunit ribosomal RNA (ssrRNA) region has allowed for further insight into the phylogenetic relationships between species. A large majority of juvenile smelt caught from the River Thames in 2018, presented with large white cysts in the gut, and this infection was tentatively identified as the microsporidian *Glugea hertwigi*. This microsporidian has never before been reported in smelt residing in UK waters. In this chapter, I aim to identify the microsporidian to species level. Furthermore, I assess its phylogenetic relationship to other closely related fish infecting microsporidians. Using bioinformatics, I was able to produce two consensus rDNA sequences from infected smelt caught in 2018 and 2020. Phylogenetic analyses placed my isolates with five other *Glugea* species, with a sequence identity > 98%. Furthermore, my isolates clustered in a phylogenetic tree with other *Glugea* species mainly found in the Northern hemisphere. Based on my morphological findings in Chapter 3 and the molecular data presented in this chapter, I suggest that smelt in the Thames may be infected with *G. hertwigi*, however current taxonomy of this genus to species level is inconsistent. This study is the first, to my knowledge, to produce an rDNA sequence for *G. hertwigi* infecting European smelt. Future studies could aim to sequence more of the genome to better understand species level differences in the *Glugea* genus. *G.* hertwigi infections have been identified morphologically in smelt from Baltic regions, but not identified genetically. DNA samples from infected Baltic smelt would provide insight into the relationship between infections and suggest possible origins.

4.1 Introduction

Microsporidia, specifically those which infect fish, are a large and diverse group of parasites (Lom & Nilsen, 2003). Microsporidian infections can have significant negative impacts in wild and farmed fish populations (Lom & Dyková, 2005; Weiss & Becnel, 2014). Certain genera, specifically xenoma-forming, such as *Glugea*, have caused mass mortalities and economic losses. Examples include mass die-offs of Rainbow smelt (*Osmerus mordax*) infected with *G. hertwigi* in North America (Haley, 1952) and ornamental killifishes (*Nothobranchius* spp.) infected with an unknown *Glugea* species (Lom, Noga & Dykova, 1995). Furthermore, *G. plecoglossi* has been responsible for significant economic losses of cultured ayu (*Plecoglossus altivelis*) in Japan due to the unsightly cysts it produces (Lee, Yokoyama & Ogawa, 2004). Identifying the microsporidian species infecting Thames smelt is essential to understand whether the infection poses any risks to the health and well-being of the local smelt population. As previously mentioned, smelt are a priority species of concern in the UK and therefore potential threats need to be understood and monitored.

Microsporidia, have a number of defining characteristics that distinguish them as a taxon, including " (i) the presence, in the spore stage, of a coiled polar filament, (ii) the posterior vacuole, (iii) the anterior polaroplast, and (iv) the diplokaryon (not present in all species)"[2] (Weiss & Becnel, 2014). Historically, identification of microsporidians was determined by light microscopy, to identify basic cell structure characteristics of spores and developmental stages (Nilsen, Endresen & Hordvik, 1998; Weiss & Becnel, 2014). The use of scanning electron microscopy (SEM) allowed for further ultra-structures to be distinguished and assist in phylogeny, however there are limitations when trying to find reliable synapomorphies (characteristics shared by two or more taxa, thus likely sharing a common ancestor) using these techniques (Nilsen, 2000). The more recent use of molecular data, specifically small subunit ribosomal RNA (ssrRNA) genes, has contributed with identification efforts by highlighting a

---

[2] (i) The polar filament is used to infiltrate the host cell.
(ii) The posterior vacuole which expands during spore germination and pushes the contents of the spore into the polar tube.
(iii) The polaroplast is a system of membrane-limited cavities in the anterior of the spore, which swells with water prior to spore discharge.
(iv) The diplokaryon is a nucleus possessing two nuclei.

number of differences between phylogenies based on morphological identification and those based on molecular identification of microsporidians (Baker et al., 1994; Nilsen, 2000).

Ribosomal RNA (rRNA) is the primary component of ribosomes (the structures in which protein synthesis takes place) (Hofmann & Clokie, 2018). Woese (1977) first proposed the use or rRNA for inferring phylogenetic frameworks of all cellular life. rRNA was found to be much more conserved than protein coding genes in bacterial studies, and appeared to be the 'functional core' of information translation in cells (Sogin & Silberman, 1998). Therefore, the first studies of protist evolution looked at comparisons of ssrRNA (Sogin & Silberman, 1998). Some of the first molecular analyses on microsporidians were based on rRNA of the genera *Nosema* and *Vairimorpha,* by sequencing the large subunit RNA (LSU RNA) (Baker et al., 1994). Microsporidian ssrRNA sequences differ greatly to ssrRNA (16S) sequences of other eukaryotes (Weiss & Becnel, 2014). Furthermore, the rRNA genes of some microsporidians are significantly shorter than eukaryotic and prokaryotic ssrRNA, with some genera 'missing' regions of the small subunit sequence considered to be 'eukaryotic' (Vossbrinck et al., 1987). Vossbrinck *et al.* (1987) chose to sequence the ssrRNA of *Vairimorpha* necatrix (of only 1244 nucleotides) region to clarify their phylogenetic position, due to the unusual molecular characteristics of these microsporidia. Vossbrinck *et al.* (1987) suggested that "using the criterion of rRNA difference as a measure of evolutionary distance, the depth of the microsporidian branching in the eukaryotic line is remarkable". A large number of microsporidian genome sequences have been determined from sequencing the ssrRNA gene, the internal transcriber spacer (ITS) (non-functional RNA situated between the small and large subunit RNA) and LSU RNA gene (Weiss & Becnel, 2014). The genome size between taxa varies greatly, with the *Encephalitozoan* genome representing the smallest known genome of 2.3 Mb (megabases), and the largest belonging to *Edhazardia aedis* at 51.3 Mb (Corradi et al., 2010).

The ssrRNA genes (both partial and complete) of a number of microsporidians, found to infect fish, have been sequenced and uploaded to GenBank (an open access sequence database; https://www.ncbi.nlm.nih.gov/genbank/). Genes are sequenced using oligonucleotide primers and polymerase chain reaction (PCR). PCR is used to

amplify a specific fragment of DNA (target DNA) from a complex mixture, known as the template DNA (Hofmann & Clokie, 2018). A pair of primers (short single-stranded nucleic acid) are chemically designed to complement a known or highly conserved region of each strand of target DNA, which provides the starting point for DNA synthesis (Hofmann & Clokie, 2018). Many ssrDNA primers have been developed for identifying and classifying microsporidians to the species level (Baker et al., 1994; Weiss et al., 1994; Vossbrinck et al., 2004) (Table 4.1.). Primers 18f and 1492r amplify most of the ssrRNA of microsporidia, while 530f and 212r1 amplify the ssrRNA and internal transcribed spacer (ITS) (Weiss & Becnel, 2014). Primer 580r amplifies the 5' end of the large subunit rRNA gene (Weiss & Becnel, 2014).

Table 4. 1. Common primers for identifying and sequencing microsporidian rDNA (adapted from Weiss & Becnel, 2014)

Name	Sequence
ss18f	CACCAGGTTGATTCTGCC
ss18sf	GTTGATTCTGCCTGACGT
ss350f	CCAAGGA(T/C)GGCAGCAGGCGCGAAA
ss350r	TTTCGCGCCTGCTGCC(G/A)TCCTTG
ss530f	GTGCCAGC(C/A)GCCGCGG
ss530r	CCGCGG(T/G)GCTGGCAC
ss1047r	AACGGCCATGCACCAC
ss1061f	GGTGGTGCATGGCCG
ss1492r	GGTTACCTTGTTACGACTT (universal primer)
ss1537	TTATGATCCTGCTAATGGTTC
ls212r1	GTT(G/A)GTTTCTTTTCCTC
ls212r2	AATCC(G/A/T/C)(G/A)GTT(G/A)GTTTCTTTTCCTC
ls580r	GGTCCGTGTTTCAAGACGG

* f = forward primer (positive strand), r = reverse primer (negative strand), ss = primer in the ssrRNA gene, ls = primer in the large subunit rRNA gene.

Approach and aims

Weiss and Becnel (2014) suggested that the combined use of traditional morphological and ecological characteristics with molecular phylogeny is the most suitable method for identifying known, and describing new microsporidian species, as well as monitoring how these parasites may change with evolutionary time. Therefore, this chapter (Chapter 4) builds on the work in **Chapter 3** (pathological description), to identify the microsporidian infecting smelt in the Thames estuary using molecular techniques. In this chapter, I aim to identify the microsporidian to species level using

polymerase chain reaction (PCR) and DNA sequencing to target and amplify rDNA genes specific to microsporidia. Microsporidians, from the genus *Glugea,* infecting European smelt (*Osmerus eperlanus*) have not been previously sequenced or uploaded to GenBank. Only one rDNA sequence of *G. hertwigi* is available on GenBank, which was extracted and sequenced from infected *O. mordax* (Rainbow smelt). My research, presented in this chapter, will be the first study (as far as I know) to sequence the ssrDNA of a microsporidian infecting European smelt (*O. eperlanus*).

4.2 Methodology

<u>Study site and smelt sample collection</u>

Approximately 10 infected juvenile smelt collected during the EA surveys in September 2018 from Chiswick and Battersea (Figure 4.1) were preserved in 100% ethanol for molecular analysis (See details on sample collection in Chapter 3).

Approximately 207 smelt had been collected during 15-minute midwater and benthic trawls (80mm cod end with 16 mm insert) at Erith in the River Thames in March, June, October and December 2019, and March, July and September 2020 (Appendix 3. Table A3.7). These samples were collected by Alex McGoran who is investigating the movement of microplastics up the food web in the River Thames.

McGoran noted 52 fish were potentially infected with a microsporidian, due to the presence of white cysts in the gut. Of these, twenty infected fish samples were sent to me for analysis that had been caught between March and September 2020 (Appendix 4. Table A4.1). Samples were immediately frozen at -20°C. Following dissection, samples were stored in 100% ethanol.

Figure 4. 1. Graphic representation of the tidal limit of the River Thames from the English Channel to Teddington lock. Red dots represent EA sampling locations at Battersea and Chiswick. The green dot represents the sampling at Erith.

Map adapted from map created at http://magic.defra.gov.uk/MagicMap.aspx.

Microsporidian cyst collection from preserved samples

Prior to dissection, all surfaces were wiped down with a 10% bleach solution and routinely wiped with 70% ethanol. All instruments were rinsed in 10% bleach and then rinsed in Milli-Q water. Cyst extraction was repeated numerous times to provide enough DNA to firstly optimise the DNA extraction method, and then for PCR optimisation and troubleshooting. Approximately 0.1-0.4 g of cyst tissue was dissected from two to six randomly selected infected smelt which had been stored at room temperature, together in one sample pot in 100% ethanol. Cyst tissue samples were pooled together to achieve a sample weight between 0.1-0.4 g. The spores/cyst tissue was rinsed in Milli-Q water, with repeated centrifugation (3 times) at 4000 x g for 1 minute to remove any ethanol residue.

Microsporidian DNA extraction

All DNA extractions were performed in a dedicated molecular laboratory. Filter tips were used for all pipetting to reduce the risk of any cross contamination. The DNeasy PowerSoil Kit (Qiagen) was used for DNA extraction. While previous authors, such as Lovy *et al.* (2009) have used standard tissue extraction kits for microsporidian genomics, the PowerSoil kit had been recommend for use at an environmental DNA (eDNA) scientific conference (Rupert Collins, pers.comm). The kit was suggested to be better at breaking down hard cyst walls, and for potential future use to detect

91

microsporidians spores in water samples. The rinsed spores/cyst tissues were transferred to the PowerBead tubes (provided in the kit) and 60 μl of C1 buffer (sodium dodecyl sulfate) was added. PowerBead tubes contain garnet beads and a buffer (guanidinium thiocyanate) to assist in tissue breakdown. Lysis efficiency was tested by leaving spore samples in a 37 °C heating block for 10 minutes, 30 minutes,1 hour and overnight, prior to homogenization in the tissue lyser. Final results suggested 1 hour in the heating block produced sufficient lysis, so all tissue samples were placed in a heating block at 37 °C for approximately 1 hour before being shaken in a tissue lyser (TissueLyser II Qiagen) for 5 minutes at 30 Hz. Next, the standard protocol (Fig. 4.2) from the DNeasy PowerSoil kit was followed, resulting in a 100 μl elution of each sample. The DNA concentration of each extracted sample was then measured on a NanoDrop One/One^C Microvolume UV-Vis Spectrophotometer (Thermo Scientific). The DNA sample with the highest DNA concentration was then selected to be used as the template DNA for PCR (See Appendix 4. Table A.3 for DNA concentrations for each extraction). Initial PCRs and optimisations were performed using template DNA from microsporidian samples collected in 2018.

DNA extraction from infected smelt samples caught in 2020 followed the same method as above, however following lysis in the heating block, I noticed that some cyst material was still visible and placed the tubes in the tissue lyser for a further 5 minutes at 30 Hz.

Prepare sample		Add sample to PowerBead Tube Add 60 µl Solution C1 Place in heating block for 1 hour at 37°C Attach to tissue lyser Vortex for 5 mins at 30 Hz
		Centrifuge tubes at 10 000 x g for 30 s
Cell lysis		Transfer supernatant (450 – 500 µl) to clean 2 ml tube Add 250 µl Solution C2 and vortex for 5 s Incubate at 2-8°C for 5 min
		Centrifuge tubes at 10 000 x g for 1 min
Inhibitor Removal Technology		Transfer up to 600 µl of supernatant to a clean 2 ml tube (avoid pellet) Add 200 µl Solution C3, vortex briefly Incubate at 2-8°C for 5 min
		Centrifuge tubes at 10 000 x g for 1 min
Bind DNA		Transfer up to 750 µl of supernatant to a clean 2 ml tube (avoid pellet) Shake to mix Solution C4, then add 1200 µl to supernatant (vortex for 5 s) Load 675 µl onto an MB Spin Column
		Centrifuge tubes at 10 000 x g for 1 min – discard flow through Repeat previous step until all of the sample has been processed
Wash		Add 500 µl Solution C5
		Centrifuge tubes at 10 000 x g for 30 s – discard flow through Centrifuge again at 10 000 x g for 1 min
Elute		Carefully place spin column onto a clean 2 ml tube Add 100 µl Solution C6 to the center of the white filter membrane Centrifuge at room temperature at 10 000 x g for 30 s – discard spin column 100 µl DNA now ready for downstream application

Figure 4. 2. Diagram showing the DNeasy PowerSoil Kit Protocol (Adapted from Qiagen, 2017)

PCR method development

First trial PCR primers, PCR troubleshooting and optimisation

Fish pathology experts at the EA National Fisheries Laboratory tentatively identified the microsporidian infecting Thames smelt as *Glugea hertwigi,* based on the morphological presentation of the disease alone and taking into account historical findings of this microsporidian species in smelt from other European rivers (Weissenberg, 1913; Sendek & Bogdanov, 2019; Pekcan-Hekim, Rahkonen & Horppila, 2005; Costa, Melo-Moreira & De Carvalho, 2016) and infecting *O. mordax* in North America (Lovy et al., 2009; Haley, 1954). Therefore, I wanted to find primers used for sequencing *G. hertwigi* to confirm or refute this assumption. When I was

conducting this research there was only one listed sequence (ssrDNA) for *Glugea hertwigi* in GenBank, extracted from infected *O. mordax* (Rainbow smelt) from Prince Edward Island, Canada (Lovy et al., 2009). My initial primer selection was based on the methods associated with the Lovy study (Lovy et al., 2009). The primers used by Lovy, were originally suggested by Vossbrinck *et al.*, (2004b) to amplify the ssrDNA in microsporidians. PCR reactions targeted approximately 1800 bp of the ssrDNA and were amplified with the following primers (Fig. 4.3); 18f (5'-CACCAGGTTGATTCTGCC-3),1492r (5'-GGTTACCTTGTTACGACTT-3'), 530f (5'-GTG CCA GCC GCC GCG G-3') and 580r (5'-GGT CCG TGT TTC AAG ACG G-3') (Vossbrinck et al., 2004). These primer pairs are also considered "universal" in terms of their ability to amplify unknown rRNA genes of microsporidia (Valenčáková & Sučik, 2020).
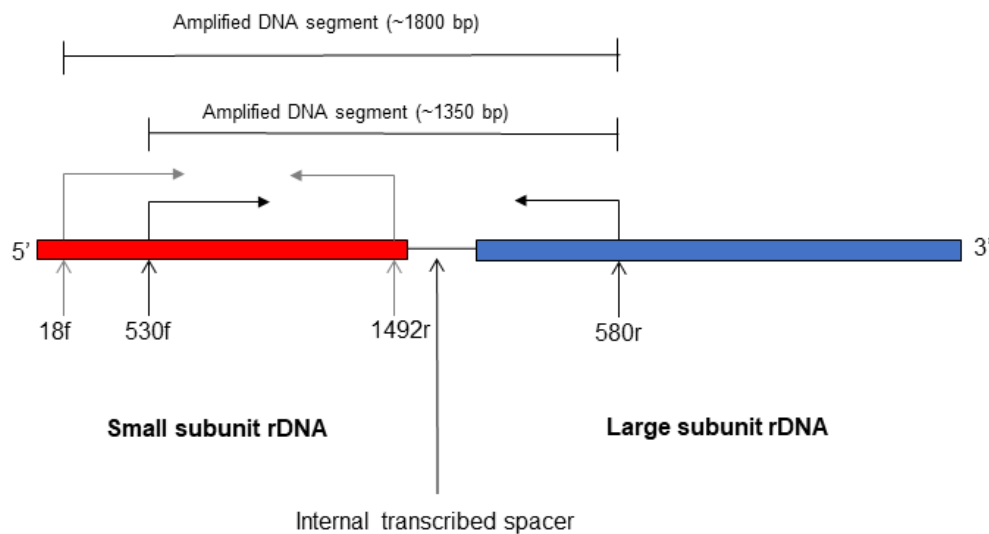
Figure 4. 3. Diagram of the small and large subunit rDNA with the internal spacer. Primer sites shown of 18f, 530f, 1492 and 580r. (Diagram adapted from Vossbrinck *et al.*, 1993)

The first PCR reactions I performed in 25 µl reactions using 1X Promega Master Mix (Promega), 10 µM of each primer (18f, 1492f, 530f and 580r), 5 µl DNA template and 6.5 µl nuclease-free water. The cycling conditions started with an initial activation at 95 °C (5 min), then 35 cycles of denaturation at 95 °C (1 min), annealing at 50 °C (30 s) and extension at 72 °C (2 min) followed by a final extension at 72 °C (10 min). The amplified products were visualised with 5X loading buffer (Bioline) on a 2% agarose

gel (1X TBE (Tris-Borate-EDTA)) stained with GelRed (Fig.4.4). Two bands could be seen but were very faint for the 18f and 1492r primer set, while two smeared bands could be seen for the 530f and 580r primer set (1600 and 1400 bp), suggesting that conditions were not optimised.

Figure 4. 4. PCR products for each set of primer pairs (18f & 1492r, and 530f &580r). The ladder on the right-hand side is a Hyperladder 50bp (Bioline). Red lines highlight the bands produced in the gel. Red arrows show the size in base pairs.

One potential issue raised was the range of strand-melting temperatures of the primers, which ranged from 53.1 – 77.6 °C. The melting temperatures of 18f and 1492r were 61.8°C and 53.1°C, while the melting temperatures of 530f and 580r were 77.6°C and 65.6°C, respectively. As a result, I chose to optimise the18f and 1492r, as they had a smaller temperature range, which I believed would be easier for optimisation. A number of separate PCRs were then run each adjusting one condition to try and optimise the PCR. These included adjusting the number of cycles, extension time, the annealing temperature, the primer concentration, and the quantity of DNA template (see Appendix 4. Table 4.4 for PCR trial conditions and results). The first optimisation I tried was to increase the number of cycles from thirty-five to thirty-nine to increase the PCR products. Increasing the number of cycles above thirty-five can increase secondary products (Lorenz, 2012), but as a second band was already visible, I

thought this was unlikely to add more products. I then reduced the extension time to 1.5 minutes. The extension or elongation step timing and temperature depends on the DNA polymerase used in the reaction (Lorenz, 2012). Optimal temperature for use with *Taq* polymerase (included in Promega Mastermix) is 70 - 80°C, with a time of 1 minute needed to elongate the first 2000 bp, and an additional minute for each additional 1000 bp amplified (Lorenz, 2012). As the expected DNA fragment size for amplification based on my primers was under 2000 bp, it was hoped that reducing the extension time would optimise the PCR. Unfortunately, two bands were still visible, so the next condition to adjust was the annealing temperature. The annealing temperature allows for optimal annealing of the primers, and therefore cannot be higher than the melting point of each primer. The annealing temperature was increased from 52 °C to 53 °C, which was just below the melting temperature of 1492R (53.1 °C). Following failure to remove the second band, I tried diluting the primer stock from 10 µM to 5 µM. It was hoped that if the primer concentration was reduced, mispriming would be reduced and only amplify one specific band. However, using 5 µM primer stock resulted in no bands visualised in the gel, suggesting in was an inefficient PCR reaction. I then tried further reducing the annealing time to 1 minute, however I could still visualise two bands in the gel. A final attempt was made using the PCR conditions suggested by Vossbrinck *et al.* (2004), however two bands were still visible.

Following the above-mentioned failed attempts to remove the second amplified band, I decided to try manual DNA extraction from the gel. Extracting bands from the gel allows for DNA to be isolated and purified based on size. This technique is commonly used in molecular labs for sequencing, cloning and restriction digestions. Both bands were cut from the gel under UV light and then processed using the MinElute gel extraction kit (Qiagen). The resulting DNA quantity was between 22 – 48 ng/ml. The minimum quantity of DNA required for Sanger sequencing was 1300 ng/ml. Therefore, even multiple extractions would not yield sufficient DNA for sequencing. While some authors were able to sequence the amplified DNA directly after PCR using primers 18f, 1492r, 530f and 580r (Ryan & Kohler, 2016), others, such as Lovy *et al.* (2009) used a cloning vector following gel extraction. Due to limited time for the project, it was decided to identify new primers rather than continue with those from the Lovy (2009) and Vossbrinck (2004) publications .

Final primer selection and PCR conditions

Following a lack of DNA amplification with the Lovy/Vossbrinck primers, new primers were selected based on the work by Pomport-Castillon, De Jonckheere & Romestand (2000). PCR amplification to target overlapping regions along the SSU rDNA were performed using the forward primer 5'-GGTTGATTCTGCCTGACGT-3' (which I will refer to as Bf) (Baker et al., 1994), the reverse primer 5'-GACGGGCGGTGTGTACAAAG-3' (which I will refer to as Vr) (Vossbrinck et al., 1993) and reverse primer 580r (Vossbrinck et al., 2004). I expected approximately 1200 bp to be amplified using primers Bf and Vr, and approximately 1800 bp to be amplified using primers Bf and 580r.

PCR reactions were carried out in 50 µl reactions using 1X Promega Master Mix (Promega), 10 µM of each primer, 5 µl DNA template and 18 µl nuclease-free water. Amplification conditions were started with an initial activation at 94 °C (3 min), then 30 cycles of denaturation at 94 °C (1 min), annealing at 55 °C (1.5 min) and extension at 72 °C (2 min) followed by a final extension at 72 °C (5 min). The amplified products were visualised on a 2% agarose gel (1 X TBE) stained with GelRed (Fig.4.5). One clear band was visible for each set of primers (Bf & Vr; Bf & 580r), meaning that the only one DNA target was amplified with the primers. The Bf and Vr primer set showed a clear, bright band and the Bf and 580r showed a faint, but clear band.

Figure 4. 5. PCR products for each set of primer pairs (Bf & Vr, and Bf & 580r). The ladder on the right-hand side is a Hyperladder 50bp (Bioline). Red arrows show the size in base pairs.

Preparation for sanger sequencing

Ten PCR reactions were performed using primers Bf and Vr, and template DNA extracted from microsporidian cysts in infected smelt from 2018. The amplified PCR products were pooled to create three samples, which were then cleaned using a PCR and DNA Clean-up Kit (Monarch T10305) and produced a final elution of 10 µl clean DNA (3 x 10 µl). DNA concentration of each sample was then measured (in duplicate) on a Qubit 3.0 with the Qubit dsDNA HS assay kit. DNA samples and associated primers were sent to the Natural History Museum (NHM) for Sanger Sequencing. PCR amplicons received by the NHM Sequencing Facility were required to have an accompanying sample sheet, including information concerning sample name(s), fragment size, primer and primer concentration. Samples were first purified using AppMag magnetic PCR beads and concentrations of each purified sample measured using a Nanodrop 8000 DNA spectrophotometer. Forward and reverse samples were then set up for sequencing using Applied Biosystems BigDye Terminator Kit V3.1 and cycled on a thermo cycler, following manufacturers guidelines. Samples were then further purified to remove unincorporated dye using AppMag Dye Terminator Removal

Magnetic Beads. Purified reactions were sequenced on an AB 3730xl capillary DNA Analyser (Applied Biosystems).

Following successful sequencing of the microsporidian DNA extracted from infected smelt collected in 2018, the process was repeated for microsporidian DNA extracted from infected smelt collected in 2020. Ten PCR reactions were performed using primers Bf and Vr, and three PCR reactions were performed using primers Bf and 580r (see Appendix 4 Table A.4.5 for PCR conditions and gel results). DNA clean-up was performed, and samples were sent for Sanger sequencing. Table 4.2 shows the DNA concentrations of each sample following clean-up. The sample column refers to the DNA extracted from infected smelt caught in 2018 and samples caught in 2020. The final DNA concentrations of replicate samples from 2020 (2020.1, 2020.2 & 2020.3) were much greater than the 2018 sample (2018.1, 2018.2 & 2018.3) concentrations; suggesting that the additional tissue lysing step conducted during the DNA extraction of the 2020 samples (additional 5 minutes at 30 Hz in the tissue lyser) assisted in breaking down the cysts and releasing DNA.

Table 4. 2. DNA concentrations (in duplicate) (ng/µl) following clean-up, including the primer set used in PCR reactions.

Date	Sample	Primers	Concentration (ng/µl)
08/02/2021	2018.1.1	Bf & Vr	13.4
08/02/2021	2018.1.2	Bf & Vr	13.3
08/02/2021	2018.2.1	Bf & Vr	12.1
08/02/2021	2018.2.2	Bf & Vr	12.4
08/02/2021	2018.3.1	Bf & Vr	13.8
08/02/2021	2018.3.2	Bf & Vr	14.3
27/05/2021	2020.1.1	Bf & Vr	70.4
27/05/2021	2020.1.2	Bf & Vr	68.9
27/05/2021	2020.2.1	Bf & Vr	67.2
27/05/2021	2020.2.2	Bf & Vr	66.9
27/05/2021	2020.3.1	Bf & Vr	63.5
27/05/2021	2020.3.2	Bf & Vr	62.5
07/06/2021	2020.4.1	Bf & 580r	21.2
07/06/2021	2020.4.2	Bf & 580r	21.1
07/06/2021	2020.4.3	Bf & 580r	21.0

Bioinformatics: consensus sequences and phylogenetic analysis

Raw sequence reads obtained after Sanger Sequencing were analysed using Geneious Prime (2021.2.1). Reads were first trimmed to remove any low-quality

regions at both ends of the read. The Heterozygote Finder tool was also used to annotate any bases where two different nucleotides were found at the same position and annotated if peak similarity was above 50%. Sequence reads were then aligned using the Geneious aligner (which uses progressive pairwise alignment) with default parameters. The consensus alignments were viewed, and heterozygote bases were edited to the original base from the original sequences. Two consensus sequences were extracted to represent the samples from 2018 and 2020.

A BLASTn search was then performed in Geneious Prime to compare the generated sequences against known microsporidian sequences in GenBank. Sequences were then selected to use for phylogenetic analyses based on their similarities to my generated sequences using their grade (A weighted score based on the pairwise identity and coverage) and host species (fish). The pairwise identity represents the pairwise residues that are identical in the alignment. The selected sequences had a grade ≥93%. *Spraguea sp.* Sdu-2008 (AB623034) was selected as an outgroup, as the sequence represented a fish-infecting microsporidian which is genetically distinct from the other sequences (Ryan & Kohler, 2016).

BioEdit (version 7.2.5 12/11/2013) and MEGA 11 were used to produce a phylogenetic tree. Using BioEdit, selected sequences (Table 4.3.) and my two sample sequences were aligned using the ClustalW multiple alignment with 1000 bootstrap. The alignment was then cropped to have the same sequence length across species. Early tests suggested that a maximum likelihood method using Tamura-Nei distance would best fit the data based on maximum likelihood fits of 24 different nucleotide substitution models. The phylogenetic tree was constructed using maximum likelihood and Tamura-Nei distance (Tamura & Nei, 1993), with 1000 bootstrap replicates. The initial tree was created by applying the Neighbor-Join and BioNJ algorithms to a matrix of pairwise distances estimated using the Maximum Composite Likelihood (MCL) approach. A discrete Gamma distribution was used to model the evolutionary rate differences among sites (5 categories (+G, parameter =0.2843)).

The sequences produced from this study (*Glugea* sp. UK 2018, *Glugea* sp. UK 2020) were then compared to a subset of other *Glugea* sequences from GenBank using p-distance and percentage identity using the Kimura-2 substitution model.

Table 4. 3. The list of microsporidian species used to construct phylogenetic trees, with their assigned GenBank accession numbers, size of sequence and source.

Microsporidian	Host	GenBank accession number	Aligned bases	Study or source
Glugea anomala	*Gasterosteus aculeatus*	AF056016	1165	Pomport-Castillon *et al.* 2000
Glugea anomala	*Gasterosteus aculeatus*	AF044391	1865	Nilsen *et al.* 1998
Glugea anomala	*Unknown*	AB923879	1775	GenBank
Glugea eda	*Caesio striata*	MK568064	1564	Mansour *et al.*, 2016
Glugea epinephelusis	*Epinephelus awoara*	AY090038	1326	GenBank
Glugea gasterostei	*Gasterosteus aculeatus*	KM977990	1305	Tokarev *et al.*, 2015
Glugea hertwigi	*Osmerus mordax*	GQ203287	1856	Lovy *et al.*, 2009
Glugea plecoglossi	*Sardina pilchardus*	KY882286	1813	GenBank
Glugea plecoglossi	*Seriola dumerili*	AB623035	1726	Miwa *et al.*, 2011
Glugea sp.	*Epinephelus polyphekadion*	KT005391	1763	Azevedo *et al.*, 2016
Glugea sp.	*Lutjanus bohar*	KP262018	1234	GenBank
Glugea sp.	*Epinephelus awoara*	AY090038	1326	GenBank
Glugea sp.	*Sardinella aurita*	MT072043	1679	GenBank
Glugea sp. CCG1	*Cottus cognatus*	KU885382	1768	Ryan & Kohler, 2016
Glugea sp. CSI-2020	*Sardinella aurita Valenciennes*	MT680621	1110	GenBank
Glugea sp. GC 2015	*Cephalopholis hemistiktos*	KJ802012	1782	Abdel-Baki *et al.*, 2015
Glugea sp. UK 2018	*Osmerus eperlanus*	-	1108	Present study
Glugea sp. UK 2020	*Osmerus eperlanus*	-	1102	Present study
Glugea sp.GC 2015	*Serranus atricauda*	KU363832	1820	GenBank
Glugea stephani	*Gasterosteus aculeatus*	AF056015	1165	Pomport-Castillon *et al.* 2000
Heterosporis anguillarum	*Anguilla japonica*	AF387331	1810	Tsai *et al.*, 2002
Ichthyosporidium weissii	*Clevelandia ios*	JQ062988	1783	Sanders *et al.*, 2012
Loma acerinae	*Gymnocephalus cernuus*	AJ252951	1312	Cheney *et al.*, 2001
Loma acerinae	*Atherina mochon pontica*	KT934810	1229	GenBank
Loma acerinae	*Neogobius fluviatilis*	KT964890	1229	GenBank
Loma acerinae	*Gymnocephalus cernuus*	AF356224	1322	Pekkarinen *et al.* 2002
Loma psittaca	*Colomesus psittacus*	FJ843104	1258	Casal *et al.*, 2009
Loma sp. SVB-PE3 (SV-1)	*Salvelinus fontinalis*	HM626217	1805	Brown *et al.* 2010
Microsporidia sp.	*Gymnocorymbus ternetzi*	MW077214	1286	Lovy, 2021
Microsporidium sp. STF	*Salmo trutta fario*	AY140647	1432	GenBank
Pleistophora sp.	*Alepes djedaba*	KF830721	1243	GenBank
Pleistophora sp.3	*Taurulus bubalis*	AF044390	1879	Nilsen *et al.* 1998
Spraguea sp. Sdu-2008	*Seriola dumerili*	AB623034	1799	Miwa *et al.*, 2011

4.3 Results

Consensus sequences

The microsporidian rDNA consensus sequence of the first sample sequenced (UK 2018) was 1182 bp in length (Fig. 4.6). The second sample microsporidian rDNA (UK 2020) was 1167 bp in length (Fig. 4.7).

The two consensus sequences had a pairwise identity of 99.3% with 1156 identical sites, suggesting that they represented the same microsporidian species in both samples. There were 8 nucleotide differences between the two sequences.

```
   1 cagcgaagcg taagtggagc ggcgcaaggc tcagtaacgg gcgagtattt gatctcctag
  61 agtggatatc ctctgtaacc ggagggcaaa acacaagatg agcgattgac gaggtcgttc
 121 gtttaacgaa tagtgtagga gagtaaaaag ccatcccatc agttagtgag tagggtaagg
 181 gcctacttaa acgaagacgg gtacggggaa ttatcgtttg attccggaga gggagcctga
 241 aagacggcta ccaggtccaa ggacagcagc cggcgcgaaa attaccgcag cctgcgttca
 301 gggcggtagt aaggagacgt gaaaacaatg tgcgggcaaa aaacgcacta aatacaggag
 361 gacaagactg gtgccagcac ccgcggtaat accagctcct ggagtgtcta tgatgattgc
 421 tgcatttaaa gagttcgtag tcgaagtggt tataacggtg taacaggcct tctctcaagg
 481 agggttatgc gccgtgattc catggaataa ggagcgttta ggggccaggt tattaagcga
 541 cgaggggtga aatctggtga ctcgcttagg agcaacagag gcgaaagcgc tggccaggag
 601 cgaatccgat gataaaggac gtaggctaga ggatcgaaga cgattagaga ccgttgtagt
 661 tctagcagta aacgatgccg ataccgtggt gcggatacgc gacgcggaag agaaatcgag
 721 tagggccctg gggagagtac acgcgcaagc gagaaattta aaggaaattg acggaagaac
 781 accacaagga gtggagtgtg cggcttaatt tgactcaacg cgggacagct taccaggccc
 841 gacggccgga cgagtgttgt acacgatagg tcgaagagtg gtgcatggcc gttaacgacg
 901 agtgaggtga cttttgggtt aaatccggga agtagtgaga cccctaccga aagggacagg
 961 tgccgaaagc acaggaagga agggtcaaga acaggtcagt gatgccctca gatggtctgg
1021 gctgcacgcg cactacagtg gtcatagaaa tgaaacgata gaattaaaga tgatcgagag
1081 ggacatgagc tttgtaagag gctcacgaac gaggaattgc tagtaatcgc ggactcatta
1141 agacgcgatg aatacgtccc tgttctttgt acacacccgc cc
```

Figure 4. 6. The consensus sequence of *Glugea* sp. UK 2018

```
   1 cggcgcaagg ctcagtaacg ggcgagtatt tgatctccta gagtggatat cctctgtaac
  61 cggagggcaa aacacaagat gagcgattga cgaggtcgtt cgtttaacga atagtgtagg
 121 agagtaagaa gccatcccat cagttagtaa gtagggtaag ggcctactta aacgaagacg
 181 ggtacgggga attatcgttt gattccggag agggagcctg aaagacggct accaggtcca
 241 aggacagcag ccggcgcgaa aattaccgca gcctgcgttc agggcggtag taaggagacg
 301 tgaaaacaat gtgcgggcaa aaaacgcact agatacagga ggacaagact ggtgccagca
 361 cccgcggtaa taccagctca tggagtgtct atgatgattg ctgcagttaa agagttcgta
 421 gtcgaagtgg ttataacggt gtaacaggcc ttctctcaag gagggttatg cgccgtgatt
 481 ccatggaata aggagcgttt aggggccagg ttattaagcg acgaggggtg aaatctggtg
 541 actcgcttag gagcaacaga ggcgaaagcg ctggccagga gcgaatccga tgataaagga
 601 cgtaggctag aggatcgaag acgattagag accgttgtag ttctagcagt aaacgatgcc
 661 gataccgtgg tgcggatacg cgacgcggaa gagaaaatcg agtagggccc tggggagagt
 721 acacgcgcaa gcgagaaatt taaaggaaat tgacggaaga acaccacaag gagtggagtg
 781 tgcggcttaa tttgactcaa cgcgggacag cttaccaggc ccgacggccg gacgagtgtt
 841 gtacacgata ggtcgaagag tggtgcatgg ccgttaacga cgagtgaggt gacttttggg
 901 ttaaatccgg gaagtagtga gacccctacc gaaagggaca ggtgccgaaa gcacaggaag
 961 gaagggtcaa gaacaggtca gtgatgccct cagatggtct gggctgcacg cgcactacag
1021 tggtcataga aatgaaacga tagaattaaa gatgatcgag agggaatgag ctttgtaaga
1081 ggctcaggaa cgaggaattg ctagtaatcg cggactcatt aagacgcgat gaatacgtcc
1141 ctgttctttg tacacacccg ccccgtc
```

Figure 4. 7. The consensus sequence of *Glugea* sp. UK 2020

Phylogenetic analysis

The *Glugea* sp. rDNA isolates from smelt reported in my study varied by less than 2% from eight other microsporidian sequences previously identified as *Glugea* species in GenBank (Table 4.4). I suggest that the species infecting smelt (*O. eperlanus*) in the River Thames is placed in the genus, *Glugea*. These sequences will be referred to as Glugea sp. UK 2018 and Glugea sp. UK 2020.

The generated phylogenetic tree (Figure 4.8.) represents the highest log likelihood of -13873.73 and had a total of 4528 positions. The tree is drawn to scale, with branch lengths measured in the number of substitutions per site. My sequences clustered together, suggesting that they represent the same species. My sequences were placed in a main clade with 12 other species of *Glugea* with a 99% bootstrap support, highlighted by the blue box. Bootstrapping values between individual species of *Glugea* within this clade were low, suggesting that there is little genetic variation between species.

Furthermore, clustering of *Glugea* clades was seen to represent geographic regions. The microsporidians most closely related to my isolates, highlighted by the blue box, were identified in countries in Europe, North America and the Baltic regions, except

for *Glugea sp.* CSI-2020a (MT680621) which was reported in *Sardinella aurita* off the Algerian coast and *G. plecoglossi* (AB623035) reported in *Seriola dumerili* off the coast of Japan (Table 4.5). The *Glugea* clade highlighted in the red box represented isolates mainly found in the Red Sea and Saudi regions.
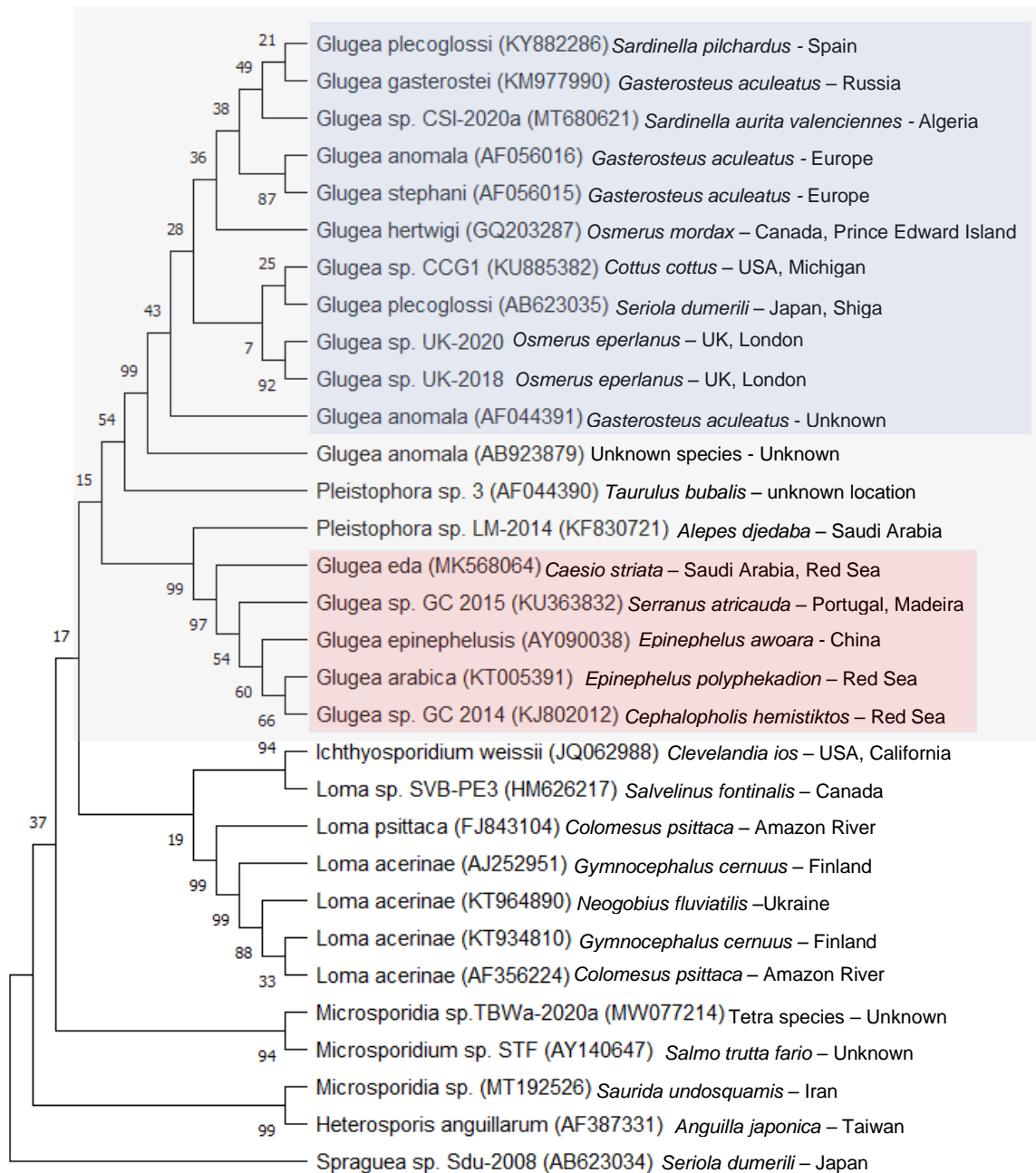
Figure 4. 8. Maximum likelihood phylogenetic tree including 31 rDNA sequences of fish infecting microsporidian species. GenBank accession numbers are included in parentheses, followed by host species and location of sample. Bootstrap probabilities are shown next to branches (%). The light grey shading highlights the main *Glugea* clade with then branches into two major sub-glades. Within the sub-glades, *Glugea* species mainly found in North America and European regions are highlighted in blue and *Glugea* species mainly found in the Red Sea and Saudi regions are highted in red.

Table 4. 4. Percent identity (bottom left diagonal) and pairwise identity (top right diagonal) for *Glugea* microsporidians with a percent identity of > 97% with the microsporidian samples from my study (7 & 8, highlighted in grey).

	Species (GenBank accession number)	1	2	3	4	5	6	7	8	9	10
1	Glugea sp. CSI-2020a (MT680621)	-	0.0046	0.0125	0.0008	0.0075	0.0083	0.0073	0.0110	0.0076	0.0048
2	Glugea plecoglossi (KY882286)	99.86	-	0.0133	0.0008	0.0067	0.0090	0.0064	0.0101	0.0033	0.0000
3	Glugea sp. CCG1 (KU885382)	98.91	99.04	-	0.0088	0.0192	0.0192	0.0148	0.0185	0.0082	0.0121
4	Glugea gasterostei (KM977990)	99.64	99.68	98.72	-	0.0039	0.0031	0.0083	0.0120	0.0062	0.0008
5	Glugea hertwigi (GQ203287)	99.36	99.5	98.63	99.18	-	0.0133	0.0092	0.0129	0.0073	0.0072
6	Glugea anomala (AF044391)	99.09	99.23	98.36	99.09	98.82	-	0.0092	0.0129	0.0127	0.0091
7	Glugea sp. UK-2020	99.27	99.41	98.54	99.09	99.00	98.73	-	0.0064	0.0101	0.0064
8	Glugea sp. UK-2018	98.56	98.69	97.84	98.38	98.29	98.02	99.10	-	0.0138	0.0101
9	Glugea plecoglossi (AB623035)	98.91	99.05	98.37	98.73	98.64	98.37	98.73	97.94	-	0.0035
10	Glugea sp. (MT072043)	99.86	99.95	99.04	99.68	99.50	99.22	99.40	98.69	99.04	-

Table 4. 5. Closely related *Glugea* species, their host species and the geographic regions where they were reported.

Glugea species (GenBank Acc.)	Host species	Geographic region	Study or source
Glugea sp. CSI-2020a (MT680621)	*Sardinella aurita Valenciennes*	Algerian coast	GenBank
Glugea plecoglossi (KY882286)	*Sardina pilchardus*	Atlantic - Spain	GenBank
Glugea sp. CCG1 (KU885382)	Cottus cognatus	USA - Michigan	Ryan & Kohler. 2016
Glugea gasterostei (KM977990)	*Gasterosteus aculeatus*	Russia: Saint-Petersburg	Tokarev et al. (2015)
Glugea hertwigi (GQ203287)	*Osmerus mordax*	Canada - Prince Edward Island	Lovy & Peckova (2009)
Glugea anomala (AF044391)	*Gasterosteus aculeatus*	Unknown	Nilsen et al. 1998
Glugea sp. UK-2020	*Osmerus eperlanus*	UK - London, River Thames	This study
Glugea sp. UK-2018	*Osmerus eperlanus*	UK - London, River Thames	This study
Glugea plecoglossi (AB623035)	*Seriola dumerili*	Japan: Shiga	Miwa et al. 2011
Glugea sp. (MT072043)	*Sardinella aurita Valenciennes*	Atlantic - Spain	GenBank

4.4 Discussion

<u>Primer selection and PCR optimisation</u>

The results of this study highlight a number of important aspects for using ssrRNA sequence data to identify microsporidian species. Although, 'universal primers' (530f &580r, 18f & 1942r) have been proposed for microsporidians, the results of my PCR trials suggest that the amplification of all microsporidian species using these primers may not always be successful. While the primers (530f &580r, 18f & 1942r) did amplify PCR products from the target genome, the amplification of a second, non-specific band suggests that the primers may not be specific enough for every microsporidian. Some authors have had success with these primers for direct sequencing following PCR (Ryan & Kohler, 2016), while Lovy *et al.* (2009) extracted amplified products from a gel and then cloned them into a cloning vector. Lovy *et al.* (2009) did not report issues with the primers, so it is possible that the cloning vector may have been used as standard practise for their laboratory or that issues regarding non-specific amplification were not disclosed. I was unable to use a cloning vector due to time

constraints, and therefore was fortunate to be able to find alternative primers (Bf, Vr & 580r) which amplified my target rRNA successfully. Furthermore, sequence comparisons of the 1200 bp fragment showed that amplified products had high sequence identity to the reported consensus sequence. In contrast, the longer sequence reads (i.e., up to 1800 bp using the 580r primer site) were relatively low in sequence identity, suggesting alternative primers must be developed to amplify sequences in the large subunit rRNA due to lack of primer specificity.

Species identification

Based on the morphological findings in **Chapter 3**, the past reports of smelt infections regionally (i.e. in the Baltic) and the phylogenetic analysis using rDNA sequence data, it could be suggested that European smelt from the River Thames are infected with *Glugea hertwigi.* However, from the current data, it seems the situation is slightly more complicated. After comparing my rDNA isolates with closely related sequences shown after a BLAST search in GenBank, the Thames isolates are most closely related to *G. plecoglossi* (KY882286), *Glugea sp.* (MT680621), *G. gasterostei* (KM977990) and *G. hertwigi* (GQ203287) with a range of 98.29 – 99.41% sequence identity. My findings agree with those of Lovy *et al.* (2009) who found that their sequence of *G. hertwigi* was very closely related to *G. anomala, G. atherinae, G. plecoglossi* and *G. stephani.* Numerous authors have hypothesized that the small variations between rDNA sequences may suggest that these different *Glugea* species may represent local isolates of a single species (Ryan & Kohler, 2016). Species have usually been named based on host species and geographic location, however this may be misleading in terms of the apparent diversity within the group.

The phylogenetic tree (Figure 4.8.) showed two distinct clades of *Glugea* species. I reviewed the host species and geographic location of infections (see Appendix 4 Table 4.6). The first clade (highlighted in blue) represented *Glugea* species mainly from North America and European regions, while the second clade (highlighted in red) represented isolates from the Red Sea and Saudi regions. I suggest that the variations seen may be representative of geographic location and some type of local adaptation.

Recent studies which have combined morphological and phylogenetic data have highlighted that individual taxa show significant plasticity in their morphological traits,

making classification difficult (Stentiford et al., 2013b, 2013a). New research has proposed that the site of infection (tissue type) within a host may also be a factor defining the relationship between microsporidian taxa (Stentiford et al., 2013b). Pomport-Castillon, De Jonckheere and Romestand (2000) suggested that *G. anomala, G. stephani* and *G. atherinae* may in fact be one species presenting slightly differently in different host species. Most *Glugea* species infect specific hosts and therefore further experimental work would be needed to assess if cross-transmissions are possible in other hosts (Lovy et al., 2009). Certain *Glugea* species have been commonly reported in multiple host species within the same genus, such as *G. hertwigi* reported in *O. eperlanus* and *O. mordax* (Lovy et al., 2009; Costa, Melo-Moreira & De Carvalho, 2016), *G. stephani* in *Pleuronectes platessa* (plaice) and *P. americanus* (winter flounder) (Cali et al., 1986; McVicar, 1975), and an unidentified *Glugea* species in *Nothobranchius korthausae*, and *N. eggersi* (Lom, Noga & Dykova, 1995). However, some of these *Glugea* species also infect other genera within the same family, such as *G. stephani* reported in other members of the Pleuronectidae, such as *Parophrys vetulus* (English sole) (Olson, 1981). This raises the question of potential cross infection between closely related fish species. Highlighting the need to be able to accurately identify microsporidians to the species level to assess potential risks to other fish populations.

Based on the literature and current classifications of *Glugea* species, it is apparent that the boundaries of species classification are not well defined. The majority of studies to taxonomically classify *Glugea* species have been based on ssrDNA with relatively small sequence lengths. More genes need to be sequenced to fully understand the genetic relationships between reported species. Limitations for reporting novel species has been noted and alternative approaches have been suggested, such as the use of non-ribosomal protein coding genes (Vossbrinck & Debrunner-Vossbrinck, 2005). A review by Stentiford *et al.* (2013b) on microsporidia in aquatic systems suggested that using alternative regions of the genome to establish relationships between microsporidia taxa. My study is the first to provide genetic data for a *Glugea* species infecting European smelt. *G.* hertwigi infections in European smelt have been reported from Baltic regions, however these studies identified the parasite via morphology alone, and did not provide molecular data or analysis (Costa, Melo-Moreira & De Carvalho, 2016; Pekcan-Hekim, Rahkonen & Horppila, 2005).

Future work could aim to gather samples from multiple European locations to establish the evolutionary placement and genetic variation of this parasite in European smelt. Additionally gathering reliable and repeated sequence information (longer reads) would assist in more accurate placement of species within the *Glugea* genus. Furthermore, comparing recent samples of *G. hertwigi* infection in *O. mordax* from the US and Canada, both morphologically and phylogenetically, would allow us to better understand the evolutionary relationship between these microsporidians in Osmerids.

Much work is still needed in the classification of microsporidia as a whole, but this provides an exciting opportunity for developing our understanding of these organisms. The increasing use of molecular techniques and ease at which to extract and sequence rDNA means that correct parasite classification will rely on a combination of morphological and molecular techniques.

Chapter 5. The hydrodynamic drag associated with parasitic disease: Microsporidia in European smelt

Abstract

The microsporidian parasite infecting juvenile smelt in the River Thames presents with large white cysts in the body cavity. These cysts, especially in heavy infections, cause deformities in the natural streamline body shape by creating large bulges, primarily along the dorsal line. I wanted to assess the impact of these infections on the fish's hydrodynamics, especially given their small size and the large numbers of infections observed. Swimming ability is an essential factor for fish survival. I collaborated with two experts to produce three-dimensional virtual models based on the micro-CT imagery produced in Chapter 3. These models were used in computational fluid dynamic (CFD) simulations to calculate surface pressure changes and drag coefficients in smelt with different microsporidian infection levels. To the best of my knowledge, this study is the first to attempt to apply CFD to calculate costs associated with parasitic infection in fish. Fish with the heaviest infections showed the highest pressure at the leading edge of the bulges. The drag (force and coefficient) significantly increased with an increasing volume of cysts. Drag values remained similar for uninfected fish and fish with a cyst burden of less than 10% volume and increased sharply when the volume of cysts was greater than 20%. The application of CFD modelling could be a useful alternative method to study costs associated with parasitic infections over traditional methods, such as swimming flume experiments. These experiments can be costly and have a number of limitations, including the difficulty of keeping certain fish species in aquaria. CFD modelling is an exciting area of research and could help fill the gaps in knowledge on biomechanics associated with parasitic diseases and provide initial data to indicate potential changes in the swimming ability of infected species.

5.1. Introduction

European smelt (*Osmerus eperlanus*) are a priority species of conservation concern in the UK (Colclough, 2013). After significant declines in the past, smelt are beginning to recover in many locations (Colclough, 2013). However, the very obvious and gross infections of this likely novel microsporidian parasite in the UK could be cause for concern for smelt recovery. The large cysts cause deformations in the infected fish's body shape, which distorts their streamlined form and could impact their swimming ability, especially given the small size of the juvenile fish and the level of infection observed (Fig. 5.1). Therefore, following on from my findings in Chapters 3 and 4, I was interested in assessing the impact of the *Glugea* cysts on the swimming ability of infected smelt.
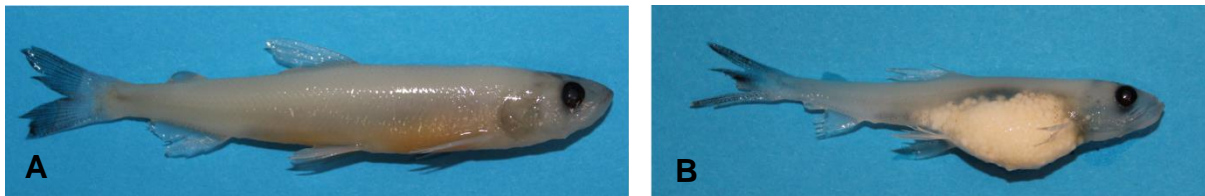
Figure 5. 1 Photographs of formalin-fixed juvenile smelt collected from the River Thames in 09/2018, representing a healthy juvenile (**A**) and a juvenile with a microsporidian infection (**B**) showing a large distortion due to white cysts in the peritoneal cavity. The discolouration of the fish was caused by the formalin fixative and they would naturally be translucent at this age. Photographs were provided by the EA National Fisheries Laboratory.

Swimming performance is a critical factor to fish survival, underpinning feeding ability, predator-prey relationships, spawning migrations and dispersal (Wolter & Arlinghaus, 2003). A large body of literature exists on the study of swimming ability in fish; however, most studies focus on the mechanics of propulsion or assessing fish health or stress based on exercise performance (Reidy, Kerr & Nelson, 2000). Furthermore, body length and shape greatly influence swimming ability, with longer fish achieving higher critical swimming velocities (Hammer, 1995). There are three commonly used methods to test swimming ability in fish. Burst swimming tests record the top speed reached over short periods (<15 s), sustained speed tests measure the top speed that can be maintained indefinitely (>200 min) and prolonged swimming tests, which combines burst speed and sustained speed to reflect how a fish would move through the environment and are measured between 2-200 minutes (Hammer, 1995).

Microsporidian infections have been noted to impact swimming ability in other fish species. Divers performing surveys in Scott Lake, Canada, reported that 3-week-old juvenile fathead minnow (*Pimephales promelas*) infected with *Glugea pimephales* swam in a 'wobbly' manner and struggled to keep up with the rest of the school when dispersed (Forest, King & Cone, 2009)*.* Another microsporidian belonging to the *Spraguea* genus has been reported to cause spiral swimming in Cultured Yellowtail (*Seriola quinqueradiata*) in Western Japan (Yokoyama, Miyazaki & Yoshinaga, 2013). A study on the effect of *Loma morhua* infection on cardiorespiratory performance in Atlantic cod (*Gadus morhua*) was conducted to measure oxygen consumption and swimming performance at critical swimming speeds (Powell & Gamperl, 2016). Powell and Gamperl (2016) found that while the infection reduced cardiac performance and maximum oxygen consumption, it did not negatively impact upper thermal tolerance or critical swimming speed. Authors studying smelt infected with *Glugea* parasites have suggested a likely negative impact on swimming ability; however, quantitative measurements have not been produced. Many studies assessing the 'costs' of parasitic infection to their fish hosts focus on pathological aspects, while few measure the indirect, physical costs that may occur due to host shape and size changes due to infection (Stewart *et al.* 2018).

When swimming, fish need to overcome the drag force exerted by the water, which comprises both frictional drag and form drag (Fig. 5.2). Frictional drag refers to the force caused by the flow of water over the body surface, while form drag is caused by differences between the pressure distribution over a body (Clough & Turnpenny, 2001).
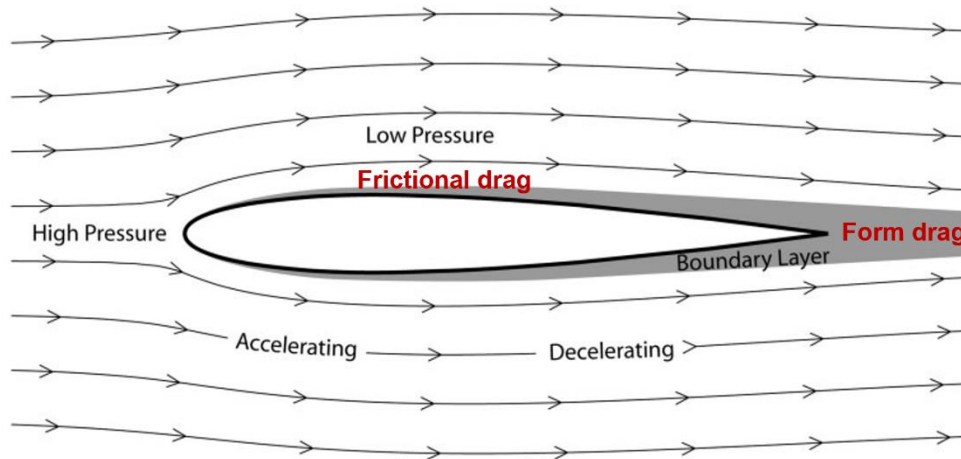
Figure 5. 2 A diagram representing streamlines of flow around a streamlined body. The highest pressure is found at the nose, while the lowest pressure will be found at the widest part of the body. A boundary layer forms as a result of frictional forces (drag force) over the surface of the body. Form drag results from the shape of the body moving through a fluid. (Diagram adapted from Windsor & McHenry, 2009).

In this chapter, I investigate the drag coefficient and surface pressure changes produced by deformities in body shape caused by microsporidian cysts, to assess potential negative impacts associated with increasing disease burden. This work was produced in collaboration with Dr Humberto G. Ferron[3] and Dr Oscar Sanisidro[4]. The micro-computer tomography (micro-CT) imagery, first shown in Chapter 3, were used by O. Sanisidro to create 3D virtual models. Following this, H. Ferron simulated water flow around the derived 3D virtual models utilising computational fluid dynamics (CFD) to calculate drag and pressure. This technique simulates fluid flow and its interaction with solid surfaces in a virtual environment, having been used widely in engineering for decades (Cengel & Cimbala, 2018). However, CFD has only recently begun to be applied in (palaeo) biological sciences, despite its potential to inform organismal function and biomechanics (Liu, 2002; Ferrón et al., 2020). Palaeobiological researchers have estimated the hydrodynamics associated with extinct species with differing morphologies (Kogan et al., 2015; Gutarra et al., 2019). However, to the best of my knowledge, CFD has not been applied to investigate morphological distortions

---

[3] Honorary Research Associate, University of Bristol

[4] Researcher, Biodiversity Institute & Natural History Museum, Kansas University

due to parasite infections in fish. This chapter presents these techniques as a novel method to model hydrodynamic effects associated with disease in fish.

5.2. Methodology

Sample collection and micro-CT protocol

Smelt samples were collected by the Environment Agency from the River Thames at sampling points at Battersea and Chiswick in March/April 2018. Fish were first euthanased by being placed in a bucket for 15 minutes with a lethal dose of benzocaine, and then preserved in 4% neutral buffered formalin (NBF) until analysis. Thirteen smelt samples were then selected to represent different infection intensities. The selection was classified by the number of, or clusters, of visible cysts, and at least three samples were chosen to represent uninfected fish, mild, moderate, and heavy infections. Scans were taken using the Nikon Metrology HMX ST 225. Post-scanning image analysis and volumetric measurements were completed using Avizo (2019.1). For full details, please refer to Chapter 3.

3D Virtual modelling

Preservation-induced shape changes can be problematic when incorporating fish specimens into hydrodynamic analyses. Preserved individuals are frequently vulnerable to deformation, resulting in misleading calculations and, therefore, smaller sample sizes. Disciplines, such as Palaeontology, have developed different techniques for recovering undistorted three-dimensional shapes (Lautenschlager, 2016). These techniques rely on bilaterally equivalent anatomical features on both sides of the specimen and define a deformed sagittal plane. The latter is then aligned into a symmetric one, correcting for the lateral bending and local lateral distortion. However, fish species bear thinner and more flexible skeletons than terrestrial vertebrates and show a higher frequency of distortions in non-uniform, plastic ways (i.e., not only lateral but also dorso-ventral bending). Unfortunately, landmark-based retrodeformation techniques cannot yet deal with these artefacts (O. Sanisidro, pers. comm). Consequently, specimen-specific manual retrodeformation was used, utilising the 'dynamic topology' tool in the 3D computer graphics software Blender v. 2.93.1 (Community, 2021). Specimens were aligned based on the shape of the lateral line and the sagittal plane, using undistorted specimens as a reference. The fins were

excluded in the final 3D images to remove any additional sources of variation between samples.

Computational fluid dynamics analyses

Simulations were performed of water flow around the three-dimensional models of the 13 studied specimens using ANSYS-Fluent 2020 R1 Academic (www.ansys.com). The computational domain consisted of a rectangular prism, with 1820 mm in length and 610 mm in width and height, in which the model was centrally fixed (Fig. 5.2 A). The inlet boundary condition was defined with a normal inflow velocity and a turbulence intensity of 0.05 at the upstream end of the domain and a zero-pressure outlet boundary condition at the downstream end. Slip symmetry boundary conditions were assigned to the sides of the rectangular prism modelling a zero-shear wall, whereas no-slip boundary conditions were assigned to the walls of the models, with fluid velocity fixed at zero (Fig.5.2 A).

The domain was meshed employing ANSYS-Meshing. Tetrahedral elements in the interior and the walls of the rectangular prism were used. An inflation layer with a maximum of 23 layers of prismatic elements and a growth rate of 1.1 was created at the no-slip boundaries (i.e. walls of the models). A volume of extra refinement was added around the wake, consisting of a rectangular prism with 700 mm in length, 200 mm in height, and 1200 in width. Finally, the domain was converted to a polyhedral mesh (Fig. 5.2 B). The number and minimum/maximum size of the mesh elements used in the CFD simulations are shown in Appendix 5 Table A5.1.
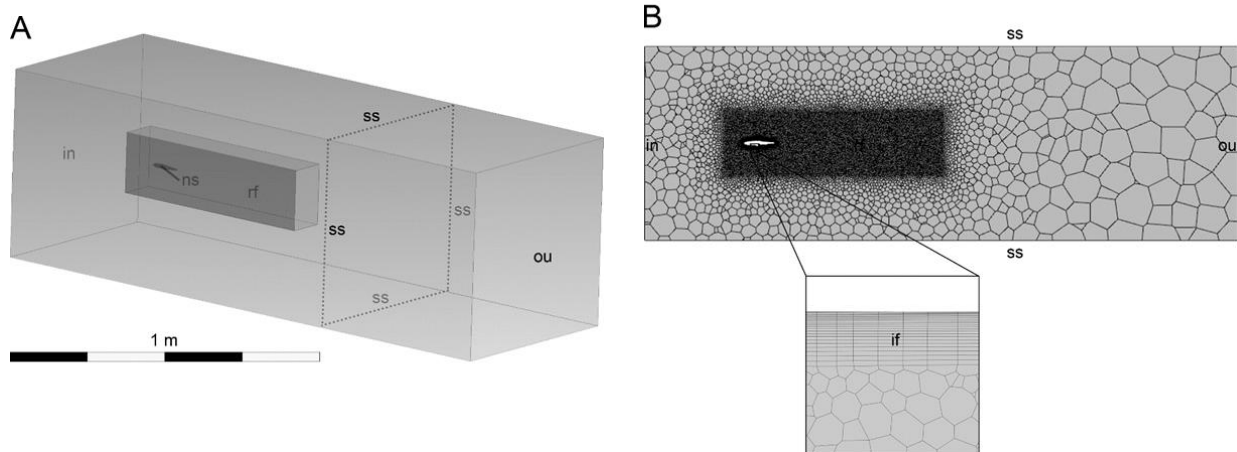
Figure 5. 2 (A) Computational domain and (B) mesh employed in the CFD analysis noting the different boundary conditions (in, inlet; ou, outlet; ns, non-slip boundary condition; ss, slip symmetry boundary condition), refinement volume (rf) and inflation layers (if).

Independence tests were performed for mesh size, domain size, and refinement volume to ensure that our results were independent of these elements. A solution was considered independent if the converged value for drag and lift forces did not change by more than 2% between a simulation and the next considering a coarser mesh or bigger domain/refinement volume. The number of inflation layers was also established by performing mesh sensitivity tests (Appendix 5 Table A5.2).

The three-dimensional incompressible flow was simulated through the domain, using a double precision stationary solver and a second-order discretisation method to compute the steady-state flow. The Spalart-Allmaras model and a pressure-based segregated algorithm solved the Reynolds averaged Navier-Stokes (RANS) equations. Convergence of the performed simulations was assessed based on a stable numerical solution for the integrated values of drag and lift forces, root-mean-square residual levels of 10^{-4}, and a mass flow rate imbalance smaller than 1%. An ambient flow velocity of 0.5 m s^{-1} was considered realistic, in agreement with swimming speed records of similar-sized living fishes (Videler, 2012)

The models were scaled to equal total length (i.e., 5 cm, corresponding to Reynolds numbers equal to 24880) and equal volume (i.e., with Reynolds numbers ranging from

22539 to 27120), both of which are considered as valid scaling criteria to assess the hydrodynamic effects of morphology (Gutarra et al., 2019) (Appendix 5 Table A5.3).

False-colour contour plots of pressure (Pa) over the surface of the models were obtained to visualise the results. Drag and lift forces were evaluated in the case of volume normalised simulations and their coefficients (C_D and C_L) in the case of Reynolds normalised simulations. The force coefficients were determined considering the whole surface of the models as the reference area.

5.3. Results

The length of each sample and the calculated volume of cysts are presented in Table 5. 1. Samples 2, 13 and 17 represented healthy, uninfected juveniles. Samples 10, 19, 22 and 36 had mild infections with cysts volumes < 2%. Samples 5, 8 and 16 represented moderate infections (> 2 - < 20%). Samples 1, 4 and 6 represented juveniles with heavy infections (< 20% volume cysts). The other samples represented mild to moderate infections. Sensitivity analyses demonstrate that our CFD results are independent of the domain and mesh size (See Appendix 5 Table A5.2).

Table 5. 1 The total length of each fish, the calculated volume of cysts within the body cavity, drag coefficient (C_{Drag}) and drag force (N). EA ID = original EA National Fisheries Laboratory reference ID.

Sample ID number (EA ID)	Total length (mm)	Volume of cysts (%)	C_{Drag} (Reynolds normalized)	Drag force (N) (Volume normalized)
1 (18/087/01)	45	32.05	0.000365	4.11E-05
2 (18/109/02)	67	0	0.000268	2.86E-05
4 (18/109/04)	37	27.08	0.000341	3.49E-05
5 (18/087/05)	44	11.23	0.000272	2.72E-05
6 (18/087/06)	54	22.36	0.000357	3.95E-05
8 (18/109/08)	50	3.21	0.000262	2.64E-05
10 (18/087/10)	66	0.09	0.000248	2.51E-05
13 (18/087/13)	63	0	0.000253	2.59E-05
16 (18/109/16)	51	4.65	0.000255	2.64E-05
17 (18/109/17)	49	0	0.000253	2.64E-05
19 (18/109/19)	77	1.02	0.000256	2.66E-05
22 (18/087/22)	53	1.07	0.000265	2.68E-05
36 (18/087/36)	62	1.56	0.000273	2.91E-05

The distributions of pressure over the fish body are visualised in Figures 5.3 and 5.4. In the fish with heavy infections, the areas of highest pressure were located at the anterior part of the head and the leading edges of the bulges (fish 1, 4 and 6 highlighted in black boxes). Fish 6 showed two regions of particularly high pressure on the leading edge of the bulges, as seen from the ventral view. The negative pressure (dark blue) areas immediately following high-pressure regions are particularly pronounced in fish with thinner body forms, as shown in fish 4 and 6. Therefore, fish with heavy infections tend to be lighter in body mass, causing protrusion of skeletal features, which distorts the natural streamline of their body shape.

Fish with mild to moderate infections (fish 10,19,22 & 36) only showed increases in surface pressure if the cysts created bulges in the peritoneal cavity on the dorsal side (fish 8, 16 and 36 highlighted in light grey boxes) (Fig. 5.3 and 5.4). There was little difference observed between fish with no infections and mild infections.

The drag (force and coefficient) significantly increases with an increasing volume of cysts (Fig. 5.5 **A** and **B**). These values remained at similar levels in fish with no infection up to approximately 10% cyst volume and then increased dramatically when the volume of the cysts was greater than 20%. According to my findings, the increases in drag (force and coefficient) were dependent on cyst volume rather than the body length of individual fish.
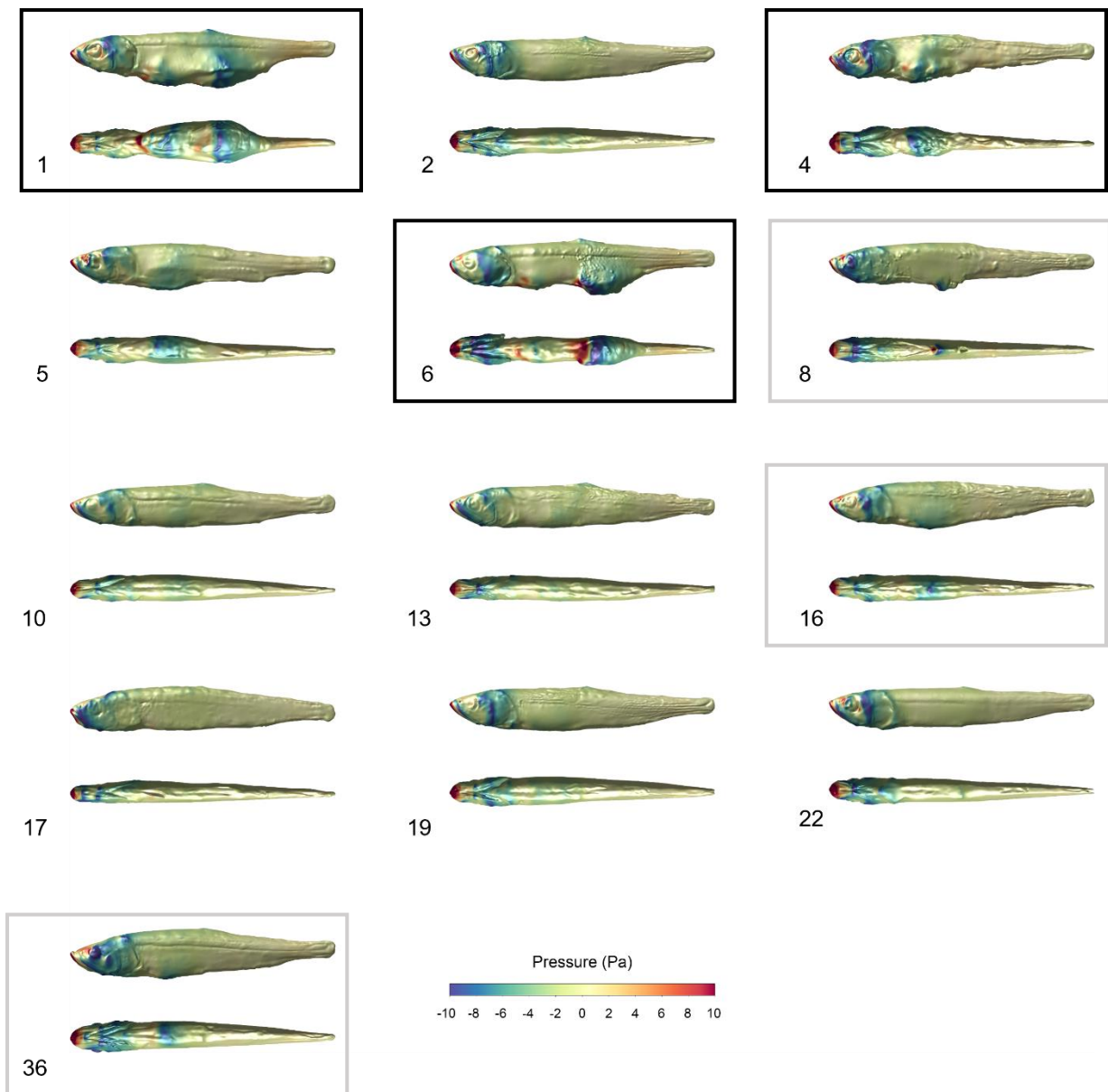
Figure 5. 3 Surface pressure distribution patterns on the models in lateral and dorsal views, considering models scaled to equal total length (Reynolds normalised). Numbers correspond to fish ID number. Heavy infections highlighted in black boxes, and moderate infections highlighted in light grey boxes.
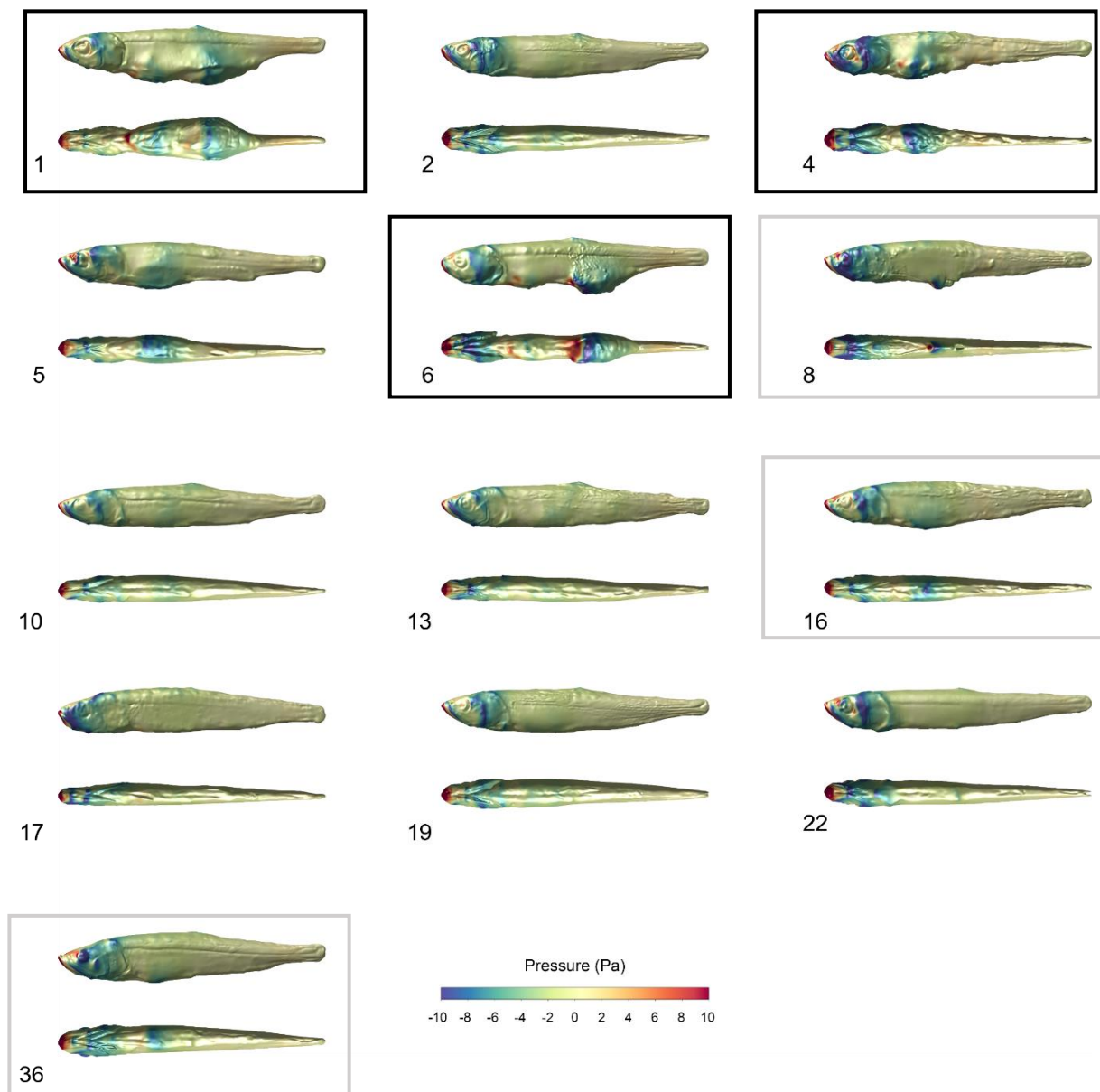
Figure 5. 4 Surface pressure distribution patterns on the models in lateral and dorsal views, considering models scaled to equal volume (volume normalised). Numbers correspond to fish ID number. Heavy infections highlighted in black boxes, and moderate infections highlighted in light grey boxes.
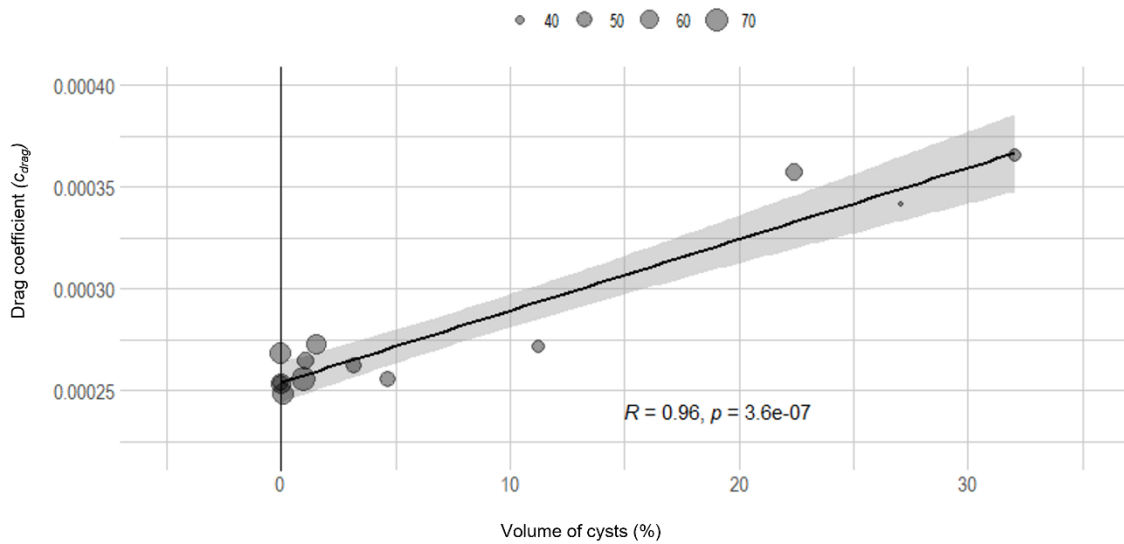
A

*Reynolds normalized
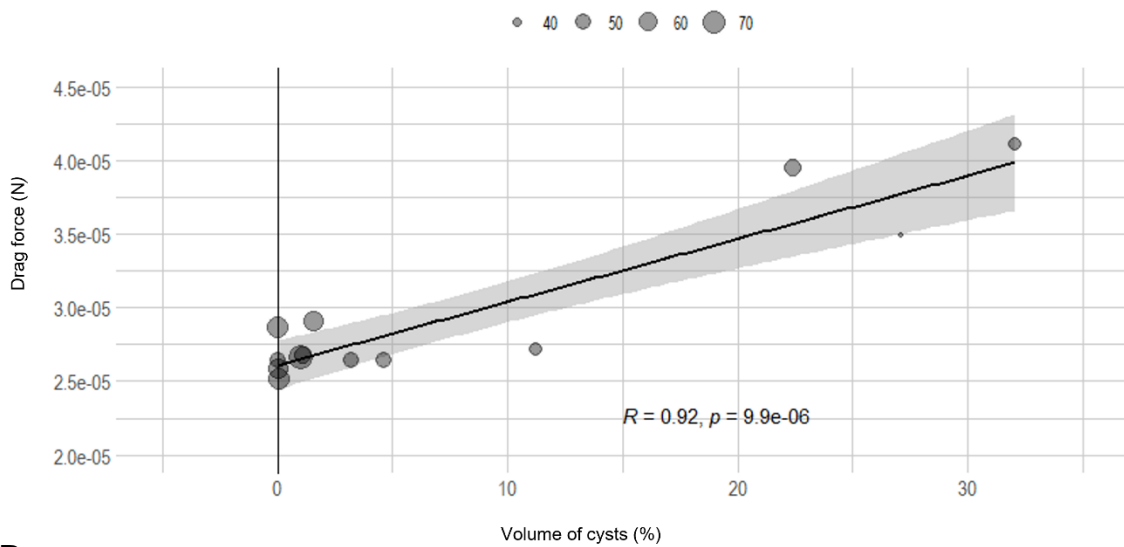
B

*Volume normalized

Figure 5. 5 Values of drag coefficient (**A**) and drag force (**B**) obtained with two different scaling criteria in relation to percentual volume of cysts. Point size is proportional to body length (in mm). Shaded area represents the 95% confidence intervals.

5.4. Discussion

Using computational fluid dynamics, this study has shown that European smelt infected with a heavy burden of Glugea microsporidian cysts experience a significant modification in pressure distribution patterns around the body, which translates into a significant increase in hydrodynamic drag. The models suggested that fish with no microsporidian infections, mild and moderate infections (up to 15% cyst volume) experienced similar surface pressures and similar drag forces to each other. However, once a fish had a cyst burden of greater than 20%, they experienced significantly higher surface pressure and drag forces.

To the best of my knowledge, this study is the first to attempt to apply CFD to calculate costs associated with parasitic infection in fish. The closest related work found was preliminary findings on the modelled effects on profile drag associated with the attachment of sea lamprey (*Petromyzon marinus*) to lake trout (*Salvelinus namaycush*) (Unpublished; Silva *et al.*, 2016). Lauder *et al.* (2016) studied fluid dynamics associated with fish skin surfaces and highlighted the gap in understanding of the surface textures of fish and hydrodynamic effects of variation around the body surface between individuals and among different species.

The application of CFD modelling could be a useful alternative method to study costs associated with parasitic infections over traditional methods, which have a number of inherent limitations. Traditional methods focus on the mechanics of propulsion or assessing fish health or stress, primarily based on exercise performance (Reidy, Kerr & Nelson, 2000). These experiments are usually conducted by placing fish in a swim tunnel and exposing them to different water flow velocities and temperatures to measure burst speed, sustained speed and prolonged speed (Clough et al., 2004; Hammer, 1995). Limitations include potential declines in swimming performance due to stress, handling, confinement and the presence of other fish (Deslauriers & Kieffer, 2011). These stressors may be further exacerbated in fish who are already stressed due to illness or parasitic infections. Furthermore, the work in this study is adding to the limited studies on the physical costs of parasitic infection instead of just the pathological costs. This issue was highlighted by Stewart *et al.* (2018), who aimed to measure the physical costs of *Argulus foliaceus* (an ectoparasite) infections on the swimming performance in three-spined sticklebacks (*Gasterosteus aculatus*). The

"cost of infection" was measured by placing infected fish in an open flume tunnel and measuring sustained (prolonged swimming against a current) and burst swimming performance. Surprisingly, the authors reported that hydrodynamic drag and stability were not impacted directly by a heavy burden of *A. foliaceus*; however, swimming ability was negatively impacted pathologically due to lethargy and sickness resulting from the infection (Stewart et al., 2018). This interesting finding emphasised the need to quantitatively measure the physical costs of infection, as species may compensate to physical changes to overcome hydrodynamic challenges.

The limited research of swimming performance of European smelt has mainly focused on critical burst swimming speeds (CBSS) and endurance swimming using flume tunnels. CBSS approximates the final velocity attained before exhaustion, where endurance swimming measured the average swimming speed maintained between 0 – 200 minutes (Clough et al., 2004). Data for swimming speeds in smelt were provided from a Thames Water Utilities Ltd (TWU) study on smelt from the River Thames and reported a mean CBSS of between 1 - 1.2 $m.s^{-1}$ in healthy individuals (Clough et al., 2004). Sprengel & Luchtenberg (1991) investigated the impact of endoparasitic worms (*Pseudoterranova decipiens*) and a microsporidian (*Pleistophora ladogensis*) on the swimming ability of smelt from German rivers. They reported that uninfected smelt (standardised length of 15 cm) had a maximum swimming speed of 0.49 $m. s^{-1}$, while individuals infected with *P. ladogensis* had on average a maximum swimming speed of 0.39 $m. s^{-1}$ and individuals infected with the microsporidian and endoparastitc worms had a greater reduction in maximum swimming speed, with an average of 0.34 $m. s^{-1}$ (Sprengel & Luchtenberg, 1991). The discrepancies between the average swimming speeds recorded in healthy smelt between the two studies highlight some of the difficulties associated with flume tunnel swimming experiments and the variability of results. Many species are also not suitable for such studies. Smelt are notoriously difficult to keep in aquaria due to their sensitivity to environmental changes. The study by TWU had difficulty collecting and transporting live smelt, with > 90% mortality during initial attempts (Clough et al., 2004). The work presented in this chapter provides a novel insight into studying the potential adverse costs of parasitic infections without needing to keep and experiment with live fish.

CFD modelling is an exciting area of research to understand better the hydrodynamic effects of variation in body surface caused by parasites. However, as with any method, there are limitations and assumptions. Firstly, specialists in 3D virtual modelling and computational fluid dynamics are needed to create and run the models. When creating 3D virtual models using preserved fish specimens, you need to account for deformation caused by the dehydration of tissues to remove sources of variation. Furthermore, the fins were removed from the 3D virtual models as I was only interested in pressure changes caused by bulges from cysts and wanted to remove other sources of variation. While the ambient flow velocity of 0.5 m s^{-1} was considered realistic for similar fishes (Videler, 2012), the CFD modelling did not account for environmental variables such as temperature, viscosity and density of the water. However, a study by Kogan *et al.* (2015), who studied the hydrodynamic properties between a fossil fish and its living relatives using CFD, found only slight differences in drag forces between ideal-theoretical and marine and lacustrine environment parameters for temperature, viscosity and density, suggesting that the values would fall within the normal range. While CFD does require skilled personnel, the costs are considered lower than those associated with experimental studies (Kogan et al., 2015). My study could have been improved with a greater number of fish samples, presenting with different intensities of infection to validate the results we have seen using a limited sample size.

Swimming performance data for fish species, especially those of conservation concern, are important for scientists and conservation managers to know what changes in water velocity can be tolerated by fish. These data are essential when managing construction and development along rivers (Clough & Turnpenny, 2001). The generalised application of CFD could help fill the gaps in knowledge on biomechanics associated with parasitic diseases and provide initial data to indicate potential changes in the swimming ability of infected species.

Chapter 6: General discussion

6.1 In summary

European smelt, a priority species of conservation importance in the UK and an indicator species on the EU Water Framework Directive, are a severely understudied migratory species across Europe. The small, cucumber scented fish was once abundant throughout rivers in the UK, however commercial overfishing, and heavy pollution of waterways in the 1800s, led to its disappearance from most UK rivers. With modern water quality legislation and conservation efforts, smelt have returned to many UK estuaries, including a large breeding population in the Thames. However, the changing climate and anthropogenic pressures remain a threat to the prosperity of this sensitive species. Furthermore, a newly reported microsporidian proliferated amongst samples collected by the EA during the summer of 2018, with < 80% of the juveniles caught presenting with large white cysts in their guts. The primary objective of this thesis was to investigate and identify this mysterious parasite, as well as to cast a light onto this nationally rare species.

<u>European smelt in English and Welsh rivers</u>

The preliminary findings reported in Chapter 2, provide the most up-to-date biological and ecological data on smelt populations in England, and a glimpse into Welsh smelt populations. Using common fisheries metrics, I assessed the trends in weights, lengths, and ages of smelt populations. My findings were comparable with previous studies which suggest a strong plasticity in lengths and weights between different sampling locations and with the average age of smelt sampled being two years, and the maximum age recorded was four (Doherty & McCarthy, 2004; Wootton, 2018; Hutchinson, 1983). Thames smelt were smaller in length and weight across all age classes when compared to fish in other rivers sampled, and some young-of-the-year had developed gonads. Smelt which are overexploited have been reported to mature earlier, and reach lower weights (Arula et al., 2017). These findings could reflect previous adaptions of this population to historic overfishing or may be due to current environmental stresses in the estuary. Though smelt are known to show plasticity in growth rates depending on environmental conditions and food availability, the findings of my study agree with previous findings reported by Colclough (2013), who suggested that the populations inhabiting different estuaries in the UK may be isolated from each

other. Further genetic analyses of different populations are needed to validate this theory. Additionally, a more robust data set is needed to account for variation in population life-history traits due to seasonal shifts and spawning times.

<u>The microsporidian infecting Thames smelt</u>

The main aim of this thesis was to provide a positive ID on the newly reported microsporidian infecting juvenile smelt in the Thames. I have produced a detailed pathological description of the microsporidian, which based on morphological characteristics and pathology I have identified as a species from the *Glugea* genus. Upon further investigation using molecular techniques, I have been able to validate that the microsporidian is in the *Glugea* genus. This finding is based on very high genetic sequence identity (> 97%) with eight other *Glugea* species. In addition, the phylogenetic tree produced showed grouping of my sample isolates with *Glugea* species mainly found in hosts inhabiting waters in the northern hemisphere. This study is the first to identify and report *Glugea* sp. infecting European smelt in the UK. Furthermore, to the best of my knowledge, I am the first to report a ssrDNA sequence for a microsporidian from the *Glugea* genus in European smelt. Based on my morphological and molecular findings, as well as historical reports of *G. hertwigi* infecting European smelt, it could be suggested that European smelt from the River Thames are infected with *Glugea hertwigi.*

It should be noted that *G. hertwigi* is believed to be host specific, with previous studies finding no evidence of similar infections in other fish species, including salmonids co-inhabiting with infected juveniles (Schrader, 1921). Environment Agency surveys did not find evidence of other species with similar infections when capturing infected juvenile smelt from the River Thames (Dr Chris Williams, pers. comm). While it is unknown if *G. hertwigi* is present in other UK rivers, no evidence of infected juvenile smelt has been raised from surveys in other UK rivers, and there is no historic record of *G. hertwigi* in the UK. Therefore, *G. hertwigi* could be considered as a non-native parasite of smelt inhabiting UK rivers and therefore raises many questions regarding its origin and the seeming presentation in juvenile smelt only from the River Thames. Previous work (Chapter 2) suggested that smelt from the River Thames may be under environmental pressures, resulting in smaller lengths at age and lower weights compared with other smelt populations in UK rivers. The River Thames population

may be under higher stress and therefore more susceptible to this microsporidian. Environmental DNA (eDNA) techniques may be useful to test other water bodies for the presence of microsporidian spores.

<u>Novel methods for investigating parasitic infections in fish</u>

In this thesis, I suggested novel methods which may be applied to assess parasitic infections in fish. The micro-CT imagery produced in Chapter 3 highlighted the ability of this technique to visualise a microsporidian infection by exploring internal morphology as a whole, in three-dimensional space. The imagery can be produced without destructive manipulations of the samples and also provides valuable quantitative data. Furthermore, the false-coloured 3D imagery is also very useful when presenting this work, as it is eye catching and captures the attention of the viewer. Such imagery may be useful when explaining parasitic infections in species of concern, especially when engaging with the public. Inspired by the 3D visualisations of infected individuals, I explored, in collaboration with expert modellers, quantitatively, the hydrodynamic impacts associated with infection. To the best of my knowledge, this study is the first to attempt to apply computational fluid dynamics (CFD) to calculate costs associated with parasitic infection in fish. The findings in Chapter 5, which suggested that drag (force and coefficient) only significantly increased with a cyst burden of > 20% may be of significance, as it suggests a potential threshold after which the fish is negatively impacted. Such findings allow us to better understand potential risks to population health, if during future monitoring, a high percentage of samples are found with heavy cyst burdens. The preliminary findings using CFD showcase the possibilities in this field of research for studying the adverse costs associated with parasitic infections in fish.

6.2 Limitations of this study

<u>Samples sizes</u>

While this study provided valuable data on an understudied and protected species, I faced a number of limitations, largely due to a limited number of samples. Due to the variable nature of fish growth depending on stage of maturation and seasonal shifts, it is essential to collect repeated samples throughout the year, and across a number of years, to rule out population shifts due to weak year classes. The data used in

Chapter 2, were collected ad hoc through EA surveys and collections by commercial netsman. Therefore, I was unable to statistically assess differences between years, and populations, due to the limited samples sizes. Furthermore, a lack of adult smelt samples from the River Thames (from EA surveys) limited my ability to accurately assess and report levels of microsporidian infection in mature individuals. The preliminary data I presented in Chapter 3 suggests that adult smelt are hosting microsporidian infections, therefore exploring if these are remnant infections picked up as juveniles or new infections should be a priority.

Molecular analysis

I faced a number of challenges conducting the molecular work in Chapter 4. I found the suggested "universal primers" and cycling conditions for microsporidians in the literature were not optimized to produce single target bands. More selective primers should be developed to improve PCR products and identify different *Glugea* species. The DNA isolates I produced for the microsporidian infecting Thames smelt, were very closely related to a number of other *Glugea* species. Several authors have suggested that many *Glugea* 'species' may be a single species presenting slightly differently in closely related host species in different geographic regions (Ryan & Kohler, 2016; Pomport-Castillon, De Jonckheere & Romestand, 2000; Lovy et al., 2009). Longer, more reliable genome sequences are needed to explore the relationships between supposed different species. Future studies on *G. hertwigi* in smelt should compare DNA samples collected from infected smelt from different Baltic regions. This would add valuable data to the limited data available for this species, as well as suggest possible relationships and origins of this parasite.

Micro-CT, 3D virtual models and computational fluid dynamics

Understanding fluid dynamics around biological specimens is complicated as it involves fluid interaction with elastic and flexible tissues, therefore any virtual and CFD modelling should try to account for such parameters (Liu, 2002). When using samples of different lengths in CFD models, complementary analyses need to be calculated to account for variations in morphology between specimens, such as standardized Reynolds number and standardised volume. Using these methods means that certain assumptions are made. Furthermore, motion should be included when simulating hydrodynamics, however 3D CFD is computationally expensive and such models

would require many assumptions of kinematics of the species (Gutarra et al., 2019). The CFD modelling in this study also did not include environmental variables which may affect hydrodynamics, including water temperature, turbidity, and density.

As seen in my findings, smelt with heavy infections were smaller in length and lower in weight compared to healthy juveniles of the same age. Future studies could perform regressions of drag versus ontogenetic stage to check for variations. Furthermore, as shown in the preliminary findings in Chapter 3, adult smelt can also present with heavy infections and should therefore be included in future CFD analyses.

6.3 Future work

<u>eDNA: Proposed study to further develop understanding of the microsporidian infecting Thames smelt</u>

As part of this thesis, I had planned to examine the applicability of using environmental DNA (eDNA) from river water to monitor for the presence of both host (smelt) and parasite (*Glugea* sp), with the ultimate aim of investigating if the microsporidian is isolated to the Thames, or if it is more widespread in the UK. This part of my research was halted by the COVID-19 outbreak and subsequent lockdowns.

The use of eDNA in fisheries science is growing exponentially to monitor aquatic organisms (Tsuji et al., 2019). However, its applicability for use in tidal systems is complex due to the inherent problems caused by the continual tidal fluctuations and saline gradients (Goldberg et al., 2016; Stoeckle, Soboleva & Charlop-Powers, 2017). eDNA has been shown to be effective for detecting rare migratory species in rivers, such as the study by Antognazza et al. (2019) who successfully developed an eDNA assay for detecting European shads (*Alosa spp*) in the River Teme. However, it should be noted that the assay was developed for detection in freshwater, and not further downstream in estuarine water (Antognazza et al., 2019).

I had planned to collect water samples using the protocol by Collins (2019) for extracting DNA from estuarine water. The timing of water sample collection is crucial, and I planned to sample at spring tides during the spawning window between March and April 2020, at both spring high and spring low, for best chances of detecting target

species. Smelt have been suggested to migrate further up rivers on spring tides to spawn, therefore these timings would provide the highest chance of detection. Furthermore, I expected that levels of potential microsporidians in the water would be highest where infected smelt would be congregating for spawning. Unfortunately, this research was halted by the COVID-19 lockdowns. Species specific primers, as well as improved microsporidian primers, needed to be developed. My molecular findings in Chapter 4, suggested that more specific microsporidian primers would be needed when testing for potential *G. hertwigi* in water samples. I had planned on testing the efficiency of primers for both smelt and the *Glugea* microsporidians by extracting and filtering aquarium tank water which had been dosed with extracted smelt and microsporidian DNA, however this experiment was never conducted. There are many generic challenges to overcome when considering the use of eDNA water sampling, including varying water flows, sediment levels and the density of the target fish species in an area (Stoeckle, Soboleva & Charlop-Powers, 2017). Furthermore, species specific challenges exist for migratory species, as samples need to be collected when fish are migrating through selected sampling sites. As part of my proposed work, I had hoped to join the ZSL team who have begun a smelt tagging project in the Thames to monitor migration and explore potential spawning grounds (Anna Cucknell, ZSL, pers. comm). With this tagging information, I had hoped that I would be notified when smelt may pass my selected sampling sites and I could more accurately time my water sample collections. Unfortunately, due to the COVID-19 restrictions, I was unable to join the ZSL team.

Monitoring population dynamics and microsporidian infections

From the findings in my thesis, it is clear that there are still knowledge gaps regarding the population dynamics between different populations of smelt around the UK. Additionally, why microsporidian infections, to the best of my knowledge and that of the EA (Dr Chris Williams, pers.comm), are only infecting Thames smelt, remains a mystery. The EA and future studies should prioritise the assessment of microsporidian infection in other smelt populations to determine potential risks. Furthermore, parasites, like the microsporidian currently infecting Thames smelt, thrive in warmer temperatures, so we are likely to see an increase in summer infection rates. The applicability of eDNA techniques should be investigated for monitoring smelt, as it

provides a non-invasive survey approach and has been found to be effective in flowing rivers (Balasingham, Walter & Heath, 2017).

6.4 Conclusion

This thesis provides the first formal report and identification of a microsporidian, most likely *Glugea hertwigi*, infecting European smelt in the River Thames, using both histopathological and molecular approaches. This parasite has not previously been reported in smelt inhabiting UK waters and therefore this work provides novel information on a possible threat to the Thames smelt population. Using micro-CT imagery and CFD to explore the pathology and hydrodynamic effects associated with microsporidian infections in smelt, I have highlighted the applicability of these modern techniques to assess parasitic diseases in fish. Furthermore, the data presented add to the limited body of knowledge regarding the biology and ecology of smelt populations in the UK and highlights the need for more routine surveys and investigations to aid fisheries management of this species in the UK.

References

Abdel-Baki, A.A.S., Al-Quraishy, S., Rocha, S., Dkhil, M.A., Casal, G. & Azevedo, C. (2015) Ultrastructure and phylogeny of *Glugea nagelia* sp. n. (Microsporidia: Glugeidae), infecting the intestinal wall of the yellowfin hind, *Cephalopholis hemistiktos* (Actinopterygii: Serranidae), from the Red Sea. *Folia Parasitologica.* 62 (1), 1–7. doi:10.14411/fp.2015.007.

Alabaster, J.S. (1982) *Water Quality Criteria for Freshwater Fish (Second Edition).* doi:10.1016/B978-0-408-10849-2.50010-1.

Antognazza, C.M., Britton, J.R., Potter, C., Franklin, E., Hardouin, E.A., Gutmann Roberts, C., Aprahamian, M. & Andreou, D. (2019) Environmental DNA as a non-invasive sampling tool to detect the spawning distribution of European anadromous shads (Alosa spp.). *Aquatic Conservation: Marine and Freshwater Ecosystems.* 29 (1), 148–152. doi:10.1002/aqc.3010.

Arula, T., Shpilev, H., Raid, T., Vetemaa, M. & Albert, A. (2017) Maturation at a young age and small size of European smelt (*Osmerus eperlanus*): A consequence of population overexploitation or climate change? *Helgoland Marine Research.* 71 (1). doi:10.1186/s10152-017-0487-x.

Azevedo, C., Abdel-Baki, A.A.S., Rocha, S., Al-Quraishy, S. & Casal, G. (2016) Ultrastructure and phylogeny of *Glugea arabica* n. sp. (Microsporidia), infecting the marine fish *Epinephelus polyphekadion* from the Red Sea. *European Journal of Protistology.* 52 (228), 11–21. doi:10.1016/j.ejop.2015.09.003.

Bailey, M.M. (1964) Age, growth, maturity, and sex composition of the American smelt, *Osmerus mordax* (Mitchill), of Western Lake Superior. *Transactions of the American Fisheries Society.* 93 (4), 382–395. doi:10.1577/1548-8659(1964)93[382:agmasc]2.0.co;2.

Baker, M.D., Vossbrinck, C.R., Maddox, J. V. & Undeen, A.H. (1994) Phylogenetic relationships among *Vairimorpha* and *Nosema* species (Microspora) based on ribosomal RNA sequence data. *Journal of Invertebrate Pathology.* 64 (2) pp.100–106. doi:10.1006/jipa.1994.1077.

Balasingham, K.D., Walter, R.P. & Heath, D.D. (2017) Residual eDNA detection sensitivity assessed by quantitative real-time PCR in a river ecosystem. *Molecular Ecology Resources.* 17 (3), 523–532. doi:10.1111/1755-0998.12598.

Barker, J. (2016) Smelt in the Tidal Thames: Modelling report. *HR Wallingford.* (October).

Barry, J., Coghlan, B., Cullagh, A., Kerr, J.R. & King, J.J. (2018) Comparison of coarse-resolution rapid methods for assessing fish passage at riverine barriers: ICE and SNIFFER protocols. *River Research and Applications*. 34 (9), 1168–1178. doi:10.1002/rra.3358.

Belletti, B., Garcia de Leaniz, C., Jones, J., Bizzi, S., Börger, L., Segura, G., Castelletti, A., van de Bund, W., Aarestrup, K., Barry, J., Belka, K., Berkhuysen, A., Birnie-Gauvin, K., Bussettini, M., Carolli, M., Consuegra, S., Dopico, E., Feierfeil, T., Fernández, S., et al. (2020) More than one million barriers fragment Europe's rivers. *Nature*. 588 (7838), 436–441. doi:10.1038/s41586-020-3005-2.

Von Bertalanffy, L. (1938) A quantitative theory of organic growth (inquiries on growth laws. II). *Human biology*. 10 (2), 181–213.

Beverton, R. & Holt, S. (1959) A review of the lifespans and mortality rates of fish in nature and the relation to growth and other physiological characteristics. In: G. Wolstenholme & M. O'Connor (eds.). *Ciba Foundation colloquia in ageing; the lifespan of animals*. Churchill. pp. 147–177. doi:10.1002/9780470715253.ch10.

Boeuf, B. & Fritsch, O. (2016) Studying the implementation of the water framework directive in Europe: A meta-analysis of 89 journal articles. *Ecology and Society*. 21 (2). doi:10.5751/ES-08411-210219.

Bogdanova, E.A. (1957) The microsporidian *Glugea hertwigi Weissenberg* in the stint (*Osmerus eperlanus m. spirinchus*) from Lake Ylyna-yarvi. *Parasites and Diseases of fish. Izvestiya Vsesoyuznoga Nauchno-Issledova-telskogo Instituta Ozernogo I Rechnogo Rybnogo Khozyaistva, Leningrad, Russia*. 1–328.

Brown, A.M.V., Kent, M.L. & Adamson, M.L. (2010) Low genetic variation in the salmon and trout parasite *Loma salmonae* (Microsporidia) supports marine transmission and clarifies species boundaries. *Diseases of Aquatic Organisms*. 91 (1), 35–46. doi:10.3354/dao02246.

Butchart, S.H.M., Walpole, M., Collen, B., van Strien, A., Scharlemann, J.P.W., Almond, R.E.A., Baillie, J.E.M., Bomhard, B., Brown, C., Bruno, J., Carpenter, K.E., Carr, G.M., Chanson, J., Chenery, A.M., Csirke, J., Davidson, N.C., Dentener, F., Foster, M., Galli, A., et al. (2010) Global biodiversity: Indicators of recent declines. *SCIENCE*. 328 (5982), 1164–1168. doi:10.1126/science.1187512.

Cali, A., Becnel, J.J. & Takvorian, P.M. (2017) Microsporidia. In: J.M. Archibald, A.G.B. Simpson, & C.H. Slamovits (eds.). *Handbook of the Protists*. Second. Springer

International Publishing. pp. 1559–1608.

Cali, A. & Takvorian, P.M. (1999) Developmental morphology and life cycles of the microsporidia. In: M. Wittner & L.M. Weiss (eds.). *The microsporidia and microsporidiosis*. American Society for Microbiology Press. pp. 85–128. doi:10.1002/9781118395264.ch2.

Cali, A., Takvorian, P.M., Ziskowski, J.J. & Sawyer, T.K. (1986) Experimental infection of American winter flounder. *Journal of Fish Biology*. (28), 199–206.

Canning, E.U. & Lom, J. (1986) *The Microsporida of Vertebrates*. Academic Press.

Carlander, K.D. (1969) *Handbook of freshwater fishery biology*. Volume 1. The Iowa State University Press.

Casal, G., Matos, E., Teles-Grilo, M.L. & Azevedo, C. (2009) Morphological and genetical description of *Loma psittaca* sp. n. isolated from the Amazonian fish species *Colomesus psittacus*. *Parasitology Research*. 105 (5), 1261–1271. doi:10.1007/s00436-009-1547-1.

Ceballos-Francisco, D., Carrillo, N.G., Pardo-Fernández, F.J., Cuesta, A. & Esteban, M. (2020a) Radiological characterization of gilthead seabream (*Sparus aurata*) by X-ray computed tomography. *Journal of Fish Biology*. 97 (5), 1440–1447. doi:10.1111/jfb.14510.

Ceballos-Francisco, D., García-Carrillo, N., Cuesta, A. & Esteban, M.Á. (2020b) Radiological characterization of gilthead seabream (*Sparus aurata*) fat by X-ray micro-computed tomography. *Scientific Reports*. 10 (1), 1–11. doi:10.1038/s41598-020-67435-2.

Cengel, Y.A. & Cimbala, J.M. (2018) *Fluid mechanics: fundamentals and applications*. McGraw-Hill Education.

Chapman, J.M., Kelly, L.A., Teffer, A.K., Miller, K.M. & Cooke, S.J. (2021) Disease ecology of wild fish: Opportunities and challenges for linking infection metrics with behaviour, condition, and survival. *Canadian Journal of Fisheries and Aquatic Sciences*. 78 (8), 995–1007. doi:10.1139/cjfas-2020-0315.

Chen, M. & Power, G. (1972) Infection of American smelt in Lake Ontario and Lake Erie with the microsporidian parasite *Glugea hertwigi* (Weissenberg). *Canadian Journal of Zoology*. 50 (9), 1183–1188. doi:10.1139/z72-159.

Chen, Y., Jackson, D. a & Harvey, H.H. (1992) A comparison of von Bertalanffy and polynomial functions in modelling fish growth data. *Canadian Journal of Fisheries and Aquatic Sciences*. 49 (Table 1), 1228–1235.

Cheney, S.A., Lafranchi-Tristem, N.J., Bourges, D. & Canning, E.U. (2001) Relationships of microsporidian genera, with emphasis on the polysporous genera, revealed by sequences of the largest subunit of RNA polymerase II (RPB1). *Journal of Eukaryotic Microbiology.* 48 (1), 111–117. doi:10.1111/j.1550-7408.2001.tb00422.x.

Clough, S. & Turnpenny, A. (2001) Swimming Speeds in Fish: Phase 1. *Environment Agency R&D Technical report W2-026/TR1.* 1–106.

Clough, S.C., Lee-Elliott, I.E., Turnpenny, A.W.H., Holden, S.D.J. & Hinks, C. (2004) Swimming Speeds in Fish : phase 2. *Environment Agency R&D Technical Report W2-049/TR1.* 1–94.

Colclough, S. (2010) *Smelt in rivers and estuaries in England 2010.*p.32.

Colclough, S. (2013) The status of Smelt *Osmerus eperlanus* (L.) in rivers and estuaries in England and Wales - 2013. *Environment Agency.*

Colclough, S.R., Gray, G., Bark, A. & Knights, B. (2002) Fish and fisheries of the tidal Thames: Management of the modern resource, research aims and future pressures. *Journal of Fish Biology.* 61 (SUPPL. A), 64–73. doi:10.1006/jfbi.2002.2068.

Collins, R. (2019) *seaDNA protocols.* 2019. https://github.com/boopsboops/seadna-protocols/tree/master/docs.

Community, B.O. (2021) *Blender - a 3D modelling and rendering package.*

Corradi, N., Pombert, J.F., Farinelli, L., Didier, E.S. & Keeling, P.J. (2010) The complete sequence of the smallest known nuclear genome from the microsporidian *Encephalitozoon intestinalis. Nature Communications.* 1 (6). doi:10.1038/ncomms1082.

Corvalan, C., Hales, S., McMichael, A., Butler, C., Campbell-Lendrum, D., Confalonieri, U., Leitner, K., Lewis, N., Patz, J., Polson, K., Scheraga, J., Woodward, A. & Younes, M. (2005) *Ecosystems and human well-being: Health synthesisa: a report of the Millennium Ecosystem Assessment.* WHO Library Cataloguing-in-Publication Data Ecosystems.

Costa, G., Melo-Moreira, E. & De Carvalho, M.A.P. (2016) Occurrence of microsporidians *Glugea hertwigi* and *Pleistophora ladogensis*, in smelt Osmerus eperlanus from two German rivers, north Sea coast. *Diseases of Aquatic Organisms.* 121 (1), 49–57. doi:10.3354/dao03040.

Cotterell, S. & Hillman, R.. (2016) Monitoring of Allis Shad and Smelt in Tamar

Estuaries - EC18234. *The Marine Biological Association of the United Kingdom and the Environment Agency.*

Davies, P., Britton, R.J., Nunn, A.D., Dodd, J.R., Crundwell, C., Velterop, R., Ó'Maoiléidigh, N., O'Neill, R., Sheehan, E. V., Stamp, T. & Bolland, J.D. (2020) Novel insights into the marine phase and river fidelity of anadromous twaite shad *Alosa fallax* in the UK and Ireland. *Aquatic Conservation: Marine and Freshwater Ecosystems.* 30 (7), 1291–1298. doi:10.1002/aqc.3343.

Day, F. (1884) *The fishes of Great Britain and Ireland.* Williams and Norgate. doi:10.5962/bhl.title.58639.

Day, T. & Taylor, P.D. (1997) von Bertalanffy's growth equation should not be used to model age and size at maturity. *The American Naturalist.* 149 (2), 381–393.

Dechtiar, A.O. (1965) Preliminary Observations on *Glugea hertwigi*, Weissenberg, 1911 (Microsporidia; Glugeidae) in American Smelt, *Osmerus mordax* (Mitchill) from Lake Erie. *The Canadian Fish Culturist.* 34, 35–38.

Delisle, C.E. (1972) Variations mensuelles de *Glugea hertwigi* (Sporozoa: Microsporida) chez différents tissus et organes de l'éperlan adulte dulcicole et conséquences de cette infection sur une mortalité massive annuelle de ce poisson. *Canadian Journal of Zoology.* 50 (12), 1589–1600. doi:10.1139/z72-209.

Department for Environment Food & Rural Affairs (2018) *Environment 25 Year Plan.* (Her Majesty's Government (2018) 'Environment 25 Year Plan', pp. 1–151.).

Deslauriers, D. & Kieffer, J.D. (2011) The influence of flume length and group size on swimming performance in shortnose sturgeon *Acipenser brevirostrum. Journal of Fish Biology.* 79 (5), 1146–1155. doi:10.1111/j.1095-8649.2011.03094.x.

Devlaming, V., Grossman, G. & Chapman, F. (1982) On the use of the gonosomatic index. *Comparative Biochemistry and Physiology -- Part A: Physiology.* 73 (1), 31–39. doi:10.1016/0300-9629(82)90088-3.

Ding, Y., Vanselow, D.J., Yakovlev, M.A., Katz, S.R., Lin, A.Y., Clark, D.P., Vargas, P., Xin, X., Copper, J.E., Canfield, V.A., Ang, K.C., Wang, Y., Xiao, X., Carlo, F. De, Rossum, D.B.V., Riviere, P. La & Cheng, K.C. (2019) Computational 3d histological phenotyping of whole zebrafish by x-ray histotomography. *eLife.* 8, 1–28. doi:10.7554/eLife.44898.

Directive, W.F. (2000) (WFD). *Directive 2000/60/EC of the European Parliament and the Council of 23 October 2000 establishing a framework for community action in the field of water policy. Official Journal of the European Communities*

(22.12.2000). L327, 1.

Doherty, D. & McCarthy, T.K. (2004) The ecology and conservation of European smelt (Osmerus eperlanus L.) from Waterford Estuary, in southeastern Ireland. *Biology and Environment.* 104 (2), 125–130. doi:10.3318/BIOE.2004.104.2.125.

Dyková, I. & Lom, J. (1978) Tissue reaction of the three-spined stickleback *Gasterosteus aculeatus* L. to infection with *Glugea anomala* (Moniez, 1887). *Journal of Fish Diseases.* 1 (1), 83–90. doi:10.1111/j.1365-2761.1978.tb00007.x.

Dyková, I. & Lom, J. (1980) Tissue reactions to microsporidian in fish. *J Fish Dis.* 3, 265–283.

Dziekonska-Rynko, J., Mierzejewska, K., Kubiak, K., Rydzewska, M. & Hliwa, P. (2018) Helminths of European smelt *Osmerus eperlanus* (Linnaeus, 1758) in Lake Hancza and the Vistula Lagoon, with special regard to their zoonotic threats. *Acta veterinaria Hungarica.* 66 (1), 96–106. doi:10.1556/004.2018.009.

FAO (1974) *Manual of Fisheries Science Part 2 - Methods of Resource Investigation and their Application.* Food and Agriculture Organization of the United Nations. http://www.fao.org/3/F0752E/F0752E00.htm.

Ferrón, H.G., Martínez-Pérez, C., Rahman, I.A., Selles de Lucas, V., Botella, H. & Donoghue, P.C.J. (2020) Computational fluid dynamics suggests ecological diversification among stem-gnathostomes. *Current Biology.* 1–6. doi:10.1016/j.cub.2020.09.031.

Forest, J.J.H., King, S.D. & Cone, D.K. (2009) Occurrence of *Glugea pimephales* in planktonic larvae of fathead minnow in Algonquin Park, Ontario. *Journal of Aquatic Animal Health.* 21 (3), 164–166. doi:10.1577/H08-057.1.

Fraser, C.M. (1916) Growth of the spring salmon. *Transaction of Pacific Fisheries Society.* (915).

Froese, R. (2006) Cube law, condition factor and weight-length relationships: History, meta-analysis and recommendations. *Journal of Applied Ichthyology.* 22 (4), 241–253. doi:10.1111/j.1439-0426.2006.00805.x.

Goldberg, C.S., Turner, C.R., Deiner, K., Klymus, K.E., Thomsen, P.F., Murphy, M.A., Spear, S.F., McKee, A., Oyler-McCance, S.J., Cornman, R.S., Laramie, M.B., Mahon, A.R., Lance, R.F., Pilliod, D.S., Strickler, K.M., Waits, L.P., Fremier, A.K., Takahara, T., Herder, J.E., et al. (2016) Critical considerations for the application of environmental DNA methods to detect aquatic species. *Methods in Ecology and Evolution.* 7 (11), 1299–1307. doi:10.1111/2041-210X.12595.

Gorodilov, Y.N. & Melnikova, E.L. (2006) Embryonic development of the European smelt *Osmerus eperlanus eperlanus* (L.) (Neva population). *Russian Journal of Marine Biology*. 32 (3), 173–185. doi:10.1134/s1063074006030059.

Grizzetti, B., Pistocchi, A., Liquete, C., Udias, A., Bouraoui, F. & Van De Bund, W. (2017) Human pressures and ecological status of European rivers. *Scientific Reports*. 7 (1), 1–11. doi:10.1038/s41598-017-00324-3.

Groot, S.J. de (2002) A review of the past and present status of anadromous fish species in the Netherlands: is restocking the Rhine feasible? *Hydrobiologia*. 478, 205–218. doi:10.1023/A:1021038916271.

Gutarra, S., Moon, B.C., Rahman, I.A., Palmer, C., Lautenschlager, S., Brimacombe, A.J. & Benton, M.J. (2019) Effects of body plan evolution on the hydrodynamic drag and energy requirements of swimming in ichthyosaurs. *Proceedings of the Royal Society B: Biological Sciences*. 286 (1898). doi:10.1098/rspb.2018.2786.

Gutiérrez, Y., Ott, D., Töpperwien, M., Salditt, T. & Scherber, C. (2018) X-ray computed tomography and its potential in ecological research: A review of studies and optimization of specimen preparation. *Ecology and Evolution*. 8 (15), 7717–7732. doi:10.1002/ece3.4149.

H.M.Government (1994) *The UK Biodiversity Action Plan*. 1–192.

Haley, A.J. (1954) Microsporidian Parasite, *Glugea Hertwigi*, in American Smelt from the Great Bay Region, New Hampshire. *Transactions of the American Fisheries Society*. 83 (1), 84–90. doi:10.1577/1548-8659(1953)83[84:MPGHIA]2.0.CO;2.

Haley, A.J. (1952) Preliminary Observations on a Severe Epidemic of Microsporidiosis in the Smelt , *Osmerus mordax* (Mitchell. *Journal of Parasitology*. 38 (2), 14–15.

Haley, A.J., Voge, M. & Read, C.P. (1954) Further Observations on *Glugea hertwigi* Weissenberg 1911 , 1913 (Microsporidia) in Fresh Water Smelt in New Hampshire. *Journal of Parasitology*. 40 (4), 482–483.

Hammar, J., Axenrot, T., Degerman, E., Asp, A., Bergstrand, E., Enderlein, O., Filipsson, O. & Kylberg, E. (2018) Smelt (*Osmerus eperlanus*): Glacial relict, planktivore, predator, competitor, and key prey for the endangered Arctic char in Lake Vättern, southern Sweden. *Journal of Great Lakes Research*. 44 (1), 126–139. doi:10.1016/j.jglr.2017.11.008.

Hammer, C. (1995) Fatigue and exercise tests with fish. *Comparative Biochemistry and Physiology -- Part A: Physiology*. 112 (1), 1–20. doi:10.1016/0300-9629(95)00060-K.

Henderson, B.A. & Nepszy, S.J. (1989) Factors affecting recruitment and mortality rates of rainbow smelt (*Osmerus Mordax*) in Lake Erie, 1963–85. *Journal of Great Lakes Research*. 15 (2), 357–366. doi:10.1016/S0380-1330(89)71488-X.

Hofmann, A. & Clokie, S. (Eds. . (2018) *Wilson and Walker's Principles and Techniques of Biochemistry and Molecular Biology*. 8th edition. Cambridge University Press. doi:10.1017/9781316677056.

Horppila, J., Nyberg, K., Peltonen, H. & Turunen, T. (1996) Effects of five years of intensive trawling on a previously unexploited smelt stock. *Journal of Fish Biology*. 49 (2), 329–340. doi:10.1006/jfbi.1996.0158.

Hulme, P.E. (2017) Climate change and biological invasions: evidence, expectations, and response options. *Biological Reviews*. 92 (3), 1297–1313. doi:10.1111/brv.12282.

Hutchings, J.A. & Reynolds, J.D. (2004) Marine fish population collapses: Consequences for recovery and extinction risk. *BioScience*. 54 (4), 297–309. doi:10.1641/0006-3568(2004)054[0297:MFPCCF]2.0.CO;2.

Hutchinson, P. (1983) The ecology of smelt, *Osmerus eperlanus* (Linnaeus), from the River Thames and the River Cree. University of Edinburgh.

Hutchinson, P. & Mills, D.H. (1987) Characteristics of spawning-run smelt, *Osmerus eperlanus* (L.), from a Scottish river, with recommendations for their conservation and management. *Aquaculture Research*. 18 (3), 249–258. doi:10.1111/j.1365-2109.1987.tb00145.x.

Jenkins, G.J., Perry, M.C. & Prior, M.J. (2008) The climate of the UK and recent trends-UKCP09. *Met Office*.

Jennings, S., Reynolds, J.D. & Mills, S.C. (1998) Life history correlates of responses to fisheries exploitation. *Proceedings of the Royal Society B: Biological Sciences*. 265 (1393), 333–339. doi:10.1098/rspb.1998.0300.

JNCC (2012) JNCC and Natural England's advice to Defra on recommended Marine Conservation Zones Marine Conservation Zone Project Executive Summary. *Joint Nature Conservation Committee*. (July), 1455.

JNCC (2010) *UK priority species pages – Version 2*. http://jncc.defra.gov.uk/_speciespages/2477.pdf.

Jolly, M.T., Aprahamian, M.W., Hawkins, S.J., Henderson, P.A., Hillman, R., O'Maoiléidigh, N., Maitland, P.S., Piper, R. & Genner, M.J. (2012) Population genetic structure of protected allis shad (*Alosa alosa*) and twaite shad (*Alosa*

fallax). *Marine Biology.* 159 (3), 675–687. doi:10.1007/s00227-011-1845-x.

Kangur, A., Kangur, P., Kangur, K. & Mols, T. (2007) The role of temperature in the population dynamics of smelt *Osmerus eperlanus eperlanus m . spirinchus Pallas* in Lake Peipsi (Estonia / Russia). *Hydrobiologia.* 584, 433–441. doi:10.1007/s10750-007-0614-9.

Katharios, P., Varvarigos, P., Keklikoglou, K., Ruetten, M., Sojan, J., Akter, M., Cascarano, M.C., Tsertou, M.I. & Kokkari, C. (2020) Native parasite affecting an introduced host in aquaculture: Cardiac henneguyosis in the red seabream *Pagrus major* Temminck & Schlegel (Perciformes: Sparidae) caused by *Henneguya aegea* n. sp. (Myxosporea: Myxobolidae). *Parasites and Vectors.* 13 (1), 1–14. doi:10.1186/s13071-020-3888-7.

Khan, R.A. (2004) Effect, distribution, and prevalence of *Glugea stephani* (microspora) in winter flounder (*Pleuronectes americanus*) living near two pulp and paper mills in newfoundland. *Journal of Parasitology.* 90 (2), 229–233. doi:10.1645/GE-107R.

King, S. & O'Hanley, J.. (2016) Optimal fish passage barrier removal - revisited. *River Research and Applications.* 32, 418–428. doi:10.1002/rra.

Klumb, R.A., Bozek, M.A. & Frie, R. V (1999) Validation of the Dahl – Lea and Fraser – Lee Back- calculation models by using Oxytetracycline-marked bluegills and bluegill × green sunfish hybrids. *North American Journal of Fisheries Management.* 19, 504–514. doi:10.1577/1548-8675(1999)019<0504.

Kogan, I., Pacholak, S., Licht, M., Schneider, J.W., Bru cker, C. & Brandt, S. (2015) The invisible fish: hydrodynamic constraints for predator-prey interaction in fossil fish Saurichthys compared to recent actinopterygians. *Biology Open.* 4 (12), 1715–1726. doi:10.1242/bio.014720.

Laudan, R., Stolen, J.S. & Cali, A. (1986) Immunoglobulin levels of the winter flounder (*Pseudopleuronectes americanus*) and the summer flounder (*Paralichthys dentatus*) injected with the microsporidan parasite *Glugea stephani*. *Developmental and Comparative Immunology.* 10 (3), 331–340. doi:10.1016/0145-305X(86)90023-6.

Lauder, G. V., Wainwright, D.K., Domel, A.G., Weaver, J.C., Wen, L. & Bertoldi, K. (2016) Structure, biomimetics, and fluid dynamics of fish skin surfaces. *Physical Review Fluids.* 1 (6), 1–18. doi:10.1103/PhysRevFluids.1.060502.

Lautenschlager, S. (2016) Reconstructing the past: Methods and techniques for the digital restoration of fossils. *Royal Society Open Science.* 3 (10).

doi:10.1098/rsos.160342.

Lee, R.M. (1920) *A review of the methods of age and growth determination in fishes by means of scales*. HM Stationery Office.

Lee, S.-J., Yokoyama, H. & Ogawa, K. (2004) Modes of transmission of *Glugea plecoglossi* (Microspora) via the skin and digestive tract in an experimental infection model using rainbow trout, *Oncorhynchus mykiss* (Walbaum). *Journal of fish diseases*. 27 (8), 435–444. doi:10.1111/j.1365-2761.2004.00556.x.

Legault, R.O. & Delisle, C. (1967) Acute infection by *Glugea hertwigi* Weissenberg in young-of-the-year rainbow smelt, *Osmerus eperlanus mordax* (Mitchill). *Canadian Journal of Zoology*. 45 (6), 1291–1292. doi:10.1139/z67-141.

Lester, N.P., Shuter, B.J. & Abrams, P.A. (2004) Interpreting the von Bertalanffy model of somatic growth in fishes: The cost of reproduction. *Proceedings of the Royal Society B: Biological Sciences*. 271 (1548), 1625–1631. doi:10.1098/rspb.2004.2778.

Liu, H. (2002) Computational biological fluid dynamics: Digitizing and visualizing animal swimming and flying. *Integrative and Comparative Biology*. 42 (5), 1050–1059. doi:10.1093/icb/42.5.1050.

Lom, J. (2002) A catalogue of described genera and species of microsporidians parasitic in fish. *Systematic Parasitology*. 53 (2), 81–99. doi:10.1023/A:1020422209539.

Lom, J. & Dyková, I. (2005) Microsporidian xenomas in fish seen in wider perspective. *Folia Parasitologica*. 52 (1–2), 69–81. doi:10.14411/fp.2005.010.

Lom, J. & Nilsen, F. (2003) Fish microsporidia: Fine structural diversity and phylogeny. *International Journal for Parasitology*. 33 (2), 107–127. doi:10.1016/S0020-7519(02)00252-7.

Lom, J., Noga, E.J. & Dykova, I. (1995) Occurrence of a microsporean with characteristics of *Glugea anomala* in ornamental fish of the family Cyprinodontidae. *Diseases of Aquatic Organisms*. 21 (3), 239–242. doi:10.3354/dao021239.

Lorenz, T.C. (2012) Polymerase chain reaction: Basic protocol plus troubleshooting and optimization strategies. *Journal of Visualized Experiments*. (63), 1–15. doi:10.3791/3998.

Lovy, J., Kostka, M., Dyková, I., Arsenault, G., Pecková, H., Wright, G.M. & Speare, D.J. (2009) Phylogeny and morphology of *Glugea hertwigi* from rainbow smelt

Osmerus mordax found in Prince Edward Island, Canada. *Diseases of Aquatic Organisms.* 86 (3), 235–243. doi:10.3354/dao02133.

Lovy, J., Yanong, R.P.E., Stilwell, J.M., Waltzek, T.B., Shelley, J.P., Pouder, D.B., Wolf, J.C. & Camus, A.C. (2021) Tetra disseminated microsporidiosis: a novel disease in ornamental fish caused by *Fusasporis stethaprioni* n. gen. n. sp. *Parasitology Research.* 120 (2), 497–514. doi:10.1007/s00436-020-06988-7.

Luna, L. (1968) *Manual of histologic staining methods of the armed forces institute of pathology.* 3rd Editio. McGraw-Hill.

Lyle, A.A. & Maitland, P.S. (1997) The spawning migration and conservation of smelt, *Osmerus eperlanus* in the River Cree, Southwest Scotland. *Biological Conservation.* 3207 (96), 303–311. doi:10.1016/S0006-3207(96)00039-0.

Maitland, P.. & Campbell, R.. (1992) *Freshwater Fishes of the British Isles (Collins New Naturalist Library, Book 75).* HarperCollins.

Maitland, P. (2003) The status of smelt *Osmerus eperlanus* in England. *English Nature Research Reports.* 516 (516), 83.

Maitland, P.S. (2007) *Scotland's Freshwater Fish: Ecology, Conservation & Folklore.* Trafford Publishing. doi:ISBN 10: 1425110649.

Maitland, P.S. & Lyle, A. (1996) The smelt *Osmerus eperlanus* in scotland. *Freshwater Forum.* 6 (Maitland), 57–68.

Mansour, L., Thabet, A., Harrath, A.H., Al Omar, S.Y., Mukhtar, A., Sayed, S.R. & Abdel-Baki, A.A.S. (2016) New microsporidia, G*lugea sardinellensis* n. Sp. (microsporea, glugeida) found in *Sardinella aurita valenciennes*, 1847, collected off tunisian coasts. *Acta Protozoologica.* 55 (4), 281–290. doi:10.4467/16890027AP.16.028.6097.

Masters, J.E.G., Jang, M.H., Ha, K., Bird, P.D., Frear, P.A. & Lucas, M.C. (2006) The commercial exploitation of a protected anadromous species, the river lamprey (*Lampetra fluviatilis* (L.)), in the tidal River Ouse, north-east England. *Aquatic Conservation: Marine and Freshwater Ecosystems.* 16 (1), 77–92. doi:10.1002/aqc.686.

Mcadam, D.S.O., Liley, N.R. & Tan, E.S.P. (1999) Comparison of reproductive indicators and analysis of the reproductive seasonality of the tinfoil barb , *Puntius schwanenfeldii* , in the Perak River , Malaysia. *Environmental Biology of Fishes.* 55 (4), 369–380. doi:https://doi.org/10.1023/A:1007563914300.

McAllister, D.E. (1984) *Fishes of the north-eastern Atlantic and Mediterranean.*

Volume 1.

McCard, J. (2015) *Smelt in the Tidal Thames (Unpublished thesis)*. University College London.

McCarthy, I.D., Jones, N.J.E., Moore, D.M. & Berlinsky, D.L. (2020) Determining the optimum temperature and salinity for larval culture, and describing a culture protocol for the conservation aquaculture for European smelt *Osmerus eperlanus* (L.). *Journal of Applied Ichthyology.* 36 (1), 113–120. doi:10.1111/jai.13992.

McVicar, A.H. (1975) Infection of plaice *Pleuronectes platessa* L. with G*lugea (Nosema) stephani* (Hagenmüller 1899)(Protozoa: Microsporidia) in a fish farm and under experimental conditions. *Journal of Fish Biology.* 7 (5), 611–619. doi:10.1111/j.1095-8649.1975.tb04634.x.

Mennerat, A., Nilsen, F., Ebert, D. & Skorping, A. (2010) Intensive farming: Evolutionary implications for parasites and pathogens. *Evolutionary Biology.* 37 (2), 59–67. doi:10.1007/s11692-010-9089-0.

Miller, J.D. & Hutchins, M. (2017) The impacts of urbanisation and climate change on urban fl ooding and urban water quality : A review of the evidence concerning the United Kingdom. *Journal of Hydrology: Regional Studies.* 12 (January), 345–362. doi:10.1016/j.ejrh.2017.06.006.

Miwa, S., Kamaishi, T., Hirae, T., Murase, T. & Nishioka, T. (2011) Encephalomyelitis associated with microsporidian infection in farmed greater amberjack, *Seriola dumerili* (Risso). *Journal of Fish Diseases.* 34 (12), 901–910. doi:10.1111/j.1365-2761.2011.01312.x.

Mladineo, I., Hrabar, J., Vidjak, O., Bočina, I., Čolak, S., Katharios, P., Cascarano, M.C., Keklikoglou, K., Volpatti, D. & Beraldo, P. (2020) Host-parasite interaction between parasitic cy-mothoid *ceratothoa oestroides* and its host, farmed european sea bass (*Dicentrarchus labrax*). *Pathogens.* 9 (3), 1–19. doi:10.3390/pathogens9030230.

Moore, A., Ives, M., Davison, P. & Privitera, L. (2016) A preliminary study on the movements of smelt, *Osmerus eperlanus*, in two East Anglian rivers. *Fisheries Management and Ecology.* 23 (2), 169–171. doi:10.1111/fme.12150.

Musk, R.S., Britton, J.R. & Axford, S.N. (2006) The effect of subjective fish scale ageing on growth and recruitment analyses: A case study from the UK. *Acta Ichthyologica et Piscatoria.* 36 (1), 81–84. doi:10.3750/AIP2006.36.1.12.

Nash, R.D.M., Valencia, A.H., Geffen, A.J. & Meek, A. (2006) *The Origin of Fulton ' s*

Condition Factor — Setting the Record Straight. 31 (5).

NBN Atlas (2021) *Osmerus eperlanus (Linnaeus, 1758).* 2021. https://records.nbnatlas.org/occurrences/search?q=lsid%3ANBNSYS000018860 9&fq=(data_resource_uid%3A%22dr741%22 OR data_resource_uid%3A%22dr815%22 OR data_resource_uid%3A%22dr1928%22)&nbn_loading=true#tab_mapView [Accessed: 9 December 2021].

Nepszy, J., Budd, J. & Dechtiar, A.O. (1978) Motality of young-of-the-year rainbow smelt (*Osmerus mordax*) in Lake Erie asscociated with the occurence of *Glugea hertwigi. Journal of Wildlife Diseases.* 14, 233–239. doi:10.7589/0090-3558-14.2.233.

Nepszy, S.J. & Dechtiar, A.O. (1972) Occurrence of *Glugea hertwigi* in Lake Erie rainbow Smelt (*Osmerus mordax*) and associated mortality of adult smelt. *Journal of the Fisheries Research Board of Canada.* 29 (11), 1639–1641. doi:10.1139/f72-254.

Nilsen, F. (2000) Small subunit ribosomal DNA phylogeny of microsporidia with particular reference to genera that infect fish. *The Journal of parasitology.* 86 (1), 128–133. doi:10.1645/0022-3395(2000)086.

Nilsen, F., Endresen, C. & Hordvik, I. (1998) Molecular phylogeny of microsporidians with particular reference to species that infect the muscles of fish. *Journal of Eukaryotic Microbiology.* 45 (5), 535–543. doi:10.1111/j.1550-7408.1998.tb05113.x.

O'Sullivan, J.D.B., Behnsen, J., Starborg, T., MacDonald, A.S., Phythian-Adams, A.T., Else, K.J., Cruickshank, S.M. & Withers, P.J. (2018) X-ray micro-computed tomography (μCT): An emerging opportunity in parasite imaging. *Parasitology.* 145 (7), 848–854. doi:10.1017/S0031182017002074.

Ogle, D.H., Brenden, T.O. & McCormick, J.L. (2017) Growth Estimation: Growth Models and Statistical Inference. In: M.C. Quist & D.A. Isermann (eds.). *Age and Growth of Fishes: Principles and Techniques.* American Fisheries Society. pp. 265–352.

Ogle, D.H., Wheeler, P. & Dinno, A. (2021) *FSA: Fisheries Stock Analysis.* https://github.com/droglenc/FSA.

Olson, R.E. (1981) Effects of low temperature on the development of the microsporidan *Glugea stephani* in English sole (*Parophrys vetulus*). *Journal of*

wildlife diseases. 17 (4), 559–562. doi:10.7589/0090-3558-17.4.559.

Pekcan-Hekim, Z., Rahkonen, R. & Horppila, J. (2005) Occurrence of the parasite *Glugea hertwigi* in young-of-the-year smelt in Lake Tuusulanjärvi. *Journal of Fish Biology*. 66 (2), 583–588. doi:10.1111/j.0022-1112.2005.00617.x.

Pekkarinen, M., Lom, J. & Nilsen, F. (2002) *Ovipleistophora gen. n.*, a new genus for *Pleistophora mirandellae*-like microsporidia. *Diseases of Aquatic Organisms*. 48 (2), 133–142. doi:10.3354/dao048133.

Peterson, T.S., Spitsbergen, J.M., Feist, S.W. & Kent, M.L. (2011) The Luna stain, an improved selective stain for detection of microsporidian spores in histologic sections. *Diseases of Aquatic Organisms*. 95 (2), 175–180. doi:10.1021/nl061786n.Core-Shell.

Pilcher, M. (1989) Tidal Thames fishery survey. *National Rivers Authority*.

Pilecka-Rapacz, M., Piasecki, W., Głoćko, M., Kesminas, V., Domagała, J., Wiśniewski, G. & Czerniawski, R. (2017) Parasitological survey of smelt, *Osmerus eperlanus* (Actinopterygii: Osmeridae), from five estuary sites along the southern coast of the Baltic Sea. *Oceanological and Hydrobiological Studies*. 46 (3), 314–324. doi:10.1515/ohs-2017-0033.

Pinsky, M.L., Jensen, O.P., Ricard, D. & Palumbi, S.R. (2011) *Unexpected patterns of fisheries collapse in the world's oceans*. 108 (20), 8317–8322. doi:10.1073/pnas.1015313108.

Pomport-Castillon, C., De Jonckheere, J.F. & Romestand, B. (2000) Ribosomal DNA sequences of *Glugea anomala, G. stephani, G. americanus and Spraguea lophii* (Microsporidia): Phylogenetic reconstruction. *Diseases of Aquatic Organisms*. 40 (2), 125–129. doi:10.3354/dao040125.

Powell, M.D. & Gamperl, A.K. (2016) Effects of *Loma morhua* (Microsporidia) infection on the cardiorespiratory performance of Atlantic cod *Gadus morhua* (L). *Journal of Fish Diseases*. 39 (2), 189–204. doi:10.1111/jfd.12352.

van Puijenbroek, P.J.T.M., Buijse, A.D., Kraak, M.H.S. & Verdonschot, P.F.M. (2019) Species and river specific effects of river fragmentation on European anadromous fish species. *River Research and Applications*. 35 (1), 68–77. doi:10.1002/rra.3386.

Putz, R.E., Hoffman, G.L. & Dunbar, C.E. (1965) Two new species of plistophora (microsporidea) from North American fish with a synopsis of microsporidea of freshwater and euryhaline fishes. *Journal of Protozoology*. 12 (2), 228–236.

doi:10.2307/3492933.

Qiagen (2017) *DNeasy PowerSoil Kit Handbook*.p.24. https://www.qiagen.com/gb/resources/resourcedetail?id=5a0517a7-711d-4085-8a28-2bb25fab828a&lang=en.

Reidy, S.P., Kerr, S.R. & Nelson, J.A. (2000) Aerobic and anaerobic swimming performance of individual atlantic cod. *Journal of Experimental Biology*. 203 (2), 347–357. doi:10.1242/jeb.203.2.347.

Repečka, R. (2003) Changes in biological indices and abundance of salmon, sea trout, smelt, vimba and twaite shad in the coastal zone of the Baltic Sea and the Curonian Lagoon at the beginning of spawning migration. *Acta Zoologica Lituanica*. 13 (2), 195–216. doi:10.1080/13921657.2003.10512563.

Reynolds, J.D., Dulvy, N.K., Goodwin, N.B. & Hutchings, J.A. (2005) Biology of extinction risk in marine fishes. *Proceedings of the Royal Society B: Biological Sciences*. 272 (1579), 2337–2344. doi:10.1098/rspb.2005.3281.

Richardson, M. & Soloviev, M. (2021) The thames: Arresting ecosystem decline and building back better. *Sustainability (Switzerland)*. 13 (11). doi:10.3390/su13116045.

Ricker, W.E. (1958) Handbook of computations for biological statistics of fish populations. *Can Fish Res Board Bull*. 119, 300.

Rodriguez-Tovar, L.E., Speare, D.J. & Markham, R.J.F. (2011) Fish microsporidia: Immune response, immunomodulation and vaccination. *Fish and Shellfish Immunology*. 30 (4–5), 999–1006. doi:10.1016/j.fsi.2011.02.011.

Rovaris, K., Queiroz, P.M., Vasconcelos, K. de F., Corpas, L. dos S., da Silveira, B.M. & Freitas, D.Q. (2018) Segmentation methods for micro CT images: A comparative study using human bone samples. *Brazilian Dental Journal*. 29 (2), 150–153. doi:10.1590/0103-6440201801385.

Ryan, J.A. & Kohler, S.L. (2016) Distribution, prevalence, and pathology of a microsporidian infecting freshwater sculpins. *Diseases of Aquatic Organisms*. 118 (3), 195–206. doi:10.3354/dao02974.

Sanders, J., Myers, M.S., Tomanek, L., Cali, A., Takvorian, P.M. & Kent, M.L. (2012) *Ichthyosporidium weissii* n. sp. (microsporidia) infecting the arrow goby (*Clevelandia ios*). *Journal of Eukaryotic Microbiology*. 59 (3), 258–267. doi:10.1111/j.1550-7408.2012.00619.x.Ichthyosporidium.

Sanders, J.L., Lawrence, C., Nichols, D.K., Brubaker, J.F., Peterson, T.S., Murray,

K.N. & Kent, M.L. (2010) *Pleistophora hyphessobryconis* (Microsporidia)infecting zebrafish danio rerio in research facilities. *Diseases of Aquatic Organisms*. 91 (1), 47–56. doi:10.3354/dao02245.

Sandlund, O.T., Stang, Y.G., Kjellberg, G., Næsje, T.F. & Hambo, M.U. (2005) European smelt (*Osmerus eperlanus*) eats all; eaten by all: Is it a key species in lakes? *SIL Proceedings, 1922-2010*. 29 (1), 432–436. doi:10.1080/03680770.2005.11902049.

Scarborough, A. & Weidner, E. (1979) Field and laboratory studies of *Glugea hertwigi* (microsporida) in the rainbow smelt *Osmerus mordax*. *The Biological Bulletin*. 157 (2), 334–343. doi:10.2307/1541059.

Schrader, F. (1921) A microsporidian occurring in the smelt. *The Journal of Parasitology*. 7 (3), 151–153. doi:10.2307/3270783.

Sendek, D.S. & Bogdanov, D. V. (2019) European smelt *Osmerus eperlanus* in the eastern Gulf of Finland, Baltic Sea: Stock status and fishery. *Journal of Fish Biology*. 94 (6), 1001–1010. doi:10.1111/jfb.14009.

Shpilev, H., Ojaveer, E. & Lankov, A. (2005) Smelt (*Osmerus eperlanus* L.) in the Baltic Sea. *Biology and Ecology*. 54, 230–241. doi:10.3176/biol.ecol.2005.3.04.

Silva, A.T., Chlebak, R.J., Dawson, J.W., Cooke, S.J., Webb, J.A., Costelloe, J.F., CasasMulet, R., Lyon, J.P. & Stewardson, M.J. (2016) Effect of parasitic sea lamprey on profile drag of lake trout: Consequences for swimming. *11th International Symposium on Ecohydraulics*. (11th Int. Symp. Ecohydraulics).

Sogin, M.L. & Silberman, J.D. (1998) Evolution of the protists and protistan parasites from the perspective of molecular systematics. *International Journal for Parasitology*. 28 (1), 11–20. doi:10.1016/S0020-7519(97)00181-1.

Sprengel, G. & Luchtenberg, H. (1991) Infection by endoparasites reduces maximum swimming speed of European smelt *Osmerus eperlanus* and European eel *Anguilla anguilla*. *Diseases of Aquatic Organisms*. 11 (1), 31–35. doi:10.3354/dao011031.

Steffens, W. (1962) Der heutige stand der verbreitung von *Plistophora hyphessobryconis Schäperclaus* 1941 (Sporozoa, Microsporidia). *Zeitschrift für Parasitenkunde*. 21 (6), 535–541. doi:10.1007/BF00260258.

Stentiford, G.D., Bateman, I.J., Hinchliffe, S.J., Bass, D., Hartnell, R., Santos, E.M., Devlin, M.J., Feist, S.W., Taylor, N.G.H., Verner-Jeffreys, D.W., van Aerle, R., Peeler, E.J., Higman, W.A., Smith, L., Baines, R., Behringer, D.C., Katsiadaki, I.,

Froehlich, H.E. & Tyler, C.R. (2020) Sustainable aquaculture through the One Health lens. *Nature Food*. 1 (8), 468–474. doi:10.1038/s43016-020-0127-5.

Stentiford, G.D., Bateman, K.S., Feist, S.W., Chambers, E. & Stone, D.M. (2013a) Plastic parasites: Extreme dimorphism creates a taxonomic conundrum in the phylum Microsporidia. *International Journal for Parasitology*. 43 (5), 339–352. doi:10.1016/j.ijpara.2012.11.010.

Stentiford, G.D., Feist, S.W., Stone, D.M., Bateman, K.S. & Dunn, A.M. (2013b) Microsporidia: Diverse, dynamic, and emergent pathogens in aquatic systems. *Trends in Parasitology*. 29 (11), 567–578. doi:10.1016/j.pt.2013.08.005.

Stewart, A., Hunt, R., Mitchell, R., Muhawenimana, V., Wilson, C.A.M.E., Jackson, J.A. & Cable, J. (2018) The cost of infection: *Argulus foliaceus* and its impact on the swimming performance of the three-spined stickleback (*Gasterosteus aculeatus*). *Journal of the Royal Society Interface*. 15 (147). doi:10.1098/rsif.2018.0571.

Stoeckle, M.Y., Soboleva, L. & Charlop-Powers, Z. (2017) Aquatic environmental DNA detects seasonal fish abundance and habitat preference in an urban estuary. *PLoS ONE*. 12 (4), 1–15. doi:10.1371/journal.pone.0175186.

Švagždys, A. (2009) Impact of environmental conditions on smelt catch fluctuations in the Nemunas River and the Curonian Lagoon. *Ekologija*. 55 (3), 204–214. doi:10.2478/v10055-009-0025-5.

Svanberg, I., Bonow, M. & Cios, S. (2016) Fishing For Smelt, *Osmerus Eperlanus* (Linnaeus, 1758): A traditional food fish – possible cuisine in post-modern Sweden? *Slovak Ethnology*. 2 (64), 136–157.

Taal, I., Saks, L., Nedolgova, S., Verliin, A., Kesler, M., Jürgens, K., Svirgsden, R., Vetemaa, M. & Saat, T. (2014) Diet composition of smelt *Osmerus eperlanus* (Linnaeus) in brackish near-shore ecosystem (Eru Bay, Baltic Sea). *Ecology of Freshwater Fish*. 23 (2), 121–128. doi:10.1111/eff.12044.

Takahashi, S. & Egusa, S. (1977) Studies on Glugea infection of the ayu, *Plecoglossus altivelis*: Description of the Glugea and a proposal of a new species , *Glugea plecoglossi*. *Fish Pathology*. 11 (175–182). doi:10.3147/jsfp.11.175.

Tamura, K. & Nei, M. (1993) Estimation of the number of nucleotide substitutions in the control region of mitochondrial DNA in humans and chimpanzees. *Molecular biology and evolution*. 10 (3), 512–526. doi:10.1093/oxfordjournals.molbev.a040023.

The Rivers Trust (2021) *State of our Rivers*. 2021. https://storymaps.arcgis.com/collections/6730f10b64184200b171a57750890643 ?item=1 [Accessed: 3 December 2021].

Tokarev, Y.S., Voronin, V.N., Senderskiy, I.V. & Issi, I.V. (2015) The microsporidium *glugea gasterostei voronin* 1974 (microsporidia: marinosporidia) from the three-spined stickleback *Gasterosteus aculeatus* (actinopterygii: gasterosteiformes) as an independent species. *Parazitologiia*. 49 (2), 81–92.

Tsai, S.J., Kou, G.H., Lo, C.F. & Wang, C.H. (2002) Complete sequence and structure of ribosomal RNA gene of *Heterosporis anguillarum*. *Diseases of Aquatic Organisms*. 49 (3), 199–206. doi:10.3354/dao049199.

Tsuji, S., Takahara, T., Doi, H., Shibata, N. & Yamanaka, H. (2019) The detection of aquatic macroorganisms using environmental DNA analysis—A review of methods for collection, extraction, and detection. *Environmental DNA*. 1 (2), 99–108. doi:10.1002/edn3.21.

Valenčáková, A. & Sučik, M. (2020) Alternatives in molecular diagnostics of encephalitozoon and enterocytozoon infections. *Journal of Fungi*. 6 (3), 1–18. doi:10.3390/jof6030114.

Verhoeven, J.T.A. (2014) Wetlands in Europe: Perspectives for restoration of a lost paradise. *Ecological Engineering*. 66, 6–9. doi:10.1016/j.ecoleng.2013.03.006.

Videler, J.J. (2012) *Fish Swimming*. Springer Science & Business Media. doi:10.1007/978-94-011-1580-3.

Vossbrinck, C.R., Andreadis, T.G., Vavra, J. & Becnel, J.J. (2004) Molecular phylogeny and evolution of mosquito parasitic microsporidia (microsporidia: Amblyosporidae). *Journal of Eukaryotic Microbiology*. 51 (1), 88–95. doi:10.1063/1.1681954.

Vossbrinck, C.R., Baker, M.D., Didier, E.S., Debrunner-Vossbrinck, B.A. & Shadduck, J.A. (1993) Ribosomal DNA sequences of *Encephalitozoon hellem* and *Encephalitozoon cuniculi:* Species identification and phylogenetic construction. *Journal of Eukaryotic Microbiology*. 40 (3), 354–362. doi:10.1111/j.1550-7408.1993.tb04928.x.

Vossbrinck, C.R. & Debrunner-Vossbrinck, B.A. (2005) Molecular phylogeny of the Microsporidia: Ecological, ultrastructural and taxonomic considerations. *Folia Parasitologica*. 52 (1–2), 131–142. doi:10.14411/fp.2005.017.

Vossbrinck, C.R., Maddox, J. V., Friedman, S., Debrunner-Vossbrinck, B.A. & Woese,

C.R. (1987) Ribosomal RNA sequence suggests microsporidia are extremely ancient eukaryotes. *Nature*. 326 (6111), 411–414. doi:10.1038/326411a0.

Weidner, E. & Sibley, L.D. (1985) Phagocytized intracellular microsporidian blocks phagosome acidification and phagosome-lysosome fusion. *The Journal of Protozoology*. 32 (2), 311–317. doi:10.1111/j.1550-7408.1985.tb03056.x.

Weinhardt, V., Shkarin, R., Wernet, T., Wittbrodt, J., Baumbach, T. & Loosli, F. (2018) Quantitative morphometric analysis of adult teleost fish by X-ray computed tomography. *Scientific Reports*. 8 (1), 1–12. doi:10.1038/s41598-018-34848-z.

Weiss, L.M. & Becnel, J.J. (2014) *Microsporidia: Pathogens of Opportunity*. First. Wiley Blackwell.

Weiss, L.M., Zhu, X., Cali, A., Tanowitz, H.B. & Wittner, M. (1994) Utility of microsporidian rRNA in diagnosis and phylogeny: A review. *Folia Parasitologica*.41 (2) pp.81–90.

Weissenberg, R. (1913) Beiträge zur Kenntnis des Zeugungskreises der Microsporidien *Glugea anomala* Moniez und *hertwigi* Weissenberg. *Archiv für mikroskopische Anatomie*. 82 (2), 81–163. doi:10.1007/BF02892181.

Weissenberg, R. (1968) Intracellular development of the microsporidan *Glugea anomala* Moniez in hypertrophying migratory cells of the fish *Gasterosteus aculeatus* L., an example of the formation of "xenoma" tumors. *The Journal of Protozoology*. 15 (1), 44–57. doi:10.1111/j.1550-7408.1968.tb02088.x.

Windsor, S.P. & McHenry, M.J. (2009) The influence of viscous hydrodynamics on the fish lateral-line system. *Integrative and Comparative Biology*. 49 (6), 691–701. doi:10.1093/icb/icp084.

Winfield, I.J., Fletcher, J.M. & Cragg-Hine, D. (1994) *Status of rare fish: A literature review of freshwater fish in the UK*. National Rivers Authority.

Woese, C.R. & Fox, G.E. (1977) Phylogenetic structure of the prokaryotic domain: The primary kingdoms (archaebacteria/eubacteria/urkaryote/16S ribosomal RNA/molecular phylogeny). *Proceedings of the National Academy of Sciences of the United States of America*. 74 (11), 5088–5090.

Wolter, C. & Arlinghaus, R. (2003) Navigation impacts on freshwater fish assemblages: The ecological relevance of swimming performance. *Reviews in Fish Biology and Fisheries*. 13 (1), 63–89. doi:10.1023/A:1026350223459.

Wootton, J.H. (2018) Assessing the sparling *Osmerus eperlanus* (L.) population of River Cree during the "Saving The Sparling" project 2018. *Galloway Fisheries*

Trust.

WWF (2018) *Living Planet Report 2018: Aiming higher. Grooten, M. and Almond, R.E.A. (eds).*

Yokoyama, H., Miyazaki, Y. & Yoshinaga, T. (2013) Microsporidian *encephalomyelitis* in cultured yellowtail Seriola quinqueradiata. *Fish Pathology.* 48 (4), 119–125. doi:10.3147/jsfp.48.119.

Zhou, Q.J., Chai, F.C. & Chen, J. (2018) First record of *Glugea plecoglossi* (Takahashi & Egusa, 1977), a microsporidian parasite of ayu (*Plecoglossus altivelis altivelis* Temminck & Schlegel, 1846) in Mainland China. *Journal of Fish Diseases.* 41 (1), 165–169. doi:10.1111/jfd.12674.

Zoological Society of London (2016) *Guidance Document Conservation of Tidal Thames Fish through the Planning Process.* doi:10.1016/j.jretconser.2010.11.006.

Zoological Society of London (2021) *The State of the Thames 2021: Environmental trends of the Tidal Thames.*

Appendix for Chapter 2.

Table A2. 1. Rivers and estuaries where smelt have been recorded between 2000-2012 in England and Wales (Colclough, 2013)

Alde	Nene
Adur	Nyfer (Nevern)
Blackwater	Orwell
Boston Haven	Plymouth Sound
Bure	Ribble
Conwy	Solway
Crouch	Stour (Suffolk)
Dee	Stour (Kent)
Esk (Yorkshire)	Swale
Great Ouse	Thames
Humber	Trent
Lune	Wash
Medway	Waveney
Mersey	Wear
Morecambe Bay	Welland

Appendix for Chapter 3

Table A3. 1 Smelt Samples collected from the Chiswick site along the River Thames in March/April 2018 by the EA, with varying levels of infection, distribution of cysts and deformity caused by cysts. Deformity refers to any deformation caused to the natural body shape by the cysts.

Fish no.	Length (mm)	Weight (g)	Overall infection	Distribution	Deformity?
C.1	-	-	Very Heavy	2 lobes	Yes
C.2	-	-	Very Heavy	2 lobes	Yes
C.3	-	-	Low	1 lobe	No
C.4	47	0.87	Moderate	1 lobe	No
C.5	-	-	Heavy	1 lobe	Yes
C.6	-	-	Very Heavy	2 lobes	Yes
C.7	-	-	Moderate	1 lobe + 2-3 cysts	No
C.8	-	-	Very Heavy	1 lobe	Yes
C.9	-	-	Very Heavy	2 lobes	Yes
C.10	-	-	Uninfected	N/A	No
C.11	52	1.41	Heavy	1 lobe	Yes
C.12	-	-	Moderate	1 lobe +3 cysts	Yes
C.13	-	-	Uninfected	N/A	No
C.14	46	0.78	Uninfected	N/A	No
C.15	-	-	Low	Throughout	No
C.16	58	1.55	Very Heavy	3 lobes	Yes
C.17	53	1.31	Very Heavy	1 lobe	Yes
C.18	-	-	Uninfected	N/A	No
C.19	-	-	Heavy	2 lobes	Yes
C.20	43	0.86	Moderate	1 lobe	Yes
C.21	71	2.96	Uninfected	N/A	No
C.22	-	-	Low	1 lobe	No
C.23	42	0.37	Moderate	1 lobe	Yes
C.24	-	-	Heavy	2 lobes	Yes
C.25	52	1.32	Very Heavy	3 lobes	Yes
C.26	74	2.36	Uninfected	N/A	No
C.27	82	4.6	Uninfected	N/A	No
C.28	85	5.06	Uninfected	N/A	No
C.29	-	-	Uninfected	N/A	N/A
C.30	53	1.22	Heavy	1 lobe	Yes
C.31	-	-	Uninfected	N/A	No
C.32	-	-	Uninfected	N/A	N/A
C.33	49	0.96	Uninfected	N/A	No
C.34	55	1.57	Very Heavy	1 lobe	Yes
C.35	-	-	Uninfected	N/A	N/A
C.36	-	-	Very low	4 cysts	N
C.37	53	1.21	Uninfected	N/A	N/A
C.38	48	0.63	Moderate	1 Lobe	Yes
C.39	43	0.6	Very Heavy	1 Lobe	Yes
C.40	53	0.94	Heavy	1 Lobe	Yes

Table A3. 2 Samples collected from the Battersea site along the River Thames in March/April 2018 by the EA, with varying levels of infection, distribution of cysts and deformity caused by cysts

Fish No.	Length (mm)	Weight (g)	Overall Infection	Distribution	Deformity?
B.1	-	-	Low	3-4 cysts	No
B.2	-	-	Uninfected	N/A	No
B.3	52	1.28	Very heavy	1 lobe	Yes
B.4	-	-	Heavy	1 lobe + cysts	Yes
B.5	-	-	Low	5 cysts	No
B.6	44	0.49	Heavy	1 lobe	Yes
B.7	-	-	Low	10 cysts	No
B.8	-	-	Moderate	1 lobe	Yes
B.9	54	1.16	Very heavy	1 lobe + cysts	Yes
B.10	50	1.05	Very heavy	1 lobe	Yes
B.11	58	1.64	Heavy	1 lobe	Yes
B.12	-	-	Very heavy	1 lobe	Yes
B.13	48	0.81	Very heavy	2 lobes	Yes
B.14	59	1.64	Very heavy	1 lobe	Yes
B.15	45	0.67	Heavy	1 lobe	Yes
B.16	-	-	Low	10 cysts	Yes
B.17	-	-	Uninfected	N/A	N/A
B.18	47	0.98	Very heavy	1 lobe + cysts	Yes
B.19	-	-	Low	1-2 cysts	No
B.20	-	-	Uninfected	N/A	N/A

Table A3. 3 Haematoxylin and eosin staining protocol using an automatic stainer

Step	Bath	Chemical	In bath time (secs)	In bath agitation	Out bath time (secs)	Out bath agitation
0	0	Histoclear	900	N	8	Y
1	1	100% IMS	120	N	8	Y
2	2	90% IMS	120	N	8	Y
3	4	70% IMS	120	N	8	Y
4	3	Water	120	N	8	Y
5	5	Haematoxylin	600	N	8	Y
6	3	Water	600	N	8	Y
7	6	Acid alcohol	20	N	8	Y
8	3	Water	20	Y	8	Y
9	7	Sat. Li_2CO_3	20	N	8	Y
10	3	Water	20	Y	8	Y
11	8	Eosin	40	N	8	Y
12	3	Water	300	N	8	Y
13	4	70% IMS	120	N	8	Y
14	9	90% IMS	120	N	8	Y
15	10	100% IMS	300	N	8	Y
16	11	Histoclear	300	N	0	N
17	11	Histoclear	0	N	0	N

Table A3. 4 Luna staining protocol (manual staining)

Step	Bath	Chemical	In bath time (secs)	In bath agitation	Out bath time (secs)	Out bath agitation
1	1	Xylene	900	N	8	Y
2	2	100% IMS	120	N	8	Y
3	3	90% IMS	120	N	8	Y
4	4	70% IMS	120	N	8	Y
5	5	Distilled water	120	N	8	Y
6	6	Haematoxylin-biebrich	300	N	8	Y
7	7	1% Acid alcohol	8 dips	Y	8	Y
8	8	Water	20	Y	8	Y
9	9	0.5% Li_2CO_3	5 dips	Y	8	Y
10	10	Running water	120	Y	8	Y
11	11	95% IMS	120	N	8	Y
12	12	95% IMS	120	N	8	Y
13	13	100% IMS	120	N	8	Y
14	14	100% IMS	120	N	8	Y
15	15	Xylene	120	N	8	N
16	16	Xylene	120	N	8	N

Table A3. 5 The solutions and their quantities needed to produce the Luna stain

Solution	Quantity
Weigert's Iron Haematoxylin Solution (A + B)	
Solution A (Haematoxylin & ethanol)	50 ml
Solution B (Hydrochloric acid & Iron trichloride hexahydrate)	50 ml
1 % Biebrich Scarlet Solution	
Biebrich scarlet	1 g
Purite water	100 ml
Haematoxylin-Biebrich Scarlet Working Solution	
Weigert's Iron Haematoxylin Solution (working)	90 ml
1 % Biebrich scarlet	10 ml
1 % Acid Alcohol Solution	
Ethanol	99 ml
Hydrochloric acid, concentrated	1 ml
0.5 % Lithium Carbonate Solution	
Lithium carbonate	2 g
Distilled water	400 ml

Table A3. 6 Instrument set up for each scan

Sample	Beam Energy		Resolution	Imaging Set Up				
	kV	uA	Voxel size (mm)	Copper Filter (mm)	Exposure (ms)	Projections	Gain (dB)	Frame Avg.
S10&S2	70	214	0.035498	0.1	354	2118	30	2
S10&S2	70	143	0.016982	0.1	354	3142	30	2
S16&S8	70	214	0.027657	0.1	354	2118	30	2
S17&S13	70	214	0.032562	0.1	354	1999	30	2
S19&S05	70	214	0.039301	0.1	354	1999	30	2
S22&S36	70	214	0.032562	0.1	354	1999	30	2
S4&S1	70	214	0.027657	0.1	354	2118	30	2
S5&S6	70	214	0.029957	0.1	354	1571	30	2
S5&S6	70	143	0.014243	0.1	354	3142	30	2
S6	70	100	0.005938	0.1	354	3142	30	2

* Projections are the number of images taken in each rotation.

** Frame avg. represents the number of images taken and averaged for each projection.

***Gain represents detector sensitivity.

Table A3. 7 Micro-CT results for each smelt sample.

TL = total length, EA ref = original reference ID from EA National Fisheries Laboratory

Fish #1 (TL: 44.63mm) (EA ref: 18/087/01)

Material	Voxel Count	Volume mm³	%
Cysts	9842305	208.21	32.05
Digestive Tract	1203851	25.47	3.92
Body Cavity	1421207	30.07	4.63
Internal	10173	0.22	0.03
Remainder	18228313	385.61	59.36
Total	**30705849**	**649.572406**	**100**
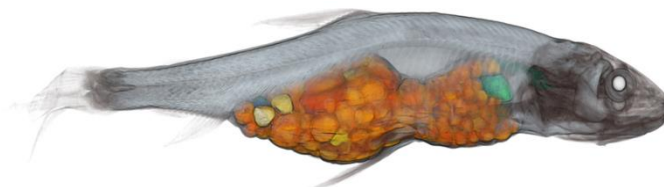
Fish #6 (TL: 53.93mm) (EA ref: 18/087/01)

Material	Voxel Count	Volume mm³	%
Cysts	6709064	180.36	22.36
Digestive Tract	865882	23.28	2.89
Body Cavity	2032075	54.63	6.77
Remainder	20402509	548.49	67.99
Total	**30009530**	**806.75**	**100**
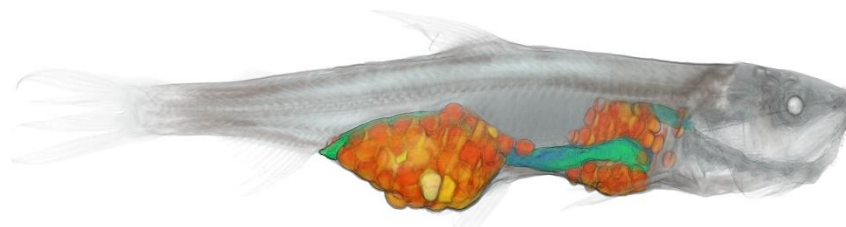
Fish #5 (TL: 43.99mm) (EA ref: 18/087/05)

Material	Voxel Count	Volume mm³	%
Cysts	1715666	46.12	11.23
Digestive Tract	884994	23.79	5.79
Internal	24728	0.66	0.16
Body Cavity	1102332	29.63	7.21
Remaining	11552671	310.57	75.60
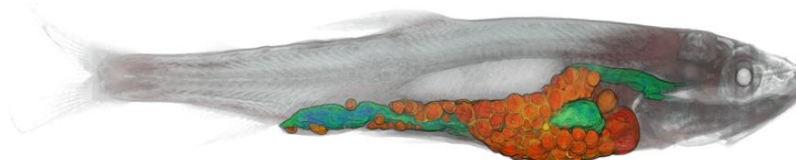
Total	15280391	410.79	100

Fish #4 (TL: 37.43mm) (EA ref: 18/109/04)

Material	Voxel Count	Volume mm³	%
Cysts	2942366	62.24	27.08
Digestive Tract	573176	12.13	5.27
Body Cavity	389245	8.23	3.58
Remaining	6961955	147.28	64.07
Total	**10866742**	**229.88**	**100**
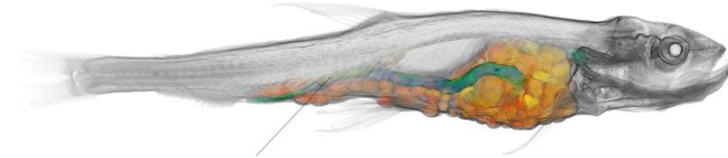
Fish #10 (TL: 65.80mm) (EA ref: 18/087/10)

Material	Voxel Count	Volume mm³	%
Cysts	32151	1.44	0.09
Digestive Tract	750244	33.56	2.17
Body Cavity	2360676	105.59	6.82
Remaining	31448942	1406.71	90.91
Total	**34592013**	**1547.30**	**100**
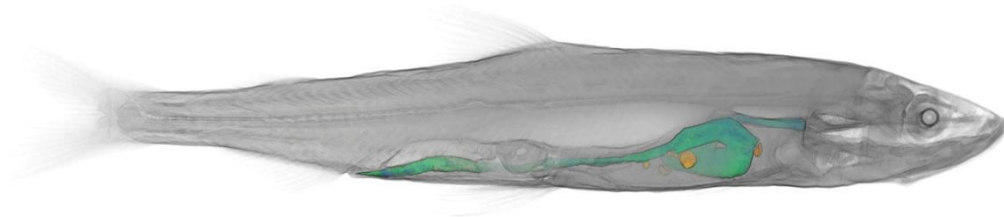
Fish #2 (TL: 66.95mm) (EA ref: 18/109/02)

Material	Voxel Count	Volume mm³	%
Cysts	0	0.00	0.00
Digestive Tract	1306732	58.45	3.63
Body Cavity	2658727	118.93	7.40
Remaining	31983900	1430.64	88.97
Bulk	**35949359**	**1608.02**	**100.00**
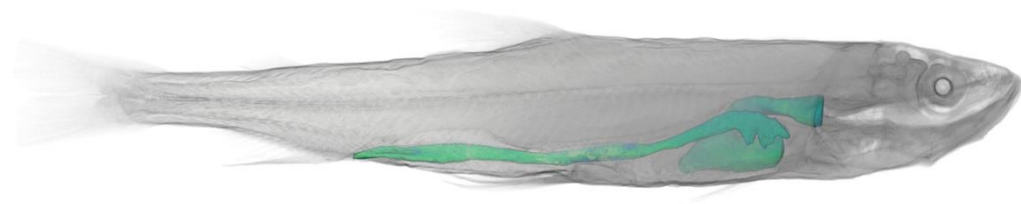
Fish #8 (TL: 49.58mm) (EA ref: 18/109/08)

Material	Voxel Count	Volume mm³	%
Cysts	1121392	23.72	3.21
Digestive Tract	836093	17.69	2.40
Body Cavity	1750970	37.04	5.02
Remaining	31196957	659.96	89.38
Bulk	**34905412**	**738.41**	**100.00**
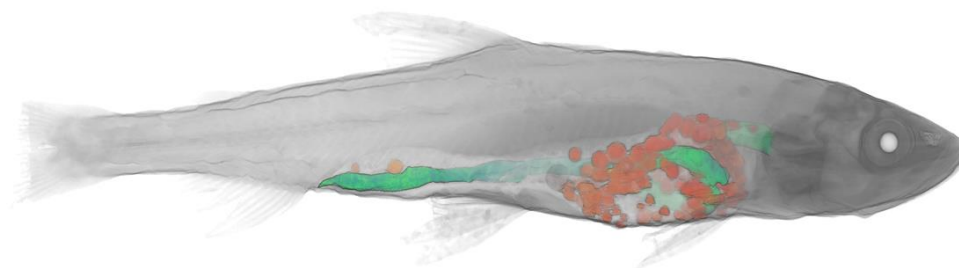
Fish #16 (TL: 50.71mm) (EA ref: 18/109/016)

Material	Voxel Count	Volume mm³	%
Cysts	1941670	41.08	4.65
Digestive Tract	1495931	31.65	3.58
Body Cavity	2650790	56.08	6.35
Remaining	35673348	754.66	85.42
Bulk	**41761739**	**883.46**	**100.00**
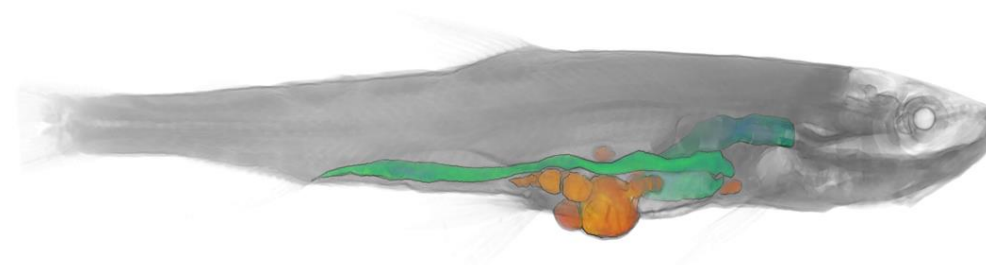
Fish #13 (TL: 63.42mm) (EA ref: 18/087/13)

Material	Voxel Count	Volume mm³	%
Cysts	0	0.00	0.00
Digestive Tract	1367069	47.20	3.41
Body Cavity	2990417	103.25	7.47
Remaining	35688009	1232.16	89.12
Bulk	**40045495**	**1382.61**	**100.00**
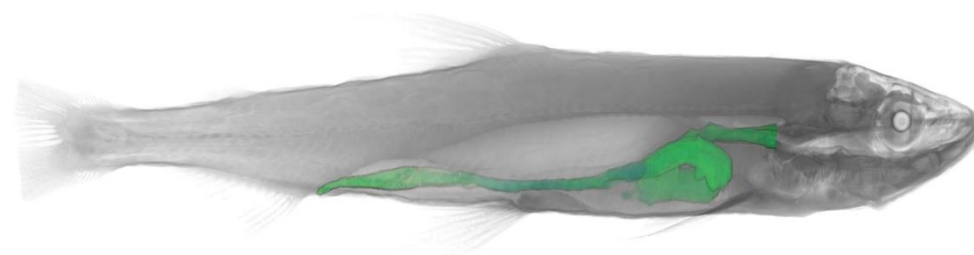
Fish #17 (TL: 49.47mm) (EA ref: 18/109/17)

Material	Voxel Count	Volume mm³	%
Cysts	0	0.00	0.00
Digestive Tract	573145	19.79	3.94
Body Cavity	612185	21.14	4.21
Remaining	13346135	460.79	91.84
Bulk	**14531465**	**501.71**	**100.00**
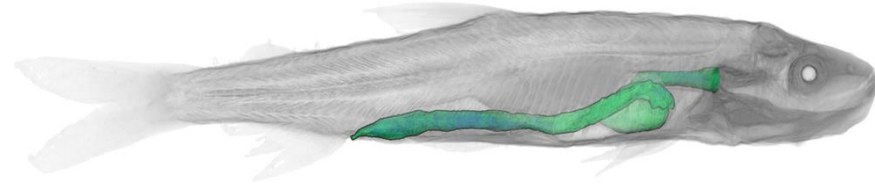
Fish #3 (TL: 66.24mm) (EA ref: 18/109/05)

Material	Voxel Count	Volume mm³	%
Cysts	150255	9.12	0.69
Digestive Tract	998047	60.59	4.58
Body Cavity	718192	43.60	3.30
Remaining	19921529	1209.34	91.43
Bulk	**21788023**	**1322.65**	**100.00**
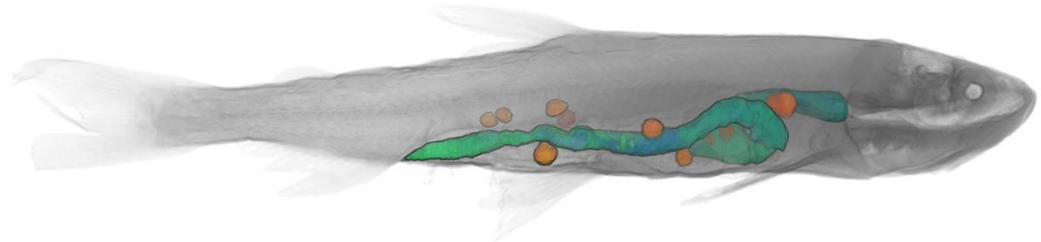
Fish #19 (TL: 77.32mm) (EA ref: 18/109/19)

Material	Voxel Count	Volume mm³	%
Cysts	419303	25.45	1.02
Digestive Tract	1830828	111.14	4.45
Body Cavity	2016678	122.42	4.91
Remaining	36847812	2236.85	89.62
Bulk	**41114621**	**2495.87**	**100.00**
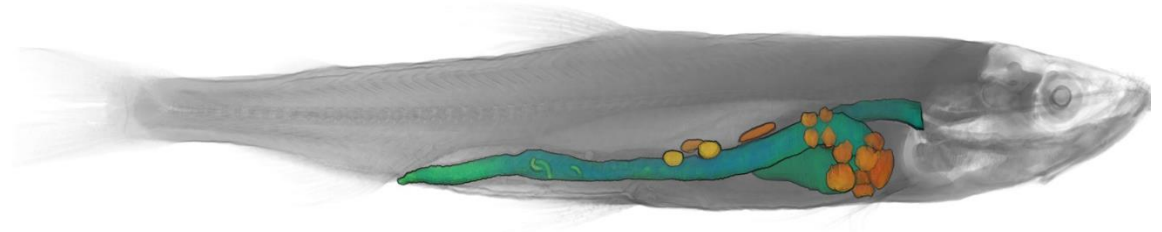
Fish #22 (TL: 52.50mm) (EA ref: 18/087/22)

Material	Voxel Count	Volume mm³	%
Cysts	190983	6.59	1.07
Digestive Tract	617610	21.32	3.47
Body Cavity	1109186	38.30	6.22
Remaining	15900942	548.99	89.24
Bulk	**17818721**	**615.21**	**100.00**
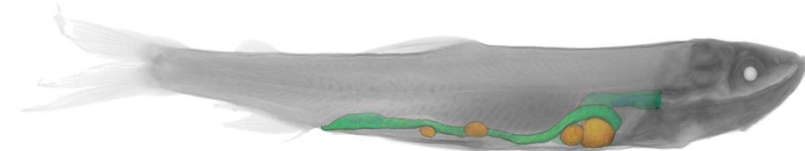
Fish #36 (TL: 62.40mm) (EA ref: 18/087/36)

Material	Voxel Count	Volume mm³	%
Cysts	830766	28.68	1.56
Digestive Tract	2934203	101.31	5.50
Body Cavity	3550370	122.58	6.65
Remaining	46044865	1589.74	86.29
Bulk	**53360204**	**1842.31**	**100.00**
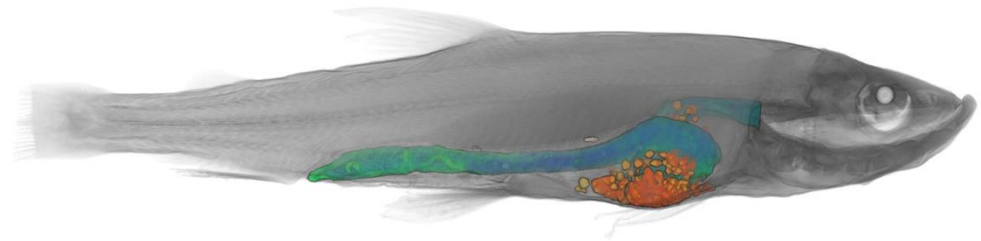
Table A3. 8 The measurements calculated for individual cysts from Micro-CT fish sample 6

Cyst	Length (mm)	Breadth (mm)	Width (mm)	Area (mm²)	Volume (mm³)
1	1.08	0.97	0.91	2.76	0.4
2	1.19	1.14	0.97	3.36	0.52
3	0.97	0.79	0.74	2.03	0.24
4	1.05	0.89	0.74	2.36	0.27
5	0.86	0.83	0.66	1.52	0.14
6	0.96	0.79	0.7	1.93	0.2
7	1.01	0.89	0.64	2.03	0.21
8	1.46	1.34	1.12	4.82	0.83
9	0.84	0.78	0.69	1.63	0.16
10	1.58	1.35	1.17	5.19	0.91
11	0.6	0.46	0.38	0.63	0.04
12	1	0.7	0.6	1.63	0.13
13	0.97	0.74	0.71	1.72	0.18
14	0.93	0.79	0.73	1.84	0.21
15	1.13	0.85	0.76	2.38	0.29
16	1.26	1.12	1.01	3.88	0.63
17	1.33	1.24	1.05	4.07	0.66
18	1.29	1.18	0.93	3.62	0.57
19	3.36	3.03	1.97	22.71	6.96
20	1.4	1.13	0.86	3.75	0.53
21	1.27	1.17	1.05	3.97	0.64
22	1.74	1.49	1.23	6.58	1.28
23	1.87	1.16	1.06	5.41	0.88
24	1.52	1.24	0.95	4.17	0.63
25	0.92	0.79	0.69	1.76	0.2
26	1.88	1.41	1.06	6.02	0.85
27	0.93	0.89	0.69	1.82	0.2
28	1.06	0.93	0.6	2.08	0.22
29	1.53	1.3	1.1	4.72	0.73
30	1.63	1.55	1.07	5.69	0.96
31	1.94	1.6	1.47	8.41	2.11
32	3.86	2.83	2.1	24.92	9.34
33	0.95	0.76	0.63	1.72	0.17
34	2.48	1.69	1.31	8.54	1.52
35	1.01	0.89	0.62	1.97	0.2
36	1.03	0.96	0.84	2.53	0.31
37	1.61	1.39	0.98	4.89	0.72
38	1.79	1.68	1.38	7.19	1.47
39	1.82	1.53	1.39	6.7	1.24
Average	**1.41**	**1.19**	**0.96**	**4.69**	**0.97**

Table A3. 9 The measurements calculated for individual cysts from Micro-CT fish sample 5.

Cyst	Length (mm)	Breadth (mm)	Width (mm)	Area (mm²)	Volume (mm³)
1	0.86	0.62	0.55	1.29	0.11
2	0.75	0.68	0.63	1.31	0.13
3	0.69	0.63	0.44	0.93	0.07
4	0.84	0.74	0.72	1.67	0.18
5	1.21	1	0.9	3.13	0.45
6	0.6	0.56	0.51	0.84	0.06
7	1.21	1.18	0.92	3.06	0.39
8	1.18	1.03	0.88	2.78	0.39
9	0.9	0.81	0.67	1.7	0.18
10	1.16	0.94	0.85	2.77	0.39
11	1.15	0.99	0.79	2.76	0.38
12	0.78	0.61	0.58	1.15	0.09
13	0.51	0.48	0.37	0.54	0.03
14	0.42	0.38	0.32	0.33	0.02
15	0.69	0.66	0.48	1.01	0.08
16	0.59	0.53	0.49	0.79	0.06
17	0.58	0.49	0.46	0.64	0.04
18	0.97	0.81	0.78	2.16	0.26
19	0.48	0.46	0.35	0.42	0.02
20	0.41	0.3	0.27	0.26	0.01
21	1.97	1.56	1.23	8.36	1.2
22	1.13	1.04	0.94	3.23	0.47
23	0.83	0.67	0.59	1.31	0.12
24	0.9	0.78	0.7	1.76	0.19
25	1.41	1.07	0.96	3.96	0.63
26	0.42	0.37	0.27	0.29	0.01
27	2.46	2.28	1.99	15.13	4.59
28	0.58	0.5	0.45	0.67	0.04
29	0.07	0.04	0.03	0.01	0
Average	**0.89**	**0.77**	**0.66**	**2.22**	**0.37**

Table A3. 10 Smelt length, weight, sex and level of infection of smelt collected in the River Thames in March, June, October and December 2019, and March, July and September 2020 (original data provided by A. McGoran). Smelt infected with a microsporidian highlighted in grey.

ID	Date	Total Length (mm)	Weight (g)	Sex	Level of infection
060319_Osmerus_eperlanus_MW1	03/2019	78	2.5	N/A	
060319_Osmerus_eperlanus_MW1	03/2019	70	1.7	N/A	
060319_Osmerus_eperlanus_MW2	03/2019	85	2.4	N/A	
060319_Osmerus_eperlanus_MW3	03/2019	80	2.4	N/A	Low
060319_Osmerus_eperlanus_MW4	03/2019	76	2	N/A	
060319_Osmerus_eperlanus_MW5	03/2019	60	1.3	N/A	Low
060319_Osmerus_eperlanus_MW6	03/2019	98	3.7	N/A	Moderate
060319_Osmerus_eperlanus_MW7	03/2019	70	1.6	N/A	Very heavy
060319_Osmerus_eperlanus_MW8	03/2019	75	2.5	N/A	
060319_Osmerus_eperlanus_MW9	03/2019	78	2.3	N/A	
060319_Osmerus_eperlanus_MW10	03/2019	65	1.1	N/A	
060319_Osmerus_eperlanus_MW11	03/2019	64	1	N/A	
060319_Osmerus_eperlanus_MW12	03/2019	75	2	N/A	Low
060319_Osmerus_eperlanus_MW13	03/2019	93	3.2	N/A	
060319_Osmerus_eperlanus_MW14	03/2019	190	39	N/A	
060319_Osmerus_eperlanus_BT1	03/2019	86	3.3	N/A	
060319_Osmerus_eperlanus_BT2	03/2019	73	1.9	N/A	
060319_Osmerus_eperlanus_BT3	03/2019	82	2.6	N/A	
060319_Osmerus_eperlanus_BT4	03/2019	80	2.7	N/A	
060319_Osmerus_eperlanus_BT5	03/2019	74	1.8	N/A	
060319_Osmerus_eperlanus_BT6	03/2019	85	3	N/A	
060319_Osmerus_eperlanus_BT7	03/2019	77	2.4	N/A	Low
060319_Osmerus_eperlanus_BT8	03/2019	95	4.6	N/A	
140619_Osmerus_eperlanus_1	06/2019	138	13.6	N/A	
140619_Osmerus_eperlanus_2	06/2019	133	13.4	N/A	
140619_Osmerus_eperlanus_3	06/2019	114	8.8	N/A	
140619_Osmerus_eperlanus_4	06/2019	136	15.1	N/A	
140619_Osmerus_eperlanus_5	06/2019	94	4.6	N/A	
140619_Osmerus_eperlanus_6	06/2019	95	4.6	N/A	
140619_Osmerus_eperlanus_7	06/2019	120	9.8	N/A	
140619_Osmerus_eperlanus_8	06/2019	104	6.7	N/A	
140619_Osmerus_eperlanus_9	06/2019	121	10.5	N/A	
140619_Osmerus_eperlanus_10	06/2019	154	24.4	N/A	
021019_Osmerus_eperlanus_1	10/2019	134	14.6	Immature	Moderate
021019_Osmerus_eperlanus_2	10/2019	112	8.4	Male	
021019_Osmerus_eperlanus_3	10/2019	133	11.9	Male	Low
021019_Osmerus_eperlanus_4	10/2019	167	28.9	Male	
021019_Osmerus_eperlanus_6	10/2019	150	18.7	Male	Low

021019_Osmerus_eperlanus_7	10/2019	130	12.2	Male	
021019_Osmerus_eperlanus_8	10/2019	136	15.4	Male	
021019_Osmerus_eperlanus_9	10/2019	146	18.1	Male	
021019_Osmerus_eperlanus_10	10/2019	140	14.8	Male	Low
021019_Osmerus_eperlanus_11	10/2019	126	11.9	Male	Low
021019_Osmerus_eperlanus_12	10/2019	145	17.3	Male	
021019_Osmerus_eperlanus_13	10/2019	130	12.4	Male	
021019_Osmerus_eperlanus_14	10/2019	123	10.9	Male	Low
021019_Osmerus_eperlanus_15	10/2019	134	15.2	Female	
021019_Osmerus_eperlanus_16	10/2019	150	19.5	Female	
021019_Osmerus_eperlanus_17	10/2019	149	18.4	Male	
021019_Osmerus_eperlanus_18	10/2019	124	11.7	Male	
191219_Osmerus_eperlanus_1	12/2019	130	18	Female	Moderate
191219_Osmerus_eperlanus_2	12/2019	103	12.5	Female	Moderate
191219_Osmerus_eperlanus_3	12/2019	110	13.8	Male	
191219_Osmerus_eperlanus_4	12/2019	98	11.7	Male	
191219_Osmerus_eperlanus_5	12/2019	223	86	Female	
191219_Osmerus_eperlanus_6	12/2019	103	6.8	Immature	Heavy
191219_Osmerus_eperlanus_7	12/2019	151	21.7	Male	Low
191219_Osmerus_eperlanus_8	12/2019	178	40.1	Female	
191219_Osmerus_eperlanus_9	12/2019	151	20.7	Female	
191219_Osmerus_eperlanus_10	12/2019	146	19.4	Female	
191219_Osmerus_eperlanus_11	12/2019	155	24	Male	Low
191219_Osmerus_eperlanus_12	12/2019	170	31.1	Female	Low
191219_Osmerus_eperlanus_13	12/2019	143	22.7	Female	Very heavy
191219_Osmerus_eperlanus_14	12/2019	127	13.6	Female	Heavy
191219_Osmerus_eperlanus_15	12/2019	171	33.4	Female	Low
191219_Osmerus_eperlanus_16	12/2019	165	25	Male	
191219_Osmerus_eperlanus_17	12/2019	177	49.1	Female	
191219_Osmerus_eperlanus_18	12/2019	170	28.3	Female	Low
191219_Osmerus_eperlanus_19	12/2019	148	21.8	Male	
191219_Osmerus_eperlanus_20	12/2019	135	15.4	Female	Very heavy
191219_Osmerus_eperlanus_21	12/2019	146	18.6	Male	Low
191219_Osmerus_eperlanus_22	12/2019	140	18.2	Female	Moderate
191219_Osmerus_eperlanus_23	12/2019	145	18	Male	
191219_Osmerus_eperlanus_24	12/2019	152	20.8	Female	
191219_Osmerus_eperlanus_25	12/2019	134	14.4	Male	
191219_Osmerus_eperlanus_26	12/2019	137	14.1	Female	
191219_Osmerus_eperlanus_27	12/2019	136	15.8	Male	Low
191219_Osmerus_eperlanus_28	12/2019	157	20.8	Female	Low
191219_Osmerus_eperlanus_29	12/2019	145	17.8	Female	
191219_Osmerus_eperlanus_30	12/2019	158	23.5	Female	
191219_Osmerus_eperlanus_31	12/2019	130	14.6	Male	Low
191219_Osmerus_eperlanus_32	12/2019	125	12.3	Female	
191219_Osmerus_eperlanus_33	12/2019	134	14.8	Female	Low
191219_Osmerus_eperlanus_34	12/2019	136	15.8	Male	-

190320_Osmerus_eperlanus_1	03/2020	136	14.1	NA	Heavy
190320_Osmerus_eperlanus_2	03/2020	145	17.7	NA	Low
190320_Osmerus_eperlanus_3	03/2020	160	23.4	NA	Low
190320_Osmerus_eperlanus_4	03/2020	119	12.5	NA	Very heavy
190320_Osmerus_eperlanus_5	03/2020	163	29.2	NA	
190320_Osmerus_eperlanus_6	03/2020	141	17.7	NA	
190320_Osmerus_eperlanus_7	03/2020	162	22	NA	
190320_Osmerus_eperlanus_8	03/2020	146	20.7	NA	
190320_Osmerus_eperlanus_9	03/2020	148	20.8	NA	
190320_Osmerus_eperlanus_10	03/2020	141	18	NA	
190320_Osmerus_eperlanus_11	03/2020	141	13	NA	Low
190320_Osmerus_eperlanus_12	03/2020	170	29.3	NA	
190320_Osmerus_eperlanus_13	03/2020	154	22.6	NA	
190320_Osmerus_eperlanus_14	03/2020	146	20.3	NA	
190320_Osmerus_eperlanus_15	03/2020	165	25.1	NA	
190320_Osmerus_eperlanus_16	03/2020	141	18.2	NA	
190320_Osmerus_eperlanus_17	03/2020	154	26.5	NA	
190320_Osmerus_eperlanus_18	03/2020	200	29.2	NA	
190320_Osmerus_eperlanus_19	03/2020	150	20.8	NA	
190320_Osmerus_eperlanus_20	03/2020	150	16.3	NA	
190320_Osmerus_eperlanus_21	03/2020	136	15.7	NA	
190320_Osmerus_eperlanus_22	03/2020	140	18.2	NA	
190320_Osmerus_eperlanus_23	03/2020	125	12	NA	Moderate
190320_Osmerus_eperlanus_24	03/2020	147	20.6	NA	
190320_Osmerus_eperlanus_25	03/2020	160	25.8	NA	
190320_Osmerus_eperlanus_26	03/2020	162	26.6	NA	
190320_Osmerus_eperlanus_27	03/2020	142	17.2	NA	Moderate
190320_Osmerus_eperlanus_28	03/2020	147	21.7	NA	
190320_Osmerus_eperlanus_29	03/2020	150	20.3	NA	Low
190320_Osmerus_eperlanus_30	03/2020	157	21.1	NA	
190320_Osmerus_eperlanus_31	03/2020	128	12.6	NA	
190320_Osmerus_eperlanus_32	03/2020	136	16	NA	Low
210720_Osmerus_eperlanus_1	07/2020	68	1.9	NA	
210720_Osmerus_eperlanus_2	07/2020	74	2.5	NA	
210720_Osmerus_eperlanus_3	07/2020	69	2	NA	
210720_Osmerus_eperlanus_4	07/2020	67	1.8	NA	
210720_Osmerus_eperlanus_5	07/2020	78	2.7	NA	
210720_Osmerus_eperlanus_6	07/2020	79	3	NA	
210720_Osmerus_eperlanus_7	07/2020	80	2.9	NA	
210720_Osmerus_eperlanus_8	07/2020	65	1.6	NA	Moderate
210720_Osmerus_eperlanus_9	07/2020	77	2.7	NA	
210720_Osmerus_eperlanus_10	07/2020	76	2.6	NA	
210720_Osmerus_eperlanus_11	07/2020	68	1.7	NA	Low
210720_Osmerus_eperlanus_12	07/2020	67	1.6	NA	Moderate
210720_Osmerus_eperlanus_13	07/2020	76	2.6	NA	
210720_Osmerus_eperlanus_14	07/2020	72	2.1	NA	

210720_Osmerus_eperlanus_15	07/2020	NA	2.3	NA	
210720_Osmerus_eperlanus_16	07/2020	87	3.8	NA	
210720_Osmerus_eperlanus_17	07/2020	72	2.3	NA	
210720_Osmerus_eperlanus_18	07/2020	71	2.2	NA	
210720_Osmerus_eperlanus_19	07/2020	80	2.8	NA	
210720_Osmerus_eperlanus_20	07/2020	74	2.4	NA	
210720_Osmerus_eperlanus_21	07/2020	74	2.5	NA	
210720_Osmerus_eperlanus_22	07/2020	81	3.7	NA	
210720_Osmerus_eperlanus_23	07/2020	80	3	NA	
210720_Osmerus_eperlanus_24	07/2020	85	3.4	NA	
210720_Osmerus_eperlanus_25	07/2020	71	2	NA	
210720_Osmerus_eperlanus_26	07/2020	81	3.1	NA	
210720_Osmerus_eperlanus_27	07/2020	157	26.4	NA	Moderate
210720_Osmerus_eperlanus_28	07/2020	158	28.6	NA	Heavy
210720_Osmerus_eperlanus_29	07/2020	160	28.4	NA	
210720_Osmerus_eperlanus_30	07/2020	154	25.4	NA	
210720_Osmerus_eperlanus_31	07/2020	159	27.3	NA	
210720_Osmerus_eperlanus_32	07/2020	187	40.5	NA	
210720_Osmerus_eperlanus_33	07/2020	180	39.5	NA	
210720_Osmerus_eperlanus_34	07/2020	162	30.6	NA	
210720_Osmerus_eperlanus_35	07/2020	168	31	NA	
210720_Osmerus_eperlanus_36	07/2020	170	32.2	NA	
210720_Osmerus_eperlanus_37	07/2020	164	30.2	NA	
210720_Osmerus_eperlanus_38	07/2020	180	39.1	NA	Moderate
210720_Osmerus_eperlanus_39	07/2020	181	39.3	NA	
210720_Osmerus_eperlanus_40	07/2020	159	28.3	NA	
210720_Osmerus_eperlanus_41	07/2020	173	33.9	NA	
210720_Osmerus_eperlanus_42	07/2020	167	32.6	NA	
210720_Osmerus_eperlanus_43	07/2020	175	36.8	NA	
210720_Osmerus_eperlanus_44	07/2020	189	42.8	NA	
210720_Osmerus_eperlanus_45	07/2020	199	55	NA	
210720_Osmerus_eperlanus_46	07/2020	169	33.7	NA	
210720_Osmerus_eperlanus_47	07/2020	153	22.8	NA	
210720_Osmerus_eperlanus_48	07/2020	158	26.1	NA	
210720_Osmerus_eperlanus_49	07/2020	160	27.2	NA	
210720_Osmerus_eperlanus_50	07/2020	132	19.8	NA	
30920_Osmerus_eperlanus_1	09/2020	205	48.7	NA	
30920_Osmerus_eperlanus_2	09/2020	170	29.1	NA	
30920_Osmerus_eperlanus_3	09/2020	178	35.8	NA	
30920_Osmerus_eperlanus_4	09/2020	182	37.1	NA	
30920_Osmerus_eperlanus_5	09/2020	198	39.6	NA	
30920_Osmerus_eperlanus_6	09/2020	146	18.5	NA	-
30920_Osmerus_eperlanus_7	09/2020	172	23.2	NA	
30920_Osmerus_eperlanus_8	09/2020	183	40.1	NA	
30920_Osmerus_eperlanus_9	09/2020	119	10.4	NA	
30920_Osmerus_eperlanus_10	09/2020	170	30.4	NA	

30920_Osmerus_eperlanus_11	09/2020	165	28	NA	
30920_Osmerus_eperlanus_12	09/2020	187	38.9	NA	
30920_Osmerus_eperlanus_13	09/2020	152	20	NA	
30920_Osmerus_eperlanus_14	09/2020	194	44	NA	-
30920_Osmerus_eperlanus_15	09/2020	149	22.1	NA	
30920_Osmerus_eperlanus_16	09/2020	156	20.1	NA	
30920_Osmerus_eperlanus_17	09/2020	154	21.5	NA	-
30920_Osmerus_eperlanus_18	09/2020	177	34.5	NA	-
30920_Osmerus_eperlanus_19	09/2020	155	16.7	NA	-
30920_Osmerus_eperlanus_20	09/2020	153	17	NA	
30920_Osmerus_eperlanus_21	09/2020	185	38.5	NA	
30920_Osmerus_eperlanus_22	09/2020	169	27.2	NA	
30920_Osmerus_eperlanus_23	09/2020	166	27.1	NA	
30920_Osmerus_eperlanus_24	09/2020	90	4	NA	
30920_Osmerus_eperlanus_25	09/2020	90	4.1	NA	
30920_Osmerus_eperlanus_26	09/2020	94	4.8	NA	
30920_Osmerus_eperlanus_27	09/2020	89	4	NA	
30920_Osmerus_eperlanus_28	09/2020	70	1.9	NA	
30920_Osmerus_eperlanus_29	09/2020	86	3.7	NA	
30920_Osmerus_eperlanus_30	09/2020	96	5.1	NA	
30920_Osmerus_eperlanus_31	09/2020	90	4.5	NA	
30920_Osmerus_eperlanus_32	09/2020	90	4.1	NA	
30920_Osmerus_eperlanus_33	09/2020	80	3.3	NA	-
30920_Osmerus_eperlanus_34	09/2020	98	5.3	NA	
30920_Osmerus_eperlanus_35	09/2020	87	3.9	NA	
30920_Osmerus_eperlanus_36	09/2020	95	4.5	NA	
30920_Osmerus_eperlanus_37	09/2020	101	6.3	NA	
30920_Osmerus_eperlanus_38	09/2020	88	3.5	NA	
30920_Osmerus_eperlanus_39	09/2020	90	4.2	NA	
30920_Osmerus_eperlanus_40	09/2020	100	5.4	NA	-

Appendix for Chapter 4

Table A4. 1. Infected (microsporidia) juvenile smelt from the River Thames (data provided by A. McGoran)

ID	Sample date	Total Length (mm)	Weight (g)
190320_Osmerus_eperlanus_3	19 March 2020	160	23.4
190320_Osmerus_eperlanus_4	19 March 2020	119	12.5
190320_Osmerus_eperlanus_11	19 March 2020	141	13
190320_Osmerus_eperlanus_23	19 March 2020	125	12
190320_Osmerus_eperlanus_27	19 March 2020	142	17.2
190320_Osmerus_eperlanus_29	19 March 2020	150	20.3
190320_Osmerus_eperlanus_32	19 March 2020	136	16
210720_Osmerus_eperlanus_8	21 July 2020	65	1.6
210720_Osmerus_eperlanus_11	21 July 2020	68	1.7
210720_Osmerus_eperlanus_12	21 July 2020	67	1.6
210720_Osmerus_eperlanus_27	21 July 2020	157	26.4
210720_Osmerus_eperlanus_28	21 July 2020	158	28.6
210720_Osmerus_eperlanus_38	21 July 2020	180	39.1
30920_Osmerus_eperlanus_6	3 September 2020	146	18.5
30920_Osmerus_eperlanus_14	3 September 2020	194	44
30920_Osmerus_eperlanus_17	3 September 2020	154	21.5
30920_Osmerus_eperlanus_18	3 September 2020	177	34.5
30920_Osmerus_eperlanus_19	3 September 2020	155	16.7
30920_Osmerus_eperlanus_33	3 September 2020	80	3.3
30920_Osmerus_eperlanus_40	3 September 2020	100	5.4

Table A4. 2. DNA concentrations for each microsporidian tissue sample after DNA extraction (DNeasy PowerSoil Kit) and the tissue lysis conditions prior to extraction

Date	Smelt sample	Sample	ng/ul	Nucleic Acid Purity Ratios A260/A280	A260/A230	Tissue Lysis conditions prior to extraction
11/02/2020	2018	1	5.5	1.4	0.06	Tissue lysis 3 x 1 minute at 30 Hz
11/02/2020	2018	2	22.1	1.55	0.27	*cyst tissue not fully broken down
11/02/2020	2018	3	22.9	1.47	0.15	
11/02/2020	2018	4	11.6	1.29	0.26	
10/03/2020	2018	1	19	1.87	1.92	Tissue lysis 2 x 5 minute at 30 HZ,
10/03/2020	2018	2	16.1	1.87	1.8	Incubate block for 10 minutes, 2 min x 2 at 30 Hz
01/10/2020	2018	1	52.5	1.8	1.98	C1 added and tube incubated overnight at 37.5 °C
01/10/2020	2018	2	45.5	1.8	2.07	C1 added and tube incubated 30 minutes at 70 °C
						Tissue lysis 2 x 5 min at 30 HZ,+ 2 min at 30 Hz
12/11/2020	2018	1.1	51.5	1.81	2.29	C1 added, vortexed 5 mins at 30 Hz
12/11/2020	2018	1.2	52	1.83	2.31	tube incubated for 60 minutes at 37 °C
12/11/2020	2018	1.3	52	1.79	2.29	
12/11/2020	2018	2.1	14.1	1.7	1.73	
12/11/2020	2018	2.2	13.6	1.77	1.72	
12/11/2020	2018	2.3	12.8	1.78	2	
07/12/2020	2018	1.1	23.1	1.87	1.77	C1 added, vortexed 5 mins at 30 Hz,
07/12/2020	2018	1.2	23.1	1.87	1.77	tube incubated for 60 minutes at 37 °C
07/12/2020	2018	2.1	50	1.9	2.13	
07/12/2020	2018	2.2	49.9	1.85	2.12	
07/12/2020	2018	3.1	25.6	1.86	2.17	
07/12/2020	2018	3.2	24.6	1.82	2.13	
07/12/2020	2018	4.1	32.2	1.84	2	
07/12/2020	2018	4.2	36.5	1.84	2	
07/12/2020	2018	5.1	17.2	1.8	1.41	
07/12/2020	2018	5.2	17.2	1.8	1.47	

07/12/2020	2018	6.1	26.3	1.84	2	
07/12/2020	2018	6.2	25.6	1.81	2	
20/05/2021	2020	1.1	21.7	1.7	0.69	C1 added, vortexed 5 mins at 30 Hz,
20/05/2021	2020	1.2	20.5	1.71	0.66	tube incubated for 60 minutes at 37 °C
20/05/2021	2020	2.1	15.1	2.07	1.36	
20/05/2021	2020	2.2	12	2.08	2.26	
20/05/2021	2020	3.1	57.1	1.92	2.24	
20/05/2021	2020	3.2	57.7	1.9	2.24	
20/05/2021	2020	4.1	17.5	1.92	1.28	
20/05/2021	2020	4.2	18.5	1.79	1.23	
20/05/2021	2020	5.1	10.9	1.81	0.57	
20/05/2021	2020	5.2	10.8	1.74	0.52	
20/05/2021	2020	6.1	7.4	1.73	0.96	
20/05/2021	2020	6.2	7.5	1.81	1.07	

Table A4. 3. PCR optimisation trials showing the reaction components, PCR cycling conditions and resulting PCR products imaged on gel

---

Date: 14/02/2020

25 µl reaction

Promega MM	1X
F Primer 18F	10 µM
R Primer 1492R	10 µM
Water (molecular grade)	3.5 µl
DNA template	8 µl

PCR conditions	Temperature (°C)	Time (min)	
Initial activation	95	3	
Denaturation	95	1	
Annealing	50	0.5	39 cycles
Extension	72	**1.5**	
Final Extension	72	10	

Date: 05/10/2020

25 µl reaction

Promega MM	1X
F Primer 18F	10 µM
R Primer 1492R	10 µM
Water (molecular grade)	3.5 µl
DNA template	8 µl

PCR conditions	Temperature (°C)	Time (min)	
Initial activation	95	3	
Denaturation	95	1	
Annealing	50	0.5	39 cycles
Extension	72	**1.5**	
Final Extension	72	10	

Date: 09/10/2020

50 µl reaction

Promega MM	1X
F Primer 18F	10 µM
R Primer 1492R	10 µM
Water (molecular grade)	15 µl
DNA template	8 µl

PCR conditions	Temperature (°C)	Time (min)	
Initial activation	95	3	
Denaturation	95	1	
Annealing	**52**	0.5	} 39 cycles
Extension	72	1.5	
Final Extension	72	10	
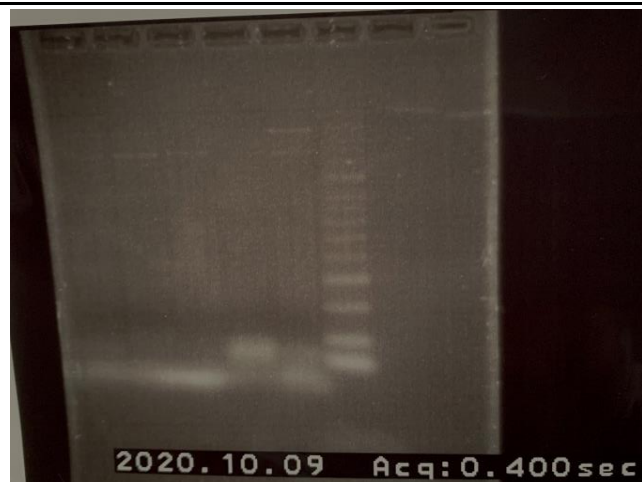
Date: 14/10/2020

50 µl reaction

Promega MM	1X
F Primer 18F	10 µM
R Primer 1492R	10 µM
Water (molecular grade)	15 µl
DNA template	8 µl

PCR conditions	Temperature (°C)	Time (min)	
Initial activation	95	3	
Denaturation	95	1	
Annealing	**53**	0.5	} 39 cycles
Extension	72	1.5	
Final Extension	72	10	

174

Date: 16/11/2020

50 µl reaction

Promega MM	1X
F Primer 18F	**5 µM**
R Primer 1492R	**5 µM**
Water (molecular grade)	15 µl
DNA template	8 µl

PCR conditions	Temperature (°C)	Time (min)	
Initial activation	95	3	
Denaturation	95	1	
Annealing	53	0.5	} 39 cycles
Extension	72	1.5	
Final Extension	72	10	

Date: 19/11/2020

50 µl reaction

Promega MM	1X
F Primer 18F	10 µM
R Primer 1492R	10 µM
Water (molecular grade)	**18 µl**
DNA template	**5 µl**

PCR conditions (PCR 1)	Temperature (°C)	Time (min)	
Initial activation	95	3	
Denaturation	95	1	
Annealing	53	0.5	} 39 cycles
Extension	72	1.5	
Final Extension	72	10	

PCR conditions (PCR 2)	Temperature (°C)	Time (min)	
Initial activation	95	3	
Denaturation	95	1	
Annealing	53	0.5	} 39 cycles
Extension	72	**1**	
Final Extension	72	10	

175
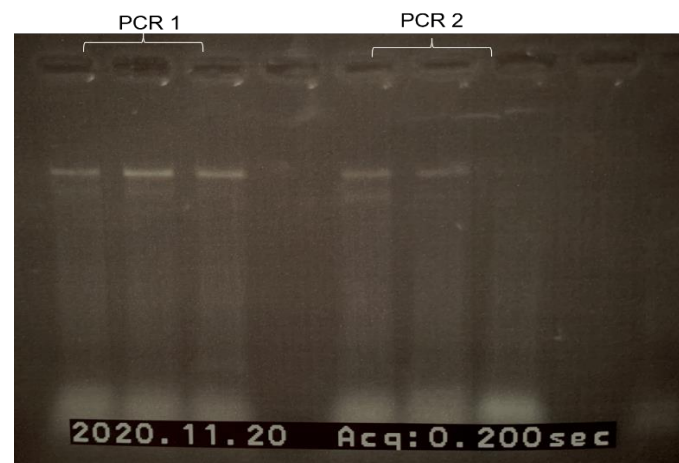
Date: 27/11/2020 (Method of Vossbrinck et al. 2004)

50 µl reaction

Promega MM	1X
F Primer 18F	10 µM
R Primer 1492R	10 µM
Water (molecular grade)	18 µl
DNA template	5 µl

PCR conditions	Temperature (°C)	Time (min)	
Initial activation	94	3	
Denaturation	94	0.75	
Annealing	45	0.5	39 cycles
Extension	72	1.5	

Table A4. 4. PCR reactions for DNA clean-up, showing PCR cycling conditions and resulting PCR products imaged on gel

Date: 05/02/2021 (Method of Pomport-Castillon et al. 2000)

50 µl reaction

Promega MM	1X
F Primer 10 uM (Bf)	10 µM
R Primer 10 uM (Vr)	10 µM
Water (molecular grade)	18 µl
DNA template (2018)	5 µl

PCR conditions	Temperature (°C)	Time (min)	
Initial activation	94	3	
Denaturation	94	1	
Annealing	55	1.5	30 cycles
Extension	72	2	
Final Extension	72	5	

176

Date: 24/05/2021   (Method of Pomport-Castillon et al. 2000)

50 µl reaction

Promega MM	1X
F Primer 10 uM (Bf)	10 µM
R Primer 10 uM (Vr)	10 µM
Water (molecular grade)	18 µl
DNA template (2020)	5 µl

PCR conditions	Temperature (°C)	Time (min)	
Initial activation	94	3	
Denaturation	94	1	
Annealing	55	1.5	30 cycles
Extension	72	2	
Final Extension	72	5	
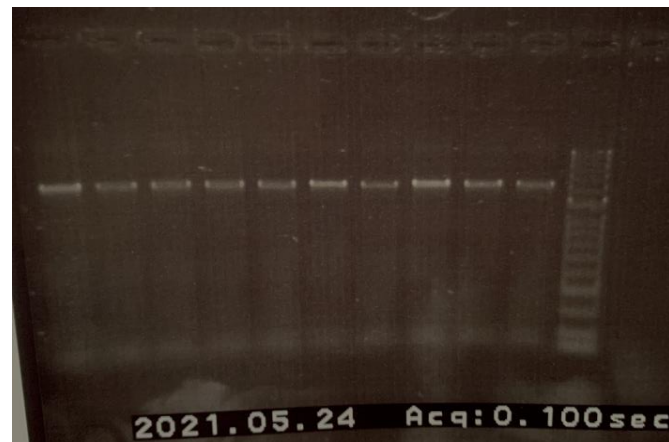
Date: 07/06/2021   (Method of Pomport-Castillon et al. 2000)

50 µl reaction

Promega MM	1X
F Primer 10 uM (Bf)	10 µM
R Primer 10 uM (580r)	10 µM
Water (molecular grade)	18 µl
DNA template (2020)	5 µl

PCR conditions	Temperature (°C)	Time (min)	
Initial activation	94	3	
Denaturation	94	1	
Annealing	55	1.5	30 cycles
Extension	72	2	
Final Extension	72	5	
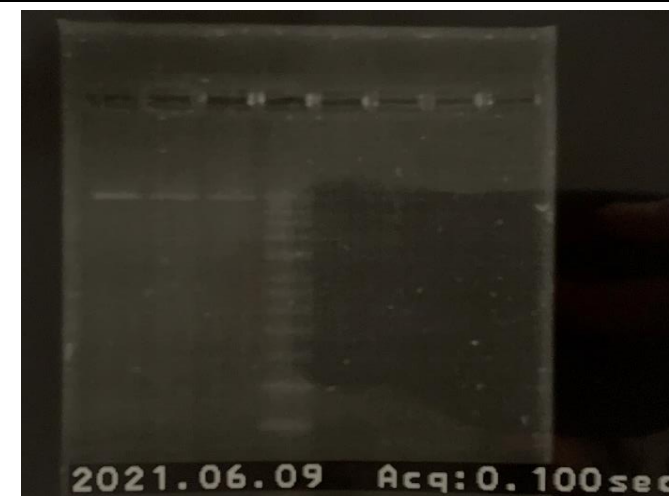
Table A4. 5. Glugea species represented in the phylogenetic analysis, showing host species and the geographic location where they were reported.

Microsporidian	Host	GenBank accession number	Geographic region	Study or source
Glugea anomala	*Gasterosteus aculeatus*	AF044391	Unknown	Nilsen et al. 1998
Glugea anomala	*Unknown*	AB923879	Unknown	GenBank
Glugea anomala	*Gasterosteus aculeatus*	AF056016	Europe	Pomport-Castillon et al. (2000)
Glugea eda	*Caesio striata*	MK568064	Saudi Arabia - Red Sea	Mansour et al. 2020
Glugea epinephelusis	*Epinephelus awoara*	AY090038	China	GenBank
Glugea gasterostei	*Gasterosteus aculeatus*	KM977990	Russia: Saint-Petersburg	Tokarev et al. (2015)
Glugea hertwigi	*Osmerus mordax*	GQ203287	Canada, Prince Edward Island	
Glugea nagelia	*Cephalopholis hemistiktos*	KJ802012	Red Sea	Abdel-Kaki et al. 2015
Glugea plecoglossi	*Sardina pilchardus*	KY882286	Atlantic - Spain	GenBank
Glugea plecoglossi	*Seriola dumerili*	AB623035	Japan: Shiga	Miwa et al. 2011
Glugea sp.	*Sardinella aurita valenciennes*	MT680621	Algerian coast	GenBank
Glugea sp.	*Sardinella aurita valenciennes*	MT072043	Atlantic - Spain	GenBank
Glugea sp.	Cottus cognatus	KU885382	USA - Michigan	Ryan & Kohler. 2016
Glugea sp.	Serranus atricauda	KU363832	Portugal: Madeira Archipelago	GenBank
Glugea sp.	*Epinephelus polyphekadion*	KT005391	Saudi Arabia - Red Sea	Azevedo et al 2015
Glugea stephani	Gasterosteus aculeatus	AF056015	Europe	Pomport-Castillon et al. (2000)

Appendix for Chapter 5

Table A5. 1 The number and minimum/maximum size of the mesh elements used in the CFD simulations

Specimen	**Scenario** Scenario	**Tetrahedric mesh** Num. nodes	Num. elem.	Flow imbalance (I)	**Results CFD** Drag force (N)	Y+
GC_O_eperlarnus_smelt_1_retrNOfins	Re normalized	1943159	6082483	2.74E-07	0.002215605	0.32738265
GC_O_eperlarnus_smelt_1_retrNOfins	V normalized	1943159	6082483	7.53E-05	0.001861623	0.3012382
GC_O_eperlarnus_smelt_2_retrNOfins	Re normalized	2337979	6940013	4.85E-07	0.001408206	0.21025652
GC_O_eperlarnus_smelt_2_retrNOfins	V normalized	2337979	6940013	-8.51E-06	0.001452701	0.21348111
GC_O_eperlarnus_smelt_4_retrNOfins	Re normalized	2219046	6674906	-1.14E-07	0.001646999	0.274095
GC_O_eperlarnus_smelt_4_retrNOfins	V normalized	2219046	6674906	-2.14E-06	0.001876676	0.29172008
GC_O_eperlarnus_smelt_5_retrNOfins	Re normalized	1499102	5146252	4.07E-06	0.001318398	0.31756997
GC_O_eperlarnus_smelt_5_retrNOfins	V normalized	1499102	5146252	-3.77E-05	0.001421433	0.32973854
GC_O_eperlarnus_smelt_6_retrNOfins	Re normalized	2038351	6296429	2.78E-07	0.002043996	0.25586964
GC_O_eperlarnus_smelt_6_retrNOfins	V normalized	2038351	6296429	8.81E-06	0.001903578	0.24724062
GC_O_eperlarnus_smelt_8_retrNOfins	Re normalized	2145652	6519373	2.78E-06	0.001247318	0.26823626
GC_O_eperlarnus_smelt_8_retrNOfins	V normalized	2145652	6519373	-5.59E-05	0.00144059	0.28807378
GC_O_eperlarnus_smelt_10_retrNOfins	Re normalized	1716311	5607077	-8.88E-07	0.001242688	0.27441012
GC_O_eperlarnus_smelt_10_retrNOfins	V normalized	1716311	5607077	1.15E-06	0.001274362	0.27781342
GC_O_eperlarnus_smelt_13_retrNOfins	Re normalized	1931106	6065642	9.47E-08	0.00128039	0.29102941
GC_O_eperlarnus_smelt_13_retrNOfins	V normalized	1931106	6065642	-1.75E-05	0.001321874	0.29564627
GC_O_eperlarnus_smelt_16_retrNOfins	Re normalized	2097063	6422293	1.32E-06	0.001298406	0.26721444
GC_O_eperlarnus_smelt_16_retrNOfins	V normalized	2097063	6422293	-1.90E-05	0.001348939	0.27236897
GC_O_eperlarnus_smelt_17_retrNOfins	Re normalized	1600575	5361030	-4.89E-06	0.001281869	0.32256038
GC_O_eperlarnus_smelt_17_retrNOfins	V normalized	1600575	5361030	-3.28E-05	0.001388465	0.33538591
GC_O_eperlarnus_smelt_19_retrNOfins	Re normalized	1914670	6028985	1.13E-07	0.001341243	0.27674783
GC_O_eperlarnus_smelt_19_retrNOfins	V normalized	1914670	6028985	8.48E-06	0.001306436	0.2731708
GC_O_eperlarnus_smelt_22_retrNOfins	Re normalized	1522022	5215172	1.26E-05	0.00130013	0.2888349
GC_O_eperlarnus_smelt_22_retrNOfins	V normalized	1522022	5215172	-3.21E-05	0.001395274	0.29912975
GC_O_eperlarnus_smelt_36_retrNOfins	Re normalized	2118105	6454538	6.07E-07	0.00149887	0.28923558
GC_O_eperlarnus_smelt_36_retrNOfins	V normalized	2118105	6454538	2.45E-05	0.001388321	0.27841968

$Re = \rho * u * L * \mu^{-1}$
where:
Re is the Reynolds number
ρ is the density of the fluid ($kg * m^{-3}$)
u is the velocity of the fluid with respect to the object ($m * s^{-1}$)
L is a characteristic linear dimension (m)
μ is the dynamic viscosity of the fluid (kg/m·s)

$C_d = 2 F_d * \rho^{-1} u^{-2} A^{-1}$
where:
C_d is the drag coefficient
F_d is the drag force (the force component in the oncoming flow direction)
ρ is the mass density of the fluid
u is the flow speed of the object relative to the fluid
A is the reference area

Specimen	Length (m) in CFD	Swimming speed (m*s-1) in CFD Re	Swimming speed (m*s-1) in CFD V	Length (m) Re normalized	Area (m2) Re normalized	Volume (m3) Re normalized	Swimming speed (m*s-1) Re	Drag force (N) Re normalized	Cd Re normalized
GC_O_eperlarnus_smelt_1_retrNOfins	0.1	0.25	0.226481875	0.05	0.000970375	1.34499E-06	0.5	4.43121E-05	0.000365319
GC_O_eperlarnus_smelt_1_retrNOfins	0.1	0.25	0.226481875	0.05	0.000970375	1.34499E-06	0.5	-	
GC_O_eperlarnus_smelt_2_retrNOfins	0.1	0.25	0.254151291	0.05	0.000840181	9.51794E-07	0.5	2.81641E-05	0.000268172
GC_O_eperlarnus_smelt_2_retrNOfins	0.1	0.25	0.254151291	0.05	0.000840181	9.51794E-07	0.5	-	
GC_O_eperlarnus_smelt_4_retrNOfins	0.1	0.25	0.268571637	0.05	0.000771908	8.06565E-07	0.5	3.294E-05	0.000341388
GC_O_eperlarnus_smelt_4_retrNOfins	0.1	0.25	0.268571637	0.05	0.000771908	8.06565E-07	0.5	-	
GC_O_eperlarnus_smelt_5_retrNOfins	0.1	0.25	0.261334293	0.05	0.00077689	8.75449E-07	0.5	2.6368E-05	0.000271523
GC_O_eperlarnus_smelt_5_retrNOfins	0.1	0.25	0.261334293	0.05	0.00077689	8.75449E-07	0.5	-	
GC_O_eperlarnus_smelt_6_retrNOfins	0.1	0.25	0.240708805	0.05	0.000915288	1.12033E-06	0.5	4.08799E-05	0.000357308
GC_O_eperlarnus_smelt_6_retrNOfins	0.1	0.25	0.240708805	0.05	0.000915288	1.12033E-06	0.5	-	
GC_O_eperlarnus_smelt_8_retrNOfins	0.1	0.25	0.272510065	0.05	0.000760784	7.72098E-07	0.5	2.49464E-05	0.000262323
GC_O_eperlarnus_smelt_8_retrNOfins	0.1	0.25	0.272510065	0.05	0.000760784	7.72098E-07	0.5	-	
GC_O_eperlarnus_smelt_10_retrNOfins	0.1	0.25	0.253941511	0.05	0.000802321	9.54155E-07	0.5	2.48538E-05	0.000247819
GC_O_eperlarnus_smelt_10_retrNOfins	0.1	0.25	0.253941511	0.05	0.000802321	9.54155E-07	0.5	-	
GC_O_eperlarnus_smelt_13_retrNOfins	0.1	0.25	0.254886593	0.05	0.000809267	9.43581E-07	0.5	2.56078E-05	0.000253146
GC_O_eperlarnus_smelt_13_retrNOfins	0.1	0.25	0.254886593	0.05	0.000809267	9.43581E-07	0.5	-	
GC_O_eperlarnus_smelt_16_retrNOfins	0.1	0.25	0.255850083	0.05	0.000813633	9.32961E-07	0.5	2.59681E-05	0.00025533
GC_O_eperlarnus_smelt_16_retrNOfins	0.1	0.25	0.255850083	0.05	0.000813633	9.32961E-07	0.5	-	
GC_O_eperlarnus_smelt_17_retrNOfins	0.1	0.25	0.262537847	0.05	0.000809103	8.63464E-07	0.5	2.56374E-05	0.00025349
GC_O_eperlarnus_smelt_17_retrNOfins	0.1	0.25	0.262537847	0.05	0.000809103	8.63464E-07	0.5	-	
GC_O_eperlarnus_smelt_19_retrNOfins	0.1	0.25	0.246028884	0.05	0.000839851	1.04921E-06	0.5	2.68249E-05	0.00025552
GC_O_eperlarnus_smelt_19_retrNOfins	0.1	0.25	0.246028884	0.05	0.000839851	1.04921E-06	0.5	-	
GC_O_eperlarnus_smelt_22_retrNOfins	0.1	0.25	0.260398226	0.05	0.000785078	8.84924E-07	0.5	2.60026E-05	0.000264968
GC_O_eperlarnus_smelt_22_retrNOfins	0.1	0.25	0.260398226	0.05	0.000785078	8.84924E-07	0.5	-	
GC_O_eperlarnus_smelt_36_retrNOfins	0.1	0.25	0.238911429	0.05	0.000879725	1.1458E-06	0.5	2.99774E-05	0.000272607
GC_O_eperlarnus_smelt_36_retrNOfins	0.1	0.25	0.238911429	0.05	0.000879725	1.1458E-06	0.5	-	

Specimen	Length (m) V normalized	Area (m2) V normalized	Volume (m3) V normalized	Swimming speed (m*s-1) V normalized	Drag force (N) V normalized
GC_O_eperlarnus_smelt_1_retrNOfins	0.045296375	0.000796391	0.000001	0.5	-
GC_O_eperlarnus_smelt_1_retrNOfins	0.045296375	0.000796391	0.000001	0.5	4.10987E-05
GC_O_eperlarnus_smelt_2_retrNOfins	0.050830258	0.000868315	0.000001	0.5	-
GC_O_eperlarnus_smelt_2_retrNOfins	0.050830258	0.000868315	0.000001	0.5	2.85794E-05
GC_O_eperlarnus_smelt_4_retrNOfins	0.053714327	0.000890852	0.000001	0.5	-
GC_O_eperlarnus_smelt_4_retrNOfins	0.053714327	0.000890852	0.000001	0.5	3.49381E-05
GC_O_eperlarnus_smelt_5_retrNOfins	0.052266859	0.000848931	0.000001	0.5	-
GC_O_eperlarnus_smelt_5_retrNOfins	0.052266859	0.000848931	0.000001	0.5	2.71957E-05
GC_O_eperlarnus_smelt_6_retrNOfins	0.048141761	0.000848519	0.000001	0.5	-
GC_O_eperlarnus_smelt_6_retrNOfins	0.048141761	0.000848519	0.000001	0.5	3.95411E-05
GC_O_eperlarnus_smelt_8_retrNOfins	0.054502013	0.000903954	0.000001	0.5	-
GC_O_eperlarnus_smelt_8_retrNOfins	0.054502013	0.000903954	0.000001	0.5	2.64319E-05
GC_O_eperlarnus_smelt_10_retrNOfins	0.050788302	0.000827819	0.000001	0.5	-
GC_O_eperlarnus_smelt_10_retrNOfins	0.050788302	0.000827819	0.000001	0.5	2.50916E-05
GC_O_eperlarnus_smelt_13_retrNOfins	0.050977319	0.000841213	0.000001	0.5	-
GC_O_eperlarnus_smelt_13_retrNOfins	0.050977319	0.000841213	0.000001	0.5	2.59306E-05
GC_O_eperlarnus_smelt_16_retrNOfins	0.051170017	0.000852157	0.000001	0.5	-
GC_O_eperlarnus_smelt_16_retrNOfins	0.051170017	0.000852157	0.000001	0.5	2.63619E-05
GC_O_eperlarnus_smelt_17_retrNOfins	0.052507569	0.000892293	0.000001	0.5	-
GC_O_eperlarnus_smelt_17_retrNOfins	0.052507569	0.000892293	0.000001	0.5	2.64431E-05
GC_O_eperlarnus_smelt_19_retrNOfins	0.049205777	0.000813382	0.000001	0.5	-
GC_O_eperlarnus_smelt_19_retrNOfins	0.049205777	0.000813382	0.000001	0.5	2.65504E-05
GC_O_eperlarnus_smelt_22_retrNOfins	0.052079645	0.000851743	0.000001	0.5	-
GC_O_eperlarnus_smelt_22_retrNOfins	0.052079645	0.000851743	0.000001	0.5	2.67911E-05
GC_O_eperlarnus_smelt_36_retrNOfins	0.047782286	0.000803417	0.000001	0.5	-
GC_O_eperlarnus_smelt_36_retrNOfins	0.047782286	0.000803417	0.000001	0.5	2.90551E-05

Table A5. 2 Mesh sensitivity test results

| Domain | | | | | | | | | | Results | | | | | |
Domain size (m)	Refinement zone size (m)	Turb. intensity	Body el. Size (m)	Face sizing (elemnt size) (m)	Face sizing (local min. size) (m)	1st layer thick.	Num. layers	Num. el.	Num. nodes	Flow imbalance (l)	Lift force (N)	Drag force (N)	Y+	Lift error (%)	Drag error (%)
Mesh independence															
1.82 x 0.61 x 0.61	0.7 x 0.2 x 0.12	0.05%	0.004	0.01	0.0001	4.06E-05	23	2196457	6624493	1.38E-06	0.0026	0.0011	0.353		
1.82 x 0.61 x 0.61	0.7 x 0.2 x 0.12	0.05%	0.004	0.01	0.00012	4.06E-05	23	2079051	6375260	-1.36E-07	0.0026	0.0011	0.352	0.01	0.03
1.82 x 0.61 x 0.61	0.7 x 0.2 x 0.12	0.05%	0.004	0.01	0.00014	4.06E-05	23	1944119	6090380	6.20E-07	0.0026	0.0011	0.355	0.03	0.14
1.82 x 0.61 x 0.61	0.7 x 0.2 x 0.12	0.05%	0.004	0.01	0.00016	4.06E-05	23	1831505	5849266	1.06E-06	0.0026	0.0011	0.355	0.04	0.11
1.82 x 0.61 x 0.61	0.7 x 0.2 x 0.12	0.05%	0.004	0.01	0.0002	4.06E-05	23	1620860	5404416	1.38E-06	0.0026	0.0011	0.360	0.03	0.10
1.82 x 0.61 x 0.61	0.7 x 0.2 x 0.12	0.05%	0.004	0.01	0.00024	4.06E-05	23	1451532	5045207	1.39E-06	0.0026	0.0011	0.364	0.08	0.01
1.82 x 0.61 x 0.61	0.7 x 0.2 x 0.12	0.05%	0.0025	0.01	0.00014	4.06E-05	23	3243218	13829993	-9.93E-08	0.0026	0.0011	0.355		
1.82 x 0.61 x 0.61	0.7 x 0.2 x 0.12	0.05%	0.003	0.01	0.00014	4.06E-05	23	2541177	9643473	1.24E-06	0.0026	0.0011	0.355	0.01	0.07
1.82 x 0.61 x 0.61	0.7 x 0.2 x 0.12	0.05%	0.0035	0.01	0.00014	4.06E-05	23	2164971	7408354	2.25E-06	0.0026	0.0011	0.355	0.02	0.10
1.82 x 0.61 x 0.61	0.7 x 0.2 x 0.12	0.05%	0.004	0.01	0.00014	4.06E-05	23	1943988	6090102	-1.79E-07	0.0026	0.0011	0.355	0.01	0.01
1.82 x 0.61 x 0.61	0.7 x 0.2 x 0.12	0.05%	0.0045	0.01	0.00014	4.06E-05	23	1810683	5295659	-1.39E-08	0.0026	0.0011	0.354	0.00	0.02
1.82 x 0.61 x 0.61	0.7 x 0.2 x 0.12	0.05%	0.005	0.01	0.00014	4.06E-05	23	1723835	4778428	2.24E-07	0.0026	0.0011	0.355	0.03	0.07
1.82 x 0.61 x 0.61	0.7 x 0.2 x 0.12	0.05%	0.0055	0.01	0.00014	4.06E-05	23	1664363	4422132	2.25E-07	0.0026	0.0011	0.355	0.02	0.01
1.82 x 0.61 x 0.61	0.7 x 0.2 x 0.12	0.05%	0.004	0.002	0.00014	4.06E-05	23	1945033	6093550	3.51E-07	0.0026	0.0011	0.355		
1.82 x 0.61 x 0.61	0.7 x 0.2 x 0.12	0.05%	0.004	0.006	0.00014	4.06E-05	23	1943277	6088252	4.62E-07	0.0026	0.0011	0.355	0.00	0.01
1.82 x 0.61 x 0.61	0.7 x 0.2 x 0.12	0.05%	0.004	0.01	0.00014	4.06E-05	23	1945092	6091343	4.04E-08	0.0026	0.0011	0.354	0.01	0.12
1.82 x 0.61 x 0.61	0.7 x 0.2 x 0.12	0.05%	0.004	0.015	0.00014	4.06E-05	23	1944330	6090391	1.37E-06	0.0026	0.0011	0.354	0.02	0.10
1.82 x 0.61 x 0.61	0.7 x 0.2 x 0.12	0.05%	0.004	0.02	0.00014	4.06E-05	23	1944246	6089453	1.66E-07	0.0026	0.0011	0.355	0.01	0.03
1.82 x 0.61 x 0.61	0.7 x 0.2 x 0.12	0.05%	0.004	0.025	0.00014	4.06E-05	23	1944009	6088954	-5.51E-07	0.0026	0.0011	0.354	0.02	0.02
1.82 x 0.61 x 0.61	0.7 x 0.2 x 0.12	0.05%	0.004	0.01	0.00014	4.06E-05	16	1572683	5496427	5.97E-07	0.0026	0.0012	0.370		
1.82 x 0.61 x 0.61	0.7 x 0.2 x 0.12	0.05%	0.004	0.01	0.00014	4.06E-05	23	1943735	6088467	1.05E-06	0.0026	0.0011	0.355	0.53	2.77
1.82 x 0.61 x 0.61	0.7 x 0.2 x 0.12	0.05%	0.004	0.01	0.00014	4.06E-05	29	2279531	6702798	-7.71E-08	0.0026	0.0011	0.346	0.18	0.50
1.82 x 0.61 x 0.61	0.7 x 0.2 x 0.12	0.05%	0.004	0.01	0.00014	0.00003	23	1954722	6153890	5.33E-07	0.0026	0.0012	0.266		
1.82 x 0.61 x 0.61	0.7 x 0.2 x 0.12	0.05%	0.004	0.01	0.00014	4.056E-05	23	1944027	6090316	1.34E-06	0.0026	0.0011	0.355	0.18	0.98
1.82 x 0.61 x 0.61	0.7 x 0.2 x 0.12	0.05%	0.004	0.01	0.00014	0.00005	23	1938836	6056232	8.75E-07	0.0026	0.0011	0.433	0.04	0.18
1.82 x 0.61 x 0.61	0.7 x 0.2 x 0.12	0.05%	0.004	0.01	0.00014	0.00006	23	1935177	6035064	4.14E-07	0.0026	0.0011	0.515	0.16	0.19
Domain size independence															
1.82 x 0.61 x 0.61	0.7 x 0.2 x 0.12	0.05%	0.004	0.01	0.00014	4.056E-05	23	1944027	6090316	1.34E-06	0.0026	0.0011	0.355		
2.32 x 0.80 x 0.80	0.7 x 0.2 x 0.12	0.05%	0.004	0.01	0.00014	4.056E-05	23	1962006	6157465	-2.70E-06	0.0026	0.0011	0.353	0.06	0.03
1.82 x 0.61 x 0.61	0.7 x 0.2 x 0.12	0.05%	0.004	0.01	0.00014	4.056E-05	23	1944027	6090316	1.34E-06	0.0026	0.0011	0.355		
1.82 x 0.61 x 0.61	1.2 x 0.4 x 0.20	0.05%	0.004	0.01	0.00014	4.056E-05	23	3843893	17387181	6.18E-06	0.0026	0.0011	0.354	0.03	0.16

Table A5. 3 Model scaling crite

Specimen	Reynolds normalized dimensions			Volume normalized dimensions			Model dimensions				
	Body length (m)	Area (m^2)	Volume (m^3)	Body length (m)	Area (m^2)	Volume (m^3)	Length model (m)	Area model (mm^2)	Area model (m^2)	Volume model (mm^3)	Volume model (m^3)
GC_O_eperlarnus_smelt_1_retrNOfins	0.050	0.0009704	0.0000013	0.045	0.0007964	0.0000010	0.100	3881.499	0.0038815	10759.935	0.0000108
GC_O_eperlarnus_smelt_2_retrNOfins	0.050	0.0008402	0.0000010	0.051	0.0008683	0.0000010	0.100	3360.725	0.0033607	7614.354	0.0000076
GC_O_eperlarnus_smelt_4_retrNOfins	0.050	0.0007719	0.0000008	0.054	0.0008909	0.0000010	0.100	3087.632	0.0030876	6452.523	0.0000065
GC_O_eperlarnus_smelt_5_retrNOfins	0.050	0.0007769	0.0000009	0.052	0.0008489	0.0000010	0.100	3107.561	0.0031076	7003.591	0.0000070
GC_O_eperlarnus_smelt_6_retrNOfins	0.050	0.0009153	0.0000011	0.048	0.0008485	0.0000010	0.100	3661.151	0.0036612	8962.601	0.0000090
GC_O_eperlarnus_smelt_8_retrNOfins	0.050	0.0007608	0.0000008	0.055	0.0009040	0.0000010	0.100	3043.135	0.0030431	6176.783	0.0000062
GC_O_eperlarnus_smelt_10_retrNOfins	0.050	0.0008023	0.0000010	0.051	0.0008278	0.0000010	0.100	3209.283	0.0032093	7633.240	0.0000076
GC_O_eperlarnus_smelt_13_retrNOfins	0.050	0.0008093	0.0000009	0.051	0.0008412	0.0000010	0.100	3237.069	0.0032371	7548.646	0.0000075
GC_O_eperlarnus_smelt_16_retrNOfins	0.050	0.0008136	0.0000009	0.051	0.0008522	0.0000010	0.100	3254.530	0.0032545	7463.685	0.0000075
GC_O_eperlarnus_smelt_17_retrNOfins	0.050	0.0008091	0.0000009	0.053	0.0008923	0.0000010	0.100	3236.410	0.0032364	6907.713	0.0000069
GC_O_eperlarnus_smelt_19_retrNOfins	0.050	0.0008399	0.0000010	0.049	0.0008134	0.0000010	0.100	3359.404	0.0033594	8393.667	0.0000084
GC_O_eperlarnus_smelt_22_retrNOfins	0.050	0.0007851	0.0000009	0.052	0.0008517	0.0000010	0.100	3140.312	0.0031403	7079.392	0.0000071
GC_O_eperlarnus_smelt_36_retrNOfins	0.050	0.0008797	0.0000011	0.048	0.0008034	0.0000010	0.100	3518.901	0.0035189	9166.409	0.0000092

Specimen	Parameters in the CFD analyses				CFD analyses (Re normalized)		CFD analyses (V normalized)	
	Density of fluid (kg*m^{-3})	Velocity (m*s^{-1})	Dynamic viscosity of fluid (kg*s^{-1}*m^{-1})	Turbulence intensity (%)	Re	Velocity CFD (m*s^{-1})	Re	Velocity CFD (m*s^{-1})
GC_O_eperlarnus_smelt_1_retrNOfins	998.2	0.500	0.001003	0.05	24880.359	0.2500000000	22539.801	0.2264818753
GC_O_eperlarnus_smelt_2_retrNOfins	998.2	0.500	0.001003	0.05	24880.359	0.2500000000	25293.501	0.2541512908
GC_O_eperlarnus_smelt_4_retrNOfins	998.2	0.500	0.001003	0.05	24880.359	0.2500000000	26728.635	0.2685716370
GC_O_eperlarnus_smelt_5_retrNOfins	998.2	0.500	0.001003	0.05	24880.359	0.2500000000	26008.364	0.2613342927
GC_O_eperlarnus_smelt_6_retrNOfins	998.2	0.500	0.001003	0.05	24880.359	0.2500000000	23955.686	0.2407088050
GC_O_eperlarnus_smelt_8_retrNOfins	998.2	0.500	0.001003	0.05	24880.359	0.2500000000	27120.593	0.2725100649
GC_O_eperlarnus_smelt_10_retrNOfins	998.2	0.500	0.001003	0.05	24880.359	0.2500000000	25272.624	0.2539415115
GC_O_eperlarnus_smelt_13_retrNOfins	998.2	0.500	0.001003	0.05	24880.359	0.2500000000	25366.680	0.2548865931
GC_O_eperlarnus_smelt_16_retrNOfins	998.2	0.500	0.001003	0.05	24880.359	0.2500000000	25462.568	0.2558500832
GC_O_eperlarnus_smelt_17_retrNOfins	998.2	0.500	0.001003	0.05	24880.359	0.2500000000	26128.143	0.2625378468
GC_O_eperlarnus_smelt_19_retrNOfins	998.2	0.500	0.001003	0.05	24880.359	0.2500000000	24485.148	0.2460288836
GC_O_eperlarnus_smelt_22_retrNOfins	998.2	0.500	0.001003	0.05	24880.359	0.2500000000	25915.205	0.2603982256
GC_O_eperlarnus_smelt_36_retrNOfins	998.2	0.500	0.001003	0.05	24880.359	0.2500000000	23776.808	0.2389114292